Chapter 8

Array Antennas

8.1 INTRODUCTION

The topic of array antennas was introduced in Sec. 3.5 with several two-element arrays as examples of simple radiating systems. Fig. 3-19 summarizes the range of pattern control that is possible by changing the spacing and phasing of two-element arrays illustrated using elements with the same excitation amplitude and isotropic patterns. Arrays are popular because of the ability to shape the pattern through spacing and excitation adjustment along with the unique capability of scanning the pattern in angular space by dynamically adjusting the excitation phases electronically. Such an array is referred to as a **phased array**. The traditional method of scanning a directive beam is to mechanically steer an aperture antenna such as a reflector antenna. Thus, the problem of mechanically slewing of one large antenna is traded for the feed network complexities associated with properly exciting many small antennas in an array. In addition to avoiding the need for a mechanical structure required to point a large antenna, a phased array can also scan a beam at electronic speeds and can even have multiple simultaneous main beams. Although a feed network is required to excite the array elements, today's low-cost electronics, computing, and digital signal processing hardware and software make electronic scanning affordable. Arrays have the additional advantage of supporting many geometries, including non-planar surfaces to conform to existing contours such as the skin of an aircraft. There are many applications for phased arrays, most notably in radar.

The first widely used array antenna was the Yagi-Uda array invented in 1926 (see Sec. 6.3). The Yagi was followed by other fixed-phase arrays that were mechanically steered. Phased arrays emerged during World War II using mechanical phase shifters. With the invention of the ferrite phase shifter in the 1950s, full electronic scanning became possible. Both array element advances and solid-state phase shifters allowed for more affordable, compact phased arrays beginning in the 1960s. The recent innovation in arrays is the active phased array in which each element has transmit/receive electronics including phase adjustment.

Both arrays and aperture antennas are capable of high gain. Arrays can be analyzed using simple mathematics by summing phasors, but reflector antenna analysis requires integration over the aperture, as we will find out in the next chapter. In this chapter, we continue the development of arrays, beginning with linear arrays of multiple isotropic elements, uniform excitations, and equal spacings. The pattern of individual elements is then included. Techniques for evaluating the directivity of linear arrays are presented, followed by addressing nonuniform excitation of linear arrays and multidimensional arrays. Implementation issues of mutual coupling and feeding techniques are treated. Finally, more detail is presented on the types of elements used in practical arrays along with the special topic of wide-bandwidth phased arrays.

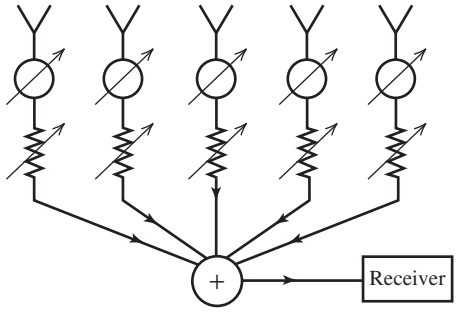

Figure 8-1 A typical linear array. The symbols ⊘ and ⚡ indicate variable phase shifters and attenuators. The output currents are summed before entering the receiver.

8.2 THE ARRAY FACTOR FOR LINEAR ARRAYS

The fundamental configuration for elements in an array is the linear array shown in Fig. 8-1. Linear arrays are used widely in practice and their operating principles can be used to understand more complex array geometries. The array of Fig. 8-1 has identical elements and is operated as a receiving antenna. The pattern characteristics of an array can be explained for operation as a transmitter or receiver, whichever is more convenient, since antennas usually satisfy the conditions for reciprocity. The output of each element can be controlled in amplitude and phase as indicated by the attenuators and phase shifters in Fig. 8-1. Amplitude and phase control provide for custom shaping of the radiation pattern and for scanning of the pattern in space.

The basic array antenna model consists of two parts, the pattern of one of the elements by itself, the element pattern, and the pattern of the array with the actual elements replaced by isotropic point sources, the array factor. The total pattern of the array is then the product of the element pattern and array factor; this will be discussed in detail in Sec. 8.4. We treat the array factor first.

The array factor corresponding to the linear array of Fig. 8-1 is found by replacing each element by an isotropic radiator, but retaining the element locations and excitations as shown in Fig. 8-2. The array is receiving a plane wave arriving at an angle θ from the line of the elements, and the planes of equal phase (i.e., wavefronts) are shown. Rays perpendicular to the wavefronts indicate the direction of travel of the wave. With the reference wavefront taken to be of zero phase, the distance to the nth element has a corresponding phase delay (found by multiplying by β) of ξ_n. That is, each element is excited with phase ξ_n, due to the spatial phase delay effect of the incoming plane wave. The amplitudes of excitation are constant, taken to be unity, because a plane wave has uniform amplitude. The resulting excitations of $1e^{j\xi_0}, 1e^{j\xi_1}, \ldots$ are shown for each element in Fig. 8-2. The elements themselves do not weight the outputs since they are isotropic radiators that respond equally to all incoming wave directions.

The array factor for the array of Fig. 8-1 is found from the array of Fig. 8-2 that has isotropic radiators for array elements in place of the actual elements. The array factor for this receiving array is then the sum of the isotropic radiator receiving antenna responses $\{e^{j\xi_0}, e^{j\xi_1}, \ldots\}$ weighted by the amplitude and phase shift represented by complex currents $\{I_0, I_1, \ldots\}$ introduced in the transmission path connected to each element. The array factor of the array shown in Fig. 8-2 is thus

$$\text{AF} = I_0 e^{j\xi_0} + I_1 e^{j\xi_1} + I_2 e^{j\xi_2} + \cdots \tag{8-1}$$

where $\xi_0, \xi_1, \ldots$ are the phases of an incoming plane wave at the element locations designated 0,1,... For convenience, these phases are usually relative to the coordinate origin; that is, the phase of the wave arriving at the nth element leads the phase of the wave arriving at the origin by ξ_n.

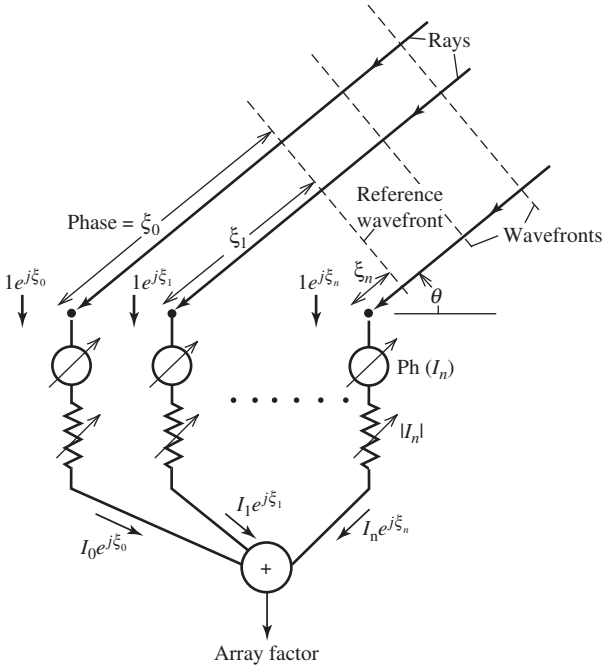

Figure 8-2 Equivalent configuration of the array in Fig. 8-1 for determining the array factor. The elements of the array are replaced by isotropic point sources.

In Sec. 3.5, we presented examples that show how to sum the phasors in (8-1) for two-element arrays of isotropic elements. For such simple cases, the major features of the radiation pattern can be found by an inspection method where the phasors for each source element are traced to the far field in principal directions and summed. We further illustrate the inspection method with the following example.

EXAMPLE 8-1 ***Two Identical Isotropic Point Sources Spaced One Wavelength Apart (see Fig. 8-3)***

Two isotropic sources spaced one wavelength apart transmit signals of the same magnitude and phase as shown in Fig. 8-3*a*. Fig. 8-3*b* shows some of the transmitted far-field rays. Because of the in-phase condition, the fields arriving in the far field add perfectly (i.e., double) in the $\pm x$-directions (broadside directions) because of the equal path length to the far field. In other words, since the rays started out in phase and experience the same propagation phase shift, they arrive in phase. Off the ends of the array in the endfire directions, the phase of the field from the more distant element to the same far-field distance lags that from the close element by 360° due to the extra one wavelength of travel. Thus, the far-field phasors sum in phase in the $\pm z$-directions. So, the phase difference between the two far-field rays varies from 0° at broadside $(\theta = 90^\circ)$ to 360° at endfire $(\theta = 0^\circ, 180^\circ)$. Therefore, there is a direction where the phase difference is 180°, corresponding to a half-wavelength path length difference, and the phasors cancel. The path length difference as a function of observation angle for the two-element array is $d \cos\theta$ (see Fig. 3-16*d*). For this example where $d = \lambda$, the angle for $\lambda/2$-path difference can be found using $\lambda \cos\theta = \pm\lambda/2$, giving $\cos\theta = \pm 1/2$ which has solutions $\theta = 60^\circ, 120^\circ$ for null locations. With these null locations and knowing that maxima occur in multiples of 90°, the radiation pattern can be sketched as in Fig. 8-3*c*. The pattern magnitude is plotted, but it should be noted that the endfire beams at 0° and 180° are negative-valued due to

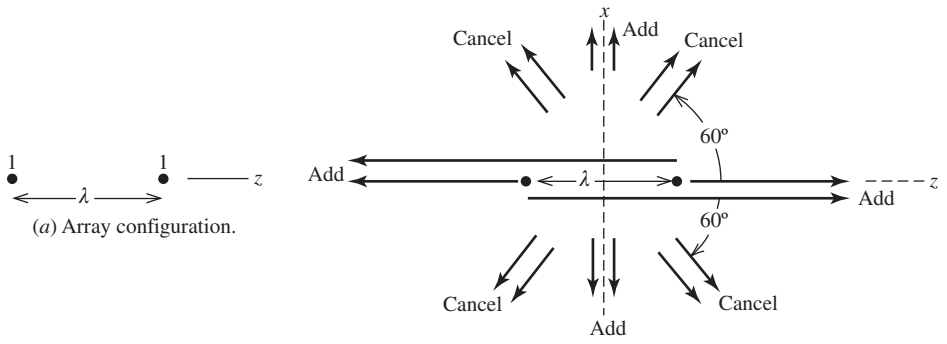

(*a*) Array configuration.

(*b*) Inspection method.

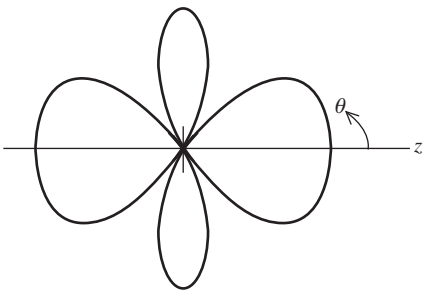

(*c*) Polar plot of array factor magnitude $|f(\theta) = |\cos(\pi \cos\theta)|$.

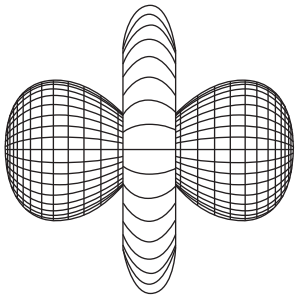

(*d*) Three-dimensional plot.

Figure 8-3 Two isotropic point sources with identical amplitude and phase currents, and spaced one wavelength apart (Example 8-1).

the 180° phase jump when passing through the null. The exact pattern expression is found from the two-element array factor expression in (3-67) with d = λ, which when normalized is

$$f(\theta) = \cos(\pi \cos\theta) \tag{8-2}$$

The three-dimensional plot of this expression is shown Fig. 8-3*d*. This example illustrates the general result that *multiple* major lobes will appear in the pattern for an element spacing of one wavelength (or greater), which can also be seen in Fig. 3-19.

We are now ready to develop more general array factor formulas. The expression in (8-1) is general and can be applied to any geometry. First, we consider linear arrays with elements equally spaced along the *z*-axis as shown in Fig. 8-4. The individual isotropic elements respond equally in all directions to an incoming plane wave. But when the outputs from each element are added in a receiver (weighted by complex currents I_n), the total array response depends on θ, which is the angle with respect to the line of elements (the *z*-axis). The phase of the arriving wave is set to zero at the origin for convenience, thus $\xi_o = 0$. The incoming waves arriving at Element 1 travel a distance of $d \cos\theta$ less than the wave arriving at the origin. The corresponding phase of waves at Element 1 relative to the origin is $\xi_1 = \beta d \cos\theta$, the spatial phase delay. In fact, across the array the phase at each element leads its immediate nearest neighbor on the left by the same amount of $\beta d \cos\theta$. Using this result in (8-1) gives

$$\text{AF} = I_0 + I_1 e^{j\beta d \cos\theta} + I_2 e^{j\beta 2d \cos\theta} + \cdots = \sum_{n=0}^{N-1} I_n e^{j\beta nd \cos\theta} \tag{8-3}$$

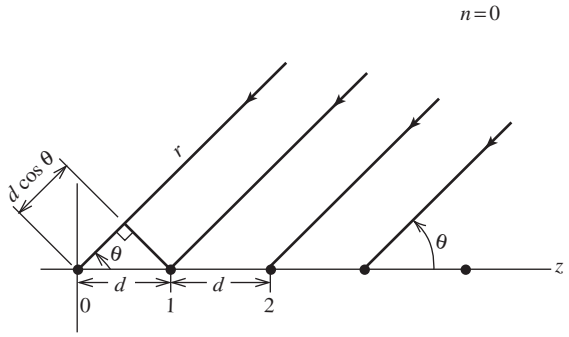

Figure 8-4 Equally spaced linear array of isotropic point sources.

Now consider the array to be transmitting. If the current has a linear phase progression (i.e., relative phase between adjacent elements is the same), we can separate the phase explicitly as

$$I_n = A_n e^{jn\alpha} \tag{8-4}$$

where the $n+1$th element leads the nth element in phase by α. Then (8-3) becomes

$$\text{AF} = \sum_{n=0}^{\text{N}-1} A_n e^{jn(\beta d\,\cos\theta+\alpha)} \tag{8-5}$$

Define

$$\psi = \beta d\,\cos\theta + \alpha \tag{8-6}$$

Then

$$\text{AF} = \sum_{n=0}^{N-1} A_n e^{jn\psi} \tag{8-7}$$

This array factor is a function of ψ and is a Fourier series. This form is convenient for calculations, but we usually want polar plots in terms of the angle θ.

The nonlinear transformation from ψ to θ given by (8-6) can be accomplished graphically. Studying this graphical procedure adds understanding to the interaction of the several array parameters.

As an example, consider two elements spaced one-half wavelength apart and with identical currents as in Example 3-2. We found the normalized array factor in (3-69) to be $f(\theta) = \cos[(\pi/2)\cos\theta]$. In this case, ψ from (8-6) is

$$\psi = \beta d\,\cos\theta + \alpha = \pi\,\cos\theta \tag{8-8}$$

since $d = \lambda/2$ and $\alpha = 0$. Now f is expressed in terms of ψ as

$$f(\psi) = \cos\frac{\psi}{2} \tag{8-9}$$

This is a rather simple function to plot. To obtain a plot of $|f|$ as a function of θ, first plot $|f(\psi)|$ from (8-9) as shown in Fig. 8-5. Then draw a circle of radius $\psi = \pi$ below it as shown, since (8-8) is a polar equation of a circle. For an arbitrary value of ψ, say, ψ_1, drop a line straight down until it intersects the circle. The values of $\theta = \theta_1$ and $|f| = f_1$ corresponding to $\psi = \psi_1$ are indicated in the figure. Locating several points taken in this fashion produces the desired pattern sketch. Note that as θ ranges for 0 to π, ψ goes from

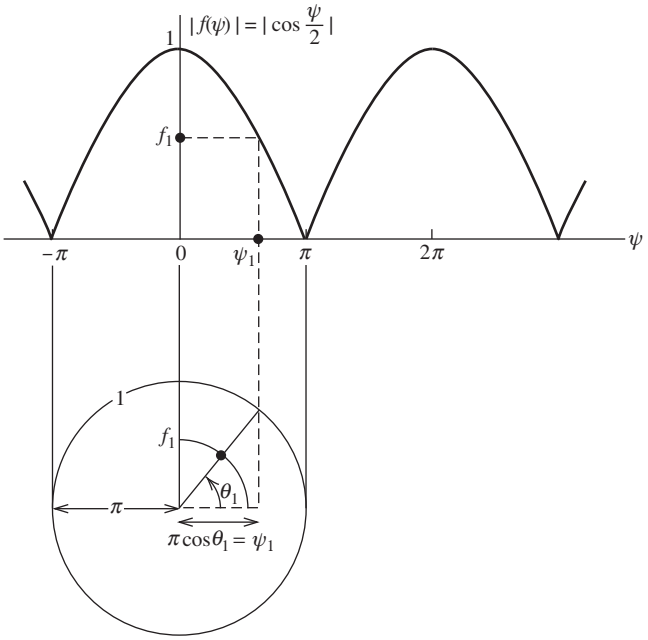

Figure 8-5 Procedure for obtaining the polar plot of the array factor of two elements spaced one-half wavelength apart with identical currents.

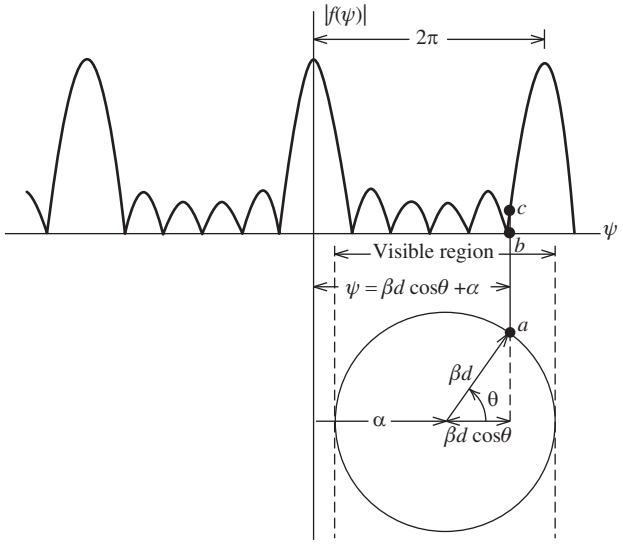

Figure 8-6 Construction technique for finding the array factor as a function of polar angle θ.

π to $-\pi$ in this case. The resulting polar plot is shown in Fig. 8-7*b*. It is the same as the result obtained in Fig. 3-16.

Before proceeding with more specific examples, we consider a general array factor and how a polar pattern is obtained from it. The magnitude of a typical array factor is plotted as a function of ψ in Fig. 8-6. Below it a circle is constructed with a radius equal to βd and its center located at $\psi = \alpha$. The angle θ is shown. It is very easy to use this plot. For a

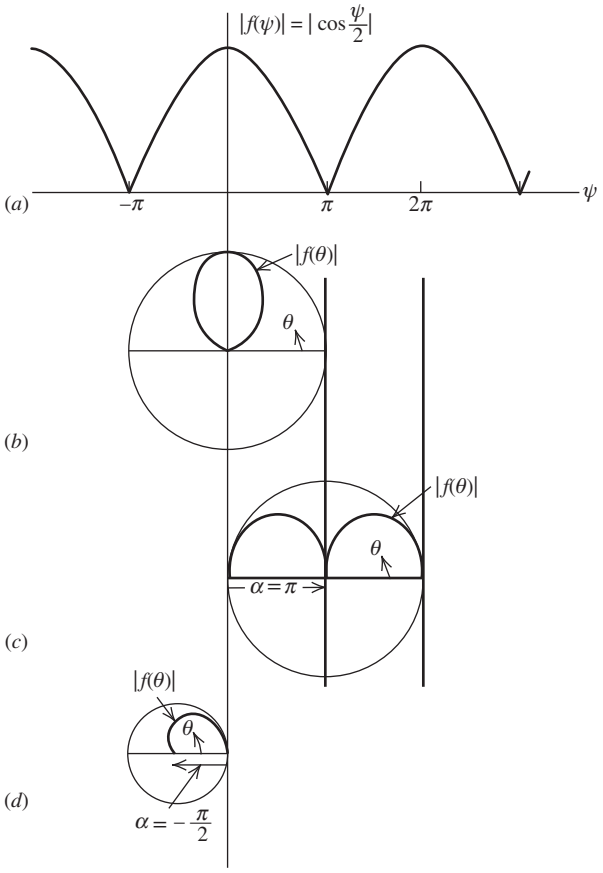

Figure 8-7 Array factors for two-element arrays with equal amplitude currents. (*a*) Universal array factor. (*b*) Polar plot for $d = \lambda/2, \beta d = \pi, \alpha = 0$ (Example 3-2). (*c*) Polar plot of $d = \lambda/2, \beta d = \pi, \alpha = \pi$ (Example 3-3). (*d*) Polar plot $d = \lambda/4$, $\beta d = \pi/2$, $\alpha = -\pi/2$ (Example 3-4).

given value of θ, locate the intersection of a radial line from the origin of the circle and the perimeter, point *a*. The corresponding value of ψ, at point *b*, is on a vertical line from *a*. The array factor value corresponding to these values of ψ and θ is then point *c*, also on the vertical line from *a*. Notice that the distance from the $\psi = 0$ axis to a point, say, at *a*, can be written as $\psi = \alpha + \beta d \cos\theta$, which is (8-6).

To illustrate the procedure further, we will find the polar plots of the array factors for some two-element arrays with uniform current amplitudes that were discussed earlier. The array factor as a function of ψ, from (8-7) with $N = 2$, is

$$\text{AF} = 1 + e^{j\psi} = e^{j(\psi/2)}(e^{-j(\psi/2)} + e^{j(\psi/2)}) = 2e^{j(\psi/2)}\cos\frac{\psi}{2} \tag{8-10}$$

where $A_0 = A_1 = 1$. Taking the magnitude eliminates the exponential factor and normalization removes the factor of 2, giving

$$|f(\psi)| = \left|\cos\frac{\psi}{2}\right| \tag{8-11}$$

which also follows from (8-9). The array factor $|f(\psi)|$ is the same for all two-element arrays with the same current amplitudes and is plotted in Fig. 8-7*a*. Of course, ψ changes with element spacing and phasing. For example, if the spacing is a half-wavelength and the phases of each element are zero ($\alpha = 0$), the pattern is obtained as shown in Fig. 8-5 with the resulting pattern plotted in Fig. 8-7*b*. This is Example 3-2 discussed earlier.

For Example 3-3, $d = \lambda/2$ and $\alpha = \pi$. The resulting polar plot of the array factor using the procedures of Fig. 8-6 is shown in Fig. 8-7*c*. The array factor for Example 3-4 with $d = \lambda/4$ and $\alpha = -\pi/2$ is shown in Fig. 8-7*d*.

By examining the general array factor expression in (8-7), some general properties can be derived that aid in the construction of pattern plots. First, the array factor is periodic in the variable ψ with period 2π. This is easily shown as follows:

$$\text{AF}(\psi + 2\pi) = \sum A_n e^{jn(\psi+2\pi)} = \sum A_n e^{jn\psi} e^{jn2\pi} = \sum A_n e^{jn\psi} = \text{AF}(\psi) \qquad (8\text{-}12)$$

The array factor of a linear array along the z-axis is a function of θ but not of ϕ (the element pattern may be though). In other words, the array factor is a pattern that has rotational symmetry about the line of the array. Therefore, its complete structure is determined by its values for

$$0 < \theta < \pi \qquad (8\text{-}13)$$

This is called the *visible region*. This corresponds to $-1 < \cos\theta < 1$ or $-\beta d < \beta d \cos\theta < \beta d$ or

$$\alpha - \beta d < \psi < \alpha + \beta d \qquad (8\text{-}14)$$

Hence, the visible region in terms of θ and ψ is given by (8-13) and (8-14), respectively. The element spacing of the array in terms of a wavelength, d/λ, determines the size of the circle in Fig. 8-6 and thus how much of the array factor appears in the visible region. The visible region in the variable ψ is of length $2\beta d$, as seen from (8-14). This is the diameter of the circle in Fig. 8-6. Suppose that exactly one period appears in the visible region. Since the period is 2π, we have $2\pi = 2\beta d = 2(2\pi/\lambda)d$ or $d/\lambda = \frac{1}{2}$. Thus, *exactly one period of the array factor appears in the visible region when the element spacing is one-half wavelength.* Less than one period is visible if $2\beta d < 2\pi$, which corresponds to $d/\lambda < \frac{1}{2}$ — that is, for spacings less than one-half wavelength. For spacings greater than one-half wavelength, more than one period will be visible. For one-wavelength spacings, two periods will be visible. For spacings larger than a half-wavelength, there may be more than one major lobe in the visible region, depending on the element phasings. Additional major lobes that rise to an intensity equal to that of the main lobe are called *grating lobes*. In the one-wavelength spaced, two-element array factor of Fig. 8-3*c*, there are grating lobes at $\theta = 0$ and 180°, in addition to the desired lobe in the $\theta = 90°$ direction. In most situations, it is undesirable to have grating lobes. As a result, most arrays are designed so the element spacings are less than one wavelength.

8.3 UNIFORMLY EXCITED, EQUALLY SPACED LINEAR ARRAYS

An array is usually comprised of identical elements positioned in a regular geometrical arrangement. In fact, this is the definition adopted by the IEEE. However, arrays are encountered in practice with unequal interelement spacings. Usually, a modifier (e.g., equally or unequally spaced) is included to be completely clear about the array geometry. The examples presented in this chapter are for equally spaced arrays, and unequally spaced arrays are treated in Sec. 8.8.

8.3.1 The Array Factor Expression

A very important special case of equally spaced linear arrays is that of the uniformly excited array. This is an array whose element current amplitudes are identical, or

$$A_0 = A_1 = A_2 = \cdots \qquad (8\text{-}15)$$

In this section, we consider only element phasings of a linear form that is accounted for by interelement phase shift α. The array factor from (8-7) is then

$$\text{AF} = A_0 \sum_{n=0}^{N-1} e^{jn\psi} = A_0(1 + e^{j\psi} + \cdots + e^{j(N-1)\psi}) \tag{8-16}$$

Only a few short steps are required to sum this geometric series. First, multiply (8-16) by $e^{j\psi}$ to obtain

$$\text{AF}\ \ e^{j\psi} = A_0(e^{j\psi} + e^{j2\psi} + \cdots + e^{jN\psi}) \tag{8-17}$$

Subtracting this from (8-16) gives

$$\text{AF}(1 - e^{j\psi}) = A_0(1 - e^{jN\psi})$$

or

$$\text{AF} = \frac{1 - e^{jN\psi}}{1 - e^{j\psi}} A_0 \tag{8-18}$$

This is rewritten in a more convenient form as follows:

$$\begin{aligned} \text{AF} = A_0 \frac{e^{jN\psi} - 1}{e^{j\psi} - 1} &= A_0 \ \frac{e^{jN\psi/2}}{e^{j\psi/2}} \frac{e^{jN\psi/2} - e^{-jN\psi/2}}{e^{j\psi/2} - e^{-j\psi/2}} \\ &= A_0 e^{j(N-1)\psi/2} \ \frac{\sin(N\psi/2)}{\sin(\psi/2)} \end{aligned} \tag{8-19}$$

The phase factor $e^{j(N-1)\psi/2}$ is not important unless the array output signal is further combined with the output from another antenna. In fact, if the array were centered about the origin, the phase factor would not be present since it represents the phase shift of the array phase center relative to the origin. Neglecting the phase factor in (8-19) gives

$$\text{AF} = A_0 \frac{\sin(N\psi/2)}{\sin(\psi/2)} \tag{8-20}$$

This expression is maximum for $\psi = 0$ and the maximum value from (8-16) is

$$\text{AF}(\psi = 0) = A_0(1 + 1 + \cdots + 1) = A_0 N \tag{8-21}$$

Dividing this into (8-20) gives the normalized array factor

$$\boxed{f(\psi) = \frac{\sin(N\psi/2)}{N\sin(\psi/2)}} \quad \textit{UE, ESLA} \tag{8-22}$$

This is the normalized array factor for an N element, uniformly excited, equally spaced linear array (UE, ESLA) that is centered about the coordinate origin. This function is similar to a $(\sin u)/u$ function, with the major difference that the side lobes do not die off without limit for increasing argument. In fact, the function (8-22) is periodic in 2π, which is true in general, as we showed in (8-12).

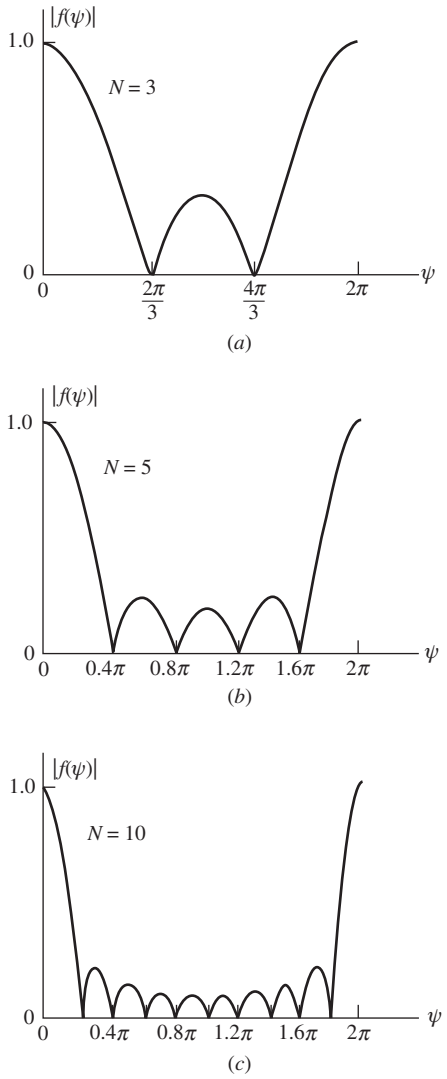

Figure 8-8 Array factor for an equally spaced, uniformly excited linear array for a few array numbers. (*a*) Three elements. (*b*) Five elements. (*c*) Ten elements.

A number of trends can be seen by examining array factor plots for various values of N as shown in Fig. 8-8:

1. As N increases, the main lobe narrows.
2. As N increases, there are more side lobes in one period of $f(\psi)$. In fact, the number of full lobes (one main lobe and the side lobes) in one period of $f(\psi)$ equals $N - 1$. Thus, there will be $N - 2$ side lobes are one main lobe in each period.
3. The minor lobes are of width $2\pi/N$ in the variable ψ and the major lobes (main and grating) are twice this width.
4. The side lobe peaks decrease with increasing N. A measure of the side lobe peaks is the *side lobe level* that we have defined as

$$\text{SLL} = \frac{|\text{maximum value of largest side lobe}|}{|\text{maximum value of main lobe}|} \tag{8-23}$$

and it is often expressed in decibels. The side lobe level of the array factor for $N = 5$ is -12 dB and it is -13 dB for $N = 20$. SLL approaches the value of a uniform line source, -13.3 dB, as N is increased.

5. $|f(\psi)|$ is symmetric about π. It is left as an exercise to show this.

The radiation (field) polar plots in the variable θ can be obtained from $f(\psi)$ as discussed in Sec. 8.2. For example, consider the two-element case. Then (8-22) becomes

$$f(\psi) = \frac{\sin\psi}{2\sin(\psi/2)} \tag{8-24}$$

This is a universal pattern function for all equal amplitude two-element arrays and is plotted in Fig 8-7*a*. Note that by the techniques used in Sec. 8.2, we found that the array factor for a two-element array was $\cos(\psi/2)$; see (8-9). It can be shown that this is identical to (8-24).

EXAMPLE 8-2 ***Four-Element Linear Array (see Fig. 8-9)***

The universal array factor for a four-element, uniformly excited, equally spaced array is plotted in Fig. 8-9*b*. Let us find the array factor plot for the special case of half-wavelength spacing and 90° interelement phasing (i.e., $\alpha = \pi/2$). The array excitations are shown in

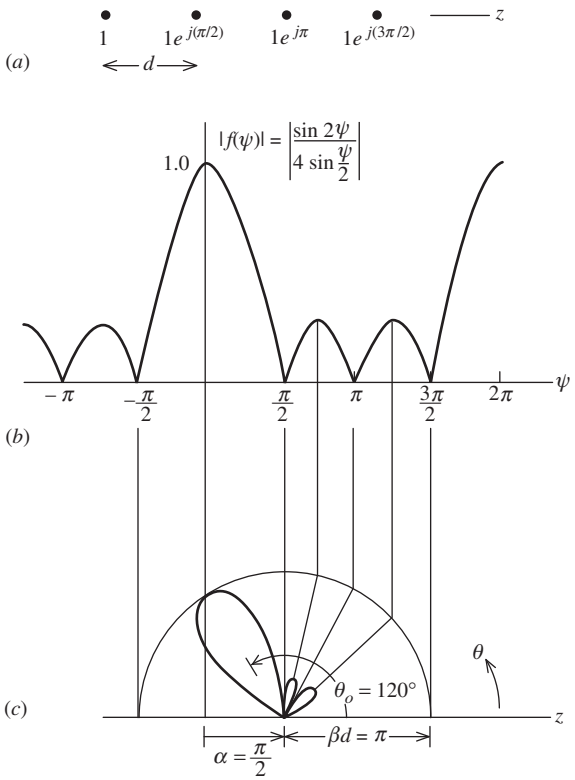

Figure 8-9 Array factor for a four-element, uniformly excited, equally spaced phased array (Example 8-2). (*a*) The array excitations. (*b*) Universal pattern for $N = 4$. (*c*) Polar plot for $d = \lambda/2$ and $\alpha = \pi/2$.

Fig. 8-9*a*. The pattern plot can be sketched quickly by locating prominent features such as maxima and zeros. Then vertical lines are dropped down from these points to the circle below. From the intersection points with the circle, straight lines are drawn in to the center of the circle. The perimeter of the circle has a pattern value of unity and the center a value of 0. For linear polar plots such as this one, the magnitude of the pattern factor is linearly proportional to the distance from the origin. For example, if the circle radius is 4 cm and the pattern value to be plotted is 0.25, the pattern point is 1 cm from the origin along a radial line at the appropriate angle θ. After locating the relative maxima and the zeros, a smooth curve is drawn, joining these points. The polar plot calculated using (8-22) is shown in Fig. 8-9*c*. Note that a polar plot can be made larger or smaller by expanding or contracting the construction circle.

8.3.2 Main Beam Scanning and Beamwidth

A maximum of an array factor occurs for $\psi = 0$. Let θ_o be the corresponding value of θ for which the array factor is maximum. Then from (8-6), we have $0 = \beta d \cos\theta_0 + \alpha$, or

$$\alpha = -\beta d \cos\theta_o \tag{8-25}$$

This is the element-to-element phase shift in the excitation currents required to produce an array factor main beam maximum in a direction θ_o relative to the line along which the array elements are disposed. Thus, if we want an array factor maximum in the $\theta = \theta_o$ direction, the required element currents from (8-4) with (8-25) are

$$I_n = e^{jn\alpha} = e^{-jn\beta d\,\cos\theta_o} \tag{8-26}$$

for a uniformly excited, equally spaced linear array. For the broadside case ($\theta_o = 90^\circ$), $\alpha = 0$. For the endfire case ($\theta_o = 0^\circ$ or 180°), $\alpha = -\beta d$ or βd. In the example illustrated in Fig. 8-9, $\alpha = \pi/2$ and $d = \lambda/2$ so $\theta_o = \cos^{-1}(-\alpha/\beta d) = \cos^{-1}\left(-\frac{1}{2}\right) = 120^\circ$.

A helpful way to remember the influence of the phase is that the beam pointing direction is toward the lagging element. In the example, each element lags its right neighbor, so the beam steers to the left of the array broadside direction as shown in Fig. 8-9*c*. This main beam scanning by phase control feature can be explicitly incorporated into ψ by substituting (8-25) into (8-6), giving

$$\psi = \beta d(\cos\theta - \cos\theta_o) \tag{8-27}$$

Scanning is discussed further in Sec. 8.9.

A measure of the width of the main beam of a uniformly excited, equally spaced linear array is given by the *beamwidth between first nulls*, BWFN, which is illustrated in Fig. 2-10*a* for a general pattern. The main beam nulls are where the array factor (8-22) first goes to zero in a plane containing the linear array. The zeros of the numerator of (8-22) occur for $N\psi_{\text{FN}}/2 = \pm n\pi$. When the denominator also goes to zero ($\frac{1}{2}\psi_{\text{FN}} = \pm n\pi$), the pattern factor is unity, corresponding to the main beam ($n = 0$) and grating lobes. The first nulls associated with the main beam occur for $N\psi_{\text{FN}}/2 = \pm\pi$. For a broadside array $\alpha = 0^\circ$ and $\psi = \beta d \cos\theta$, so the angles θ for the first nulls are found from

$$\pm\pi = \frac{N}{2}\frac{2\pi}{\lambda} d \cos\theta_{\text{FN}} \tag{8-28}$$

or

$$\theta_{\text{FN}} = \cos^{-1}\left(\pm\frac{\lambda}{Nd}\right) \tag{8-29}$$

The BWFN is then

$$\text{BWFN} = |\theta_{\text{FN left}} - \theta_{\text{FN right}}| \tag{8-30}$$

$$= \left|\cos^{-1}\left(-\frac{\lambda}{Nd}\right) - \cos^{-1}\left(+\frac{\lambda}{Nd}\right)\right| \tag{8-31}$$

For long arrays (length $L = Nd \gg \lambda$), we can approximate (8-31) as follows:

$$\text{BWFN} \approx \left|\frac{\pi}{2} + \frac{\lambda}{Nd} - \left(\frac{\pi}{2} - \frac{\lambda}{Nd}\right)\right| = \frac{2\lambda}{Nd} \qquad \textit{near broadside} \tag{8-32}$$

For an endfire array (see Fig. 2-11*c*), the beamwidth between first nulls is twice that from the main beam maximum to the first null. For long arrays it is approximately

$$\text{BWFN} \approx 2\sqrt{\frac{2\lambda}{Nd}} \qquad \textit{endfire} \tag{8-33}$$

Half-power beamwidth (HP) is a more popular measure of the main beam size than BWFN. Both depend on the array length Nd and main beam pointing angle θ_o. For a long $(Nd \gg \lambda)$ uniformly excited linear array, the HP is approximately [1]

$$\text{HP} \approx 0.886\frac{\lambda}{Nd}\ \csc\theta_o \quad \textit{near broadside} \tag{8-34}$$

and

$$\text{HP} \approx 2\sqrt{0.886\frac{\lambda}{Nd}} \qquad \textit{endfire} \tag{8-35}$$

Comparing the formulas for HP and BWFN, we can see that HP is roughly one-half of the corresponding BWFN value for long, uniformly excited linear arrays.

8.3.3 The Ordinary Endfire Array

In many applications, antennas are required to produce a single pencil beam. The array factor for a broadside array produces a fan beam (such as in Fig. 8-3), although the proper selection of array elements may yield a total pattern that has a single pencil beam. Another way to achieve a single pencil beam is by the proper design of an endfire array. We have said that an endfire condition results when $\theta_o = 0°$ or 180°, which corresponds to $\alpha = -\beta d$ or $+\beta d$. Such arrays for which $\alpha = \pm\beta d$ are referred to as *ordinary endfire* arrays. If the spacing d is a half-wavelength, there will be two identical endfire lobes (see Fig. 3-17). There are several ways to eliminate one of these lobes, thus leaving a single pencil beam. Already mentioned was the use of a backing ground plane in Example 3-5. For an array, the back lobe can be reduced by decreasing the spacing below a half-wavelength. The visible region is $2\beta d$ wide in the variable ψ, and to eliminate the unwanted major lobe (grating lobe), we should reduce the visible region (and thus the spacing d) below the half-wavelength spacing value of 2π. Since the grating lobe half-width (maximum to null) is $2\pi/N$, so that $2\beta d \leq 2\pi - \pi/N$. Dividing this by $2\beta d$ gives the condition on spacing, which is given below along with the associated condition on phasing for ordinary endfire operation:

$$d < \frac{\lambda}{2}\left(1 - \frac{1}{2N}\right) \tag{8-36a}$$

Ordinary endfire conditions

$$\alpha = \pm\beta d \tag{8-36b}$$

An array satisfying these conditions produces a single endfire beam and no grating lobe with a peak in the direction $\theta = 0^\circ$ for $\alpha = -\beta d$ and in the direction $\theta = 180^\circ$ for $\alpha = \beta d$, which follows from (8-25). The example below, like many to follow in this chapter, uses five elements because there are enough lobes to fully illustrate general pattern trends.

EXAMPLE 8-3 *Five-Element Ordinary Endfire Linear Array (see Fig. 8-10)*

From (8-36*a*) for a five-element ordinary endfire array, we must have $d \leq (\lambda/2)(1 - 1/10) = 0.45\lambda$. If we select $d = 0.45\lambda$ and the $\theta_o = 180^\circ$ endfire direction, the required element-to-element phase shift from (8-36*b*) is $\alpha = \beta d = (2\pi/\lambda)(0.45\lambda) = 0.9\pi$. The pattern construction

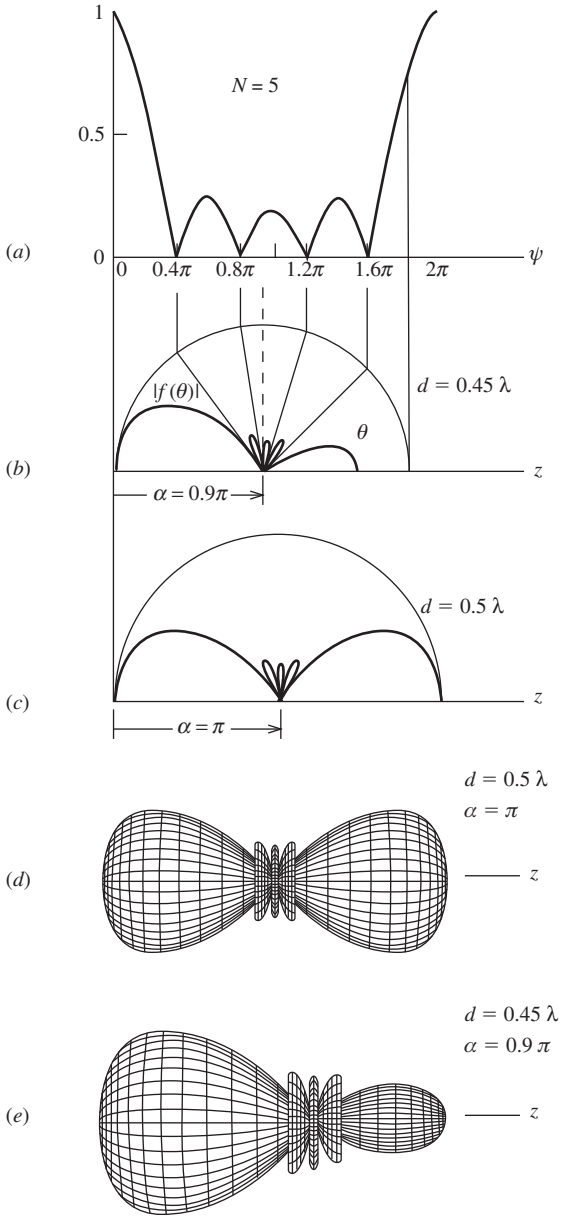

Figure 8-10 Five-element uniformly excited, equally spaced linear array (Example 8-3). (*a*) Universal pattern plot. (*b*) Polar plot for ordinary endfire case with $d = 0.45\lambda$ and $\alpha = 0.9\pi$. (*c*) and (*d*) Plots for endfire case with $d = 0.5\lambda$. (*e*) 3D plot for case of (*c*).

process is shown in Figs. 8-10*a* and *b*, and the three-dimensional pattern plot is shown in Fig. 8-10*e*. Note there is a single main lobe. For comparison, if a spacing of a half-wavelength had been used, two major lobes would appear as shown in Figs. 8-10*c* and *d*.

8.3.4 The Hansen-Woodyard Endfire Array

In the ordinary endfire case, the interelement excitation phase, $\alpha = \pm\beta d$, exactly equals the spatial phase delay of waves in the endfire direction. If the phase delay is increased beyond that for ordinary endfire by an amount δ, the *excess phase delay*, the interelement phase shift is

$$\alpha = \pm(\beta d + \delta) \tag{8-37}$$

with the $+$ and $-$ signs corresponding to beam peak directions of $\theta_o = 180^\circ$ and 0°, respectively. This excitation moves the maximum of the universal array factor out of the visible region ($0^\circ \leq \theta \leq 180^\circ$) as shown by example in Fig. 8-11, leading to a narrowing of the main beam. A popular choice for the excess phase delay is $\delta = \pi/N$. Because the phase delay is increased, the construction circle moves off the origin, which can lead to the appearance of grating lobes or high side lobes. To avoid this, the circle radius is decreased more than in the ordinary endfire case, corresponding to an element spacing d that is smaller than a half-wavelength by twice that used in the ordinary endfire case. These conditions on spacing and phasing are referred to as the *Hansen-Woodyard endfire conditions* for endfire operation and are given by:

$$d < \frac{\lambda}{2}\left(1 - \frac{1}{N}\right) \tag{8-38a}$$

Hansen-Woodyard endfire conditions

$$\alpha = \pm\left(\beta d + \frac{\pi}{N}\right) \tag{8-38b}$$

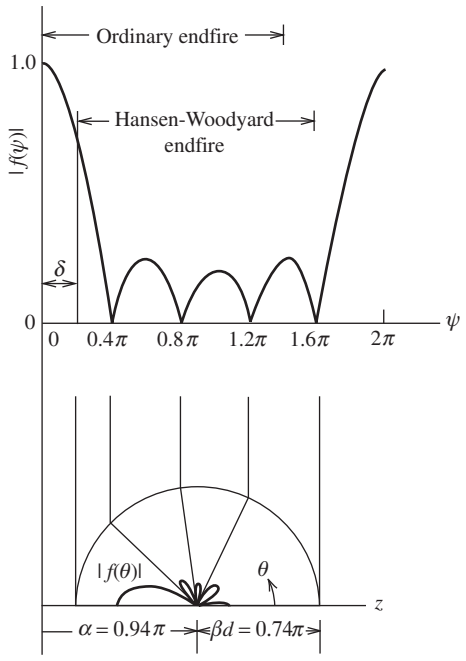

Figure 8-11 Single endfire beam for a five-element Hansen–Woodyard increased directivity array with $\alpha = 0.94\pi$ and $d = 0.37\lambda$ (Example 8-4).

where again the + and − signs are used with main beam peak directions of $\theta_o = 180^\circ$ and 0°, respectively. The original derivation by Hansen and Woodyard [2] assumed a continuous current distribution, but the result holds for an array of many closely spaced elements. The value that yields maximum directivity is $\delta_{\max} = 2.92/N$, which is close to the Hansen-Woodyard value of π/N used in (8-39*b*). Array directivity is discussed further in Sec. 8.5.

The pattern of an endfire array with a non-zero δ value has the pattern shape of (8-22) but is not normalized to unity maximum due to the peak of the universal array factor being invisible. Using (8-37) in (8-6) gives the modified expression for ψ of $\beta d(\cos\theta - 1) - \delta$. Solving this for the pattern maximum at $\theta_o = 0^\circ$ or 180° gives $\psi_o = -\delta$ or δ, and the pattern from (8-22) is $\sin(N\delta/2)/N\sin(\delta/2)$. Using this to renormalize the general array factor to include non-zero δ gives

$$f(\psi) = \frac{N\sin\left(\dfrac{\delta}{2}\right)\sin\left(\dfrac{N\psi}{2}\right)}{\sin\left(\dfrac{N\delta}{2}\right)N\sin\left(\dfrac{\psi}{2}\right)} \tag{8-39}$$

The consequence of increased directivity for Hansen-Woodyard type arrays is higher side lobes, as illustrated in the following example.

EXAMPLE 8-4 ***Five-Element Hansen-Woodyard Endfire Linear Array (see Fig. 8-11)***

From (8-38*a*) for a five-element Hansen-Woodyard endfire array, we must have $d \leq (\lambda/2)(1 - 1/5) = 0.4\lambda$. Choosing $d = 0.37\lambda$ and the $\theta_o = 180^\circ$ endfire direction, the required element-to-element phase shift from (8-38*b*) is $\alpha = \beta d + \pi/N = 0.74\pi + 0.2\pi = 0.94\pi$.The pattern shown in Fig. 8-11 has a single main beam that is narrower than for the ordinary endfire case in Example 8-3 (also using five elements), but the side lobes are higher. Nevertheless, the array exhibits increased directivity, as we will examine in more detail in Sec. 8.5.

It is helpful to summarize the endfire array design process. First, select the number of elements, using enough to achieve the required directivity. Next, choose an element spacing that is less than a half-wavelength; for example, satisfying (8-36*a*) or (8-38*a*) for ordinary or Handsen-Woodyard endfire cases. Finally, evaluate the interelement phase shift α using (8-36*b*) or (8-38*b*) for ordinary or Handsen-Woodyard endfire cases.

8.4 THE COMPLETE ARRAY PATTERN AND PATTERN MULTIPLICATION

Our treatment of arrays so far has assumed that all elements in the array are isotropic point sources. Actual arrays, of course, employ real elements that do not have an isotropic pattern. In the remainder of this chapter, we include element effects, starting in this section with the principle of pattern multiplication which gives the complete array pattern as the product of the element pattern and the array factor.

When the elements of an array are placed along a line and the currents in each element also flow in the direction of that line, the array is said to be *collinear*. As a simple example of a collinear array, suppose we have N short dipoles as shown in Fig. 8-12. The elements are equally spaced a distance d apart and have currents $I_0, I_1, I_2, \ldots, I_{N-1}$. The total current is the sum of the z-directed short dipole currents and thus is z-directed,

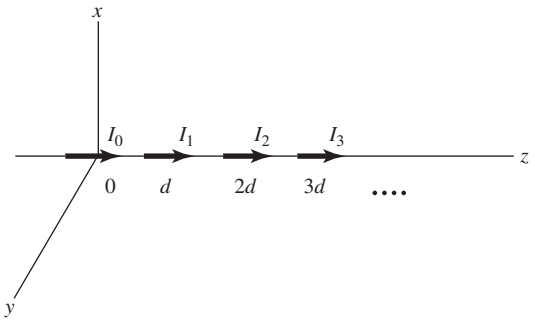

Figure 8-12 A collinear array of short dipoles.

as is the vector potential. The vector potential integral in (2-103) reduces to a sum over the element currents (modeled as ideal dipoles) as[1]

$$\begin{aligned} A_z &= \mu \frac{e^{-j\beta r}}{4\pi r} \Delta z \left[I_0 + I_1 e^{j\beta d \cos\theta} + I_2 e^{j\beta 2d \cos\theta} + \cdots + I_{N-1} e^{j\beta(N-1)d \cos\theta} \right] \\ &= \mu \frac{e^{-j\beta r}}{4\pi r} \Delta z \sum_{n=0}^{N-1} I_n e^{j\beta nd \cos\theta} \end{aligned} \tag{8-40}$$

in the far field. Then from (2-106),

$$E_\theta = j\omega\mu \frac{e^{-j\beta r}}{4\pi r} \Delta z \sin\theta \sum_{n=0}^{N-1} I_n e^{j\beta nd \cos\theta} \tag{8-41}$$

From this expression, we can identify $\sin\theta$ as the pattern of a single element by itself, called the *element pattern*. The remaining factor

$$\text{AF} = \sum_{n=0}^{N-1} I_n e^{j\beta nd \cos\theta} \tag{8-42}$$

is the array factor of (8-3). The array factor is a sum of fields from isotropic point sources located at the center of each array element and is found from the element currents (amplitudes and phases) and their locations. On the other hand, the element pattern is that factor of the radiation pattern determined by the individual properties of an element based on its current distribution and orientation in space. We shall see that this factoring process holds in general if the elements have the same pattern and are similarly oriented.

We now consider a slightly more complicated case. Suppose for the sake of explanation, we have N identical general, line-source elements forming a collinear array along

---

[1] This result could also be obtained by writing the z-directed current density as

$$J_z = \delta(x')\ \delta(y')[I_0\ \delta(z') + I_1\ \delta(z' - d) + I_2\ \delta(z' - 2d) + \cdots I_{N-1}\ \delta(z' - (N-1)\ d)]\ \Delta z$$

and substituting this into (2-102), giving

$$A_z = \mu \frac{e^{-j\beta r}}{4\pi r} \Delta z \int_{-\infty}^{\infty} [I_0\ \delta(z') + I_1\ \delta(z' - d) + \cdots] e^{j\beta z' \cos\theta} dz'$$

from which (8-40) follows.

the z-axis. The nth element is centered at $z = z_n$ and has a current distribution $i_n(z')$. We are now relaxing the equal spacing constraint. The total current along the z-axis is

$$I(z') = \sum_{n=0}^{N-1} i_n(z') \tag{8-43}$$

The vector potential is then

$$A_z = \mu \frac{e^{-j\beta r}}{4\pi r} \int_{-\infty}^{\infty} \sum_{n=0}^{N-1} i_n(z') e^{j\beta z' \cos\theta} dz' \tag{8-44}$$

The far-field electric field from this and (2-106) is

$$E_\theta = j\omega\mu \frac{e^{-j\beta r}}{4\pi r} \sum_{n=0}^{N-1} E_n(\theta) \tag{8-45}$$

where

$$E_n(\theta) = \sin\theta \int_{-\infty}^{\infty} i_n(z') e^{j\beta z' \cos\theta} dz' \tag{8-46}$$

is the pattern of the nth element.

If the array possesses no symmetry, (8-45) cannot be simplified. But if the array elements are similar, a great deal of simplification is possible. By *similar* we mean that the currents of each antenna element are in the same direction, of the same length, and have the same distribution (although there may be different current amplitudes and phases for each element). Then the patterns of (8-46) will be similar; that is, they will have the same spatial variation but may have different amplitudes and phases. In the example at hand, the currents are all z-directed. Now assume that each element is of length ℓ, has a normalized current distribution over its length of $i(z')$, and an input current of I_n. Then

$$i_n(z') = \mathrm{I}_n i(z' - z_n) \tag{8-47}$$

where z_n is the position of the nth element center along the z-axis. Substituting this into (8-46) gives

$$E_n(\theta) = \sin\theta \; I_n \int_{z_n - \ell/2}^{z_n + \ell/2} i(\xi - z_n) e^{j\beta\xi \cos\theta} d\xi \tag{8-48}$$

where ξ replaced z'. Let $\tau = \xi - z_n$; then (8-48) becomes

$$\begin{aligned} E_n(\theta) &= \sin\theta \; I_n \int_{-\ell/2}^{\ell/2} i(\tau) e^{j\beta(\tau + z_n)\cos\theta} d\tau \\ &= \sin\theta \left[\int_{-\ell/2}^{\ell/2} i(\tau) e^{j\beta\tau \cos\theta} d\tau \right] I_n e^{j\beta z_n \cos\theta} \end{aligned} \tag{8-49}$$

To maintain consistent notation, we replace τ by z', yielding

$$E_n(\theta) = \sin\theta \left[\int_{-\ell/2}^{\ell/2} i(z') e^{j\beta z' \cos\theta} dz' \right] I_n e^{j\beta z_n \cos\theta} \tag{8-50}$$

The pattern for each element of an array of similar elements given by (8-50) is a product of the pattern of the current distribution, and the amplitude and phase of excitation I_n, and the last factor represents the spatial phase due to the displacement from the origin. Substituting (8-50) into (8-45) gives

$$E_\theta = j\omega\mu \frac{e^{-j\beta r}}{4\pi r} \left[\sin\theta \int_{-\ell/2}^{\ell/2} i(z') e^{j\beta z' \cos\theta} \, dz' \right] \sum_{n=0}^{N-1} I_n e^{j\beta z_n \cos\theta} \tag{8-51}$$

The factor

$$\sin\theta \int_{-\ell/2}^{\ell/2} i(z') e^{j\beta z' \cos\theta} \, dz' \tag{8-52}$$

when normalized is the element pattern $g_a(\theta)$ of any element in the array of similar elements. The sum

$$\text{AF} = \sum_{n=0}^{N-1} I_n e^{j\beta z_n \cos\theta} \tag{8-53}$$

is the unnormalized array factor.

In going from (8-45) to (8-51), it was necessary to assume that the elements of the array were similar. When this is true, the electric field can be written as a product of an element pattern, as in (8-52), and an array factor, as in (8-53). Note that the array factor is the pattern of a linear array of N point sources located at positions $\{z_n\}$ on the z-axis. If the elements are equally spaced, $z_n = nd$ and (8-53) reduces to (8-42). If further, they are uniformly excited, the array reduces to (8-20). This result is not restricted to collinear elements but can be applied to any array of similar elements. This is discussed next.

The process of factoring the pattern of an array into an element pattern and an array factor is referred to as the *principle of pattern multiplication*. It is stated as follows: The electric field pattern of an array consisting of similar elements is the product of the pattern of one of the elements (the element pattern) and the pattern of an array of isotropic point sources with the same locations, relative amplitudes, and phases as the original array (the array factor).

In Sec. 2.4, we wrote the normalized electric field pattern of a single antenna as a product of a normalized element factor g and a normalized pattern factor f. For array antennas, we expand this concept and call the pattern of one element in the array an element pattern g_a. It, in turn, is composed of an element factor that is the pattern of an infinitesimal piece of current on the array element (i.e., an ideal dipole) and a pattern factor that is the pattern due to its current distribution as in (8-52). The complete (normalized) pattern of an array antenna is

$$F(\theta, \phi) = g_a(\theta, \phi) f(\theta, \phi) \tag{8-54}$$

where $g_a(\theta, \phi)$ is the normalized pattern of a single element antenna of the array (the *array element pattern*, or *element pattern*) and $f(\theta, \phi)$ is the familiar normalized array factor.

EXAMPLE 8-5 *Two Collinear, Half-Wavelength-Spaced Short Dipoles (see Fig. 8-13)*

To illustrate pattern multiplication, consider two collinear short dipoles spaced a half-wavelength apart and equally excited. The element pattern is $\sin\theta$ for an element along the z-axis and the array factor was found in (3-69) to be $\cos[(\pi/2)\cos\theta]$. The total pattern is then $\sin\theta \cos[(\pi/2)\cos\theta]$. The patterns are illustrated in Fig. 8-13. The 3D pattern, which has been

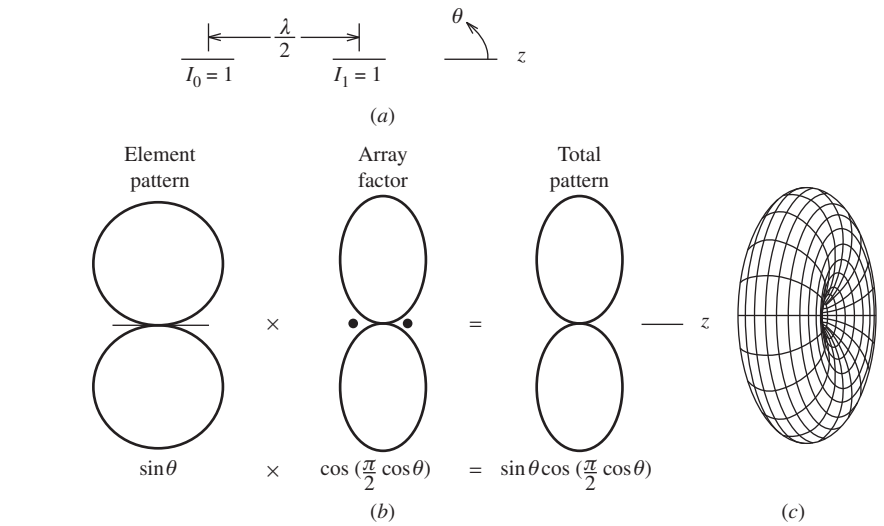

Figure 8-13 Array of two half-wavelength spaced, equal amplitude, equal phase, collinear short dipoles (Example 8-5). (*a*) The array. (*b*) The pattern. (*c*) The 3D pattern (rotated).

rotated slightly to see inside, illustrates the omnidirectional shape. The half-power beamwidth of the array factor is 60° and is 51° for the complete pattern. So, the complete pattern is essentially a slightly narrower version of the array factor.

Collinear arrays are in widespread use in base stations for land mobile communications. Half-wave dipoles spaced more than a half-wavelength apart are popular elements. The array axis is oriented vertically, producing an omnidirectional pattern in the horizontal plane as required for point-to-multipoint communications. Lengthening the array by adding elements narrows the beamwidth in the elevation plane, increasing the directivity and extending the usable range to a mobile unit. Base station antennas are treated further in Sec. 12.2.

Arrays that have parallel elements, as illustrated in Fig. 8-14, have more complicated pattern expressions because the axis of symmetry of the array (the z-axis) is no longer aligned with the axis of symmetry of the elements (the x-axis), as for a collinear array. So the pattern will be a function of both θ and ϕ rather than just θ. The element pattern for the line source element parallel to the x-axis is found from an expression analogous to (8-52):

$$\sin\gamma \int_{-\ell/2}^{\ell/2} i(x')e^{j\beta x'\cos\ \gamma}dx' \tag{8-55}$$

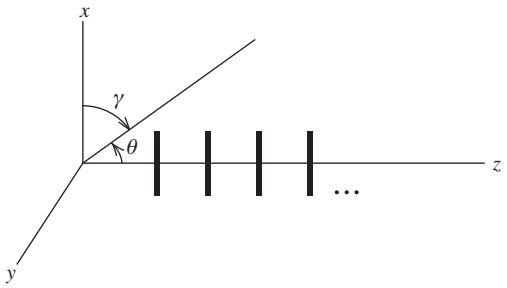

Figure 8-14 A linear array of parallel line sources.

where γ is the spherical polar angle from the x-axis with $0 \le \gamma \le 180°$. γ is expressed in terms of θ and ϕ through the relations [H.3: Kraus, 3rd ed., Ch. 16]:

$$\cos\gamma = \sin\theta\cos\phi \quad \text{and} \quad \sin\gamma = \sqrt{1 - \sin^2\theta\cos^2\phi} \tag{8-56}$$

The array factor of (8-53) also applies to this case of parallel elements because the elements are still along the z-axis.

EXAMPLE 8-6 *Two Parallel, Half-Wavelength Spaced Short Dipoles (see Fig. 8-15)*

The pattern of the short dipole elements parallel the x-axis is $\sin\gamma$ analogous to its $\sin\theta$ pattern when parallel to the z-axis. Using (8-56), the element pattern expressed in θ and ϕ is $\sin\gamma = \sqrt{1 - \sin^2\theta\cos^2\phi}$. The array factor is the same as for the previous example because the element locations are the same. The complete pattern is the product of the element pattern and array factor as shown in Figs. 8-15*b* and *c*. The fact that the axes of symmetry for the element and the array are orthogonal leads to different principal plane patterns and to the complicated 3D pattern of Fig. 8-15*d*, which has the axes tilted to show the broad null in the z-direction and the narrow null in the x-direction. While such a pattern has few applications, it is presented here to illustrate how an element pattern can have a major influence on the array pattern and for additional practice in visualizing array patterns.

EXAMPLE 8-7 *Five-Element Endfire Array of Parallel Half-Wave Dipoles*

To illustrate parallel element arrays further, suppose the element antennas of Fig. 8-14 are half-wave dipoles. Also suppose there are five elements arranged and excited for ordinary endfire as in Example 8-3. The complete pattern is the product of the single half-wave dipole element pattern and the array factor found from five isotropic sources. The element pattern for a half-wave dipole element along the x-axis is

$$g_a(\gamma) = \frac{\cos[(\pi/2)\cos\gamma]}{\sin\gamma} \tag{8-57}$$

which is (3-4) with θ replaced by γ. Using (8-56), this becomes

$$g_a(\theta, \phi) = \frac{\cos[(\pi/2)\sin\theta\cos\phi]}{\sqrt{1 - \sin^2\theta\cos^2\phi}} \tag{8-58}$$

The array factor is (8-22) with $N = 5$, or

$$f(\psi) = \frac{\sin\left(\frac{5}{2}\psi\right)}{5\sin\left(\frac{1}{2}\psi\right)} \tag{8-59}$$

For this example, $\alpha = 0.9\pi$ and $d = 0.45\lambda$ so $\psi = \beta d\cos\theta + \alpha = 0.9\pi\cos\theta + 0.9\pi$, and (8-59) is

$$f(\theta) = \frac{\sin(2.25\pi\cos\theta + 2.25\pi)}{5\sin(0.45\pi\cos\theta + 0.45\pi)} \tag{8-60}$$

The total pattern of the array in terms of θ and ϕ is then the product of (8-58) and (8-60):

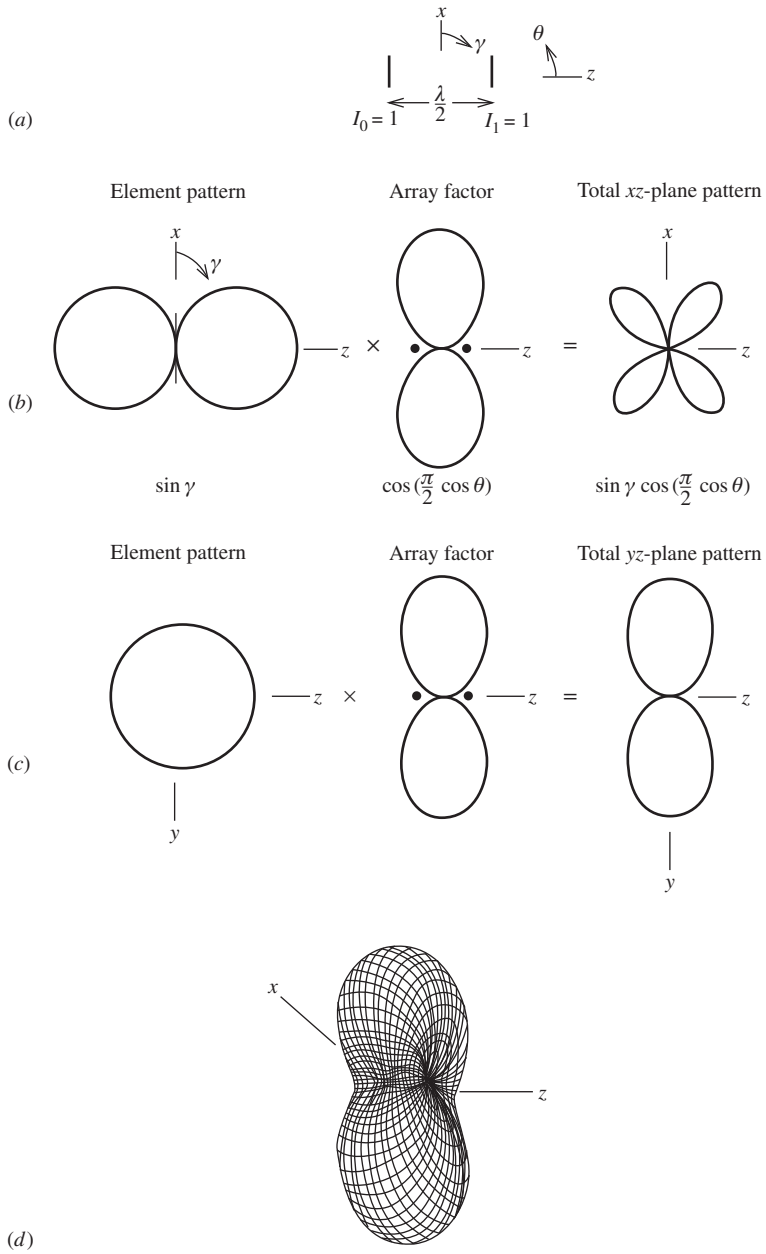

Figure 8-15 Array of two half-wavelength spaced, equal amplitude, equal phase parallel short dipoles (Example 8-6). (*a*) The array. (*b*) The *xz*-plane pattern. (*c*) The *yz*-plane pattern. (*d*) The three-dimensional pattern.

$$F(\theta,\phi) = \frac{\cos[(\pi/2)\sin\theta\cos\phi]}{\sqrt{1-\sin^2\theta\cos^2\phi}} \frac{\sin(2.25\pi\cos\theta + 2.25\pi)}{5\sin(0.45\pi\cos\theta + 0.45\pi)} \tag{8-61}$$

The polar plot of this pattern is easily obtained by multiplying the plot in Fig. 3-5*b*, where the axis of symmetry is now the *x*-axis instead of the *z*-axis, times the polar plot of Fig. 8-10*b*. This is a polar plot similar to the array factor plot except that the endfire lobes are slightly narrower, and there is a pattern zero in the $\gamma = 0^\circ$ direction caused by the element pattern.

8.5 DIRECTIVITY OF UNIFORMLY EXCITED, EQUALLY SPACED LINEAR ARRAYS

The directivity of an antenna is solely determined by its radiation pattern in all space surrounding the antenna. The techniques of the previous section for determining the pattern of an array have prepared us to develop, in this section, exact and approximate formulas for the directivity of uniformly excited, equally spaced linear arrays (UE, ESLA). As expected, array gain equals array directivity multiplied by the array radiation efficiency. To derive directivity expressions, we use $D = 4\pi/\Omega_A$, first finding the beam solid angle as

$$\Omega_A = \iint |F(\theta,\phi)|^2 d\Omega = \iint |g_a(\theta,\phi)|^2 |f(\theta)|^2 \, d\Omega \tag{8-62}$$

where $g_a(\theta,\phi)$ and $f(\theta)$ are the normalized element pattern and linear array factor and $d\Omega = \sin\theta \, d\theta \, d\phi$.

We begin by assuming the elements are equally spaced, uniformly excited, and isotropic. This assumption leads to approximate results for situations where the element pattern is much broader than the array factor and the main beams of both are aligned. The appropriate array factor from (8-22) is

$$|f|^2 = \left| \frac{\sin(N\psi/2)}{N\sin(\psi/2)} \right|^2 \tag{8-63}$$

$$= \frac{1}{N} + \frac{2}{N^2} \sum_{m=1}^{N-1} (N-m) \cos m\psi \tag{8-64}$$

where (8-64) is another form for (8-63). This identity can be shown to be true for $N = 2$ since from (8-64), $|f(\psi)|^2 = \frac{1}{2} + \frac{1}{2}\cos\psi = \cos^2(\psi/2)$ as in (8-9). With the simple expression in (8-64), it is easier to perform the integration in (8-62) in terms of the variable ψ. Using $g_a(\theta,\phi) = 1$, $\psi = \beta d \cos\theta + \alpha$, and $\sin\theta \, d\theta = -(1/\beta d) d\psi$ in (8-62) gives

$$\Omega_A = \int_0^{2\pi} d\phi \int_0^{\pi} |f(\theta)|^2 \sin\theta \; d\theta = 2\pi \int_{\beta d+\alpha}^{-\beta d+\alpha} |f(\psi)|^2 \left(-\frac{1}{\beta d} \right) d\psi$$

$$= \frac{2\pi}{\beta d} \int_{-\beta d+\alpha}^{\beta d+\alpha} |f(\psi)|^2 \, d\psi \tag{8-65}$$

Substituting (8-64) in the above yields

$$\Omega_A = \frac{2\pi}{\beta d} \left[\frac{1}{N} \int_{-\beta d+\alpha}^{\beta d+\alpha} d\psi + \frac{2}{N^2} \sum_{m=1}^{N-1} (N-m) \int_{-\beta d+\alpha}^{\beta d+a} \cos m\psi \; d\psi \right]$$

$$= \frac{2\pi}{\beta d} \left[\frac{1}{N} \psi \Big|_{-\beta d+\alpha}^{\beta d+\alpha} + \frac{2}{N^2} \sum_{m=1}^{N-1} (N-m) \frac{\sin m\psi}{m} \Big|_{-\beta d+\alpha}^{\beta d+\alpha} \right]$$

$$= \frac{2\pi}{\beta d} \left[\frac{1}{N} (2\beta d) + \frac{2}{N^2} \sum_{m=1}^{N-1} \frac{N-m}{m} [\sin m(\beta d+\alpha) - \sin m(-\beta d+\alpha)] \right]$$

$$= \frac{4\pi}{N} + \frac{4\pi}{N^2} \sum_{m=1}^{N-1} \frac{N-m}{m\beta d} 2\cos m\alpha \sin m\beta d \tag{8-66}$$

where (D-6) was used in the last step.

The directivity is now found from its basic definition of $D = 4\pi/\Omega_A$ with (8-66) as [H.8.2: Ma. p. 23].

$$D = \frac{\left|\dfrac{\sin(N\,\delta/2)}{N\sin(\delta/2)}\right|^2}{\dfrac{1}{N} + \dfrac{2}{N^2}\displaystyle\sum_{m=1}^{N-1}\frac{N-m}{m\beta d}\sin\, m\beta d\cos\, m\alpha} \qquad \textit{UE, ESLA of istropic elements} \tag{8-67}$$

The numerator of this expression is the pattern normalization factor from (8-39), which is required to normalize the pattern to unity peak in the visible region in cases where an additional phase of δ beyond that for ordinary endfire is used; see (8-37). The formula applies for any number of elements N, any spacing d, and any interelement phasing α, but is restricted to isotropic elements. Fig. 8-16 plots this formula for various numbers of elements as a function of element spacing for the broadside case with α and δ zero. Tai [1] presented a family of such plots. All of the directivity curves fall off steeply as the spacing approaches one wavelength. This effect is due to the emergence of grating lobes in the visible region. See Fig. 8-3 as an example where full grating lobes are visible for one-wavelength spacing. Eq. (8-67) reduces to a simple result for elements spaced a multiple of a half-wavelength apart:

$$D = N \qquad \textit{for isotropic elements and } d = n\frac{\lambda}{2} \tag{8-68}$$

These values can be located on the graph in Fig. 8-16 for the broadside case, but (8-68) applies for any scan angle.

It is obvious from Fig. 8-16 that maximum directivity is achieved with a broadside UE, ESLA for a spacing of just under a wavelength, with the peak directivity becoming closer to a wavelength for larger numbers of elements. Arrays are often designed to have an element spacing near a wavelength to keep the number of elements as low as possible to limit the cost and complexity of the antenna and associated feed network. A simple formula for the directivity of a broadside array of uniformly excited isotropic elements follows directly from the uniform line source case in (5-19):

$$D \approx 2\frac{L}{\lambda} = 2\frac{Nd}{\lambda} \qquad \textit{broadside, UELA} \tag{8-69}$$

where we used the array length of $L = Nd$. This straight line approximation, shown in Fig. 8-16 for the case of 10 elements, is an excellent fit to the exact result up to almost

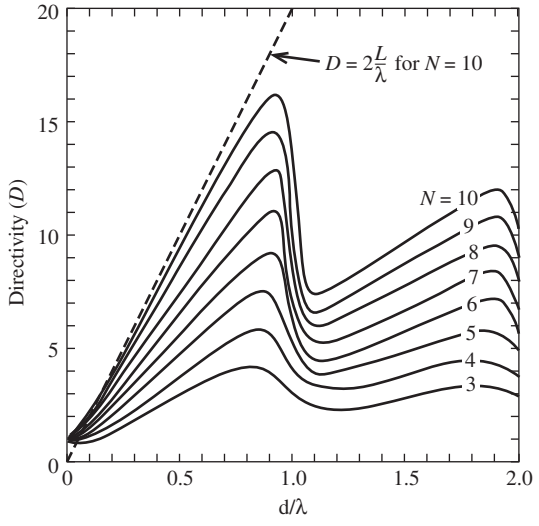

Figure 8-16 Directivity as a function of element spacing for a broadside array of isotropic elements for several element numbers N computed using (8-67).

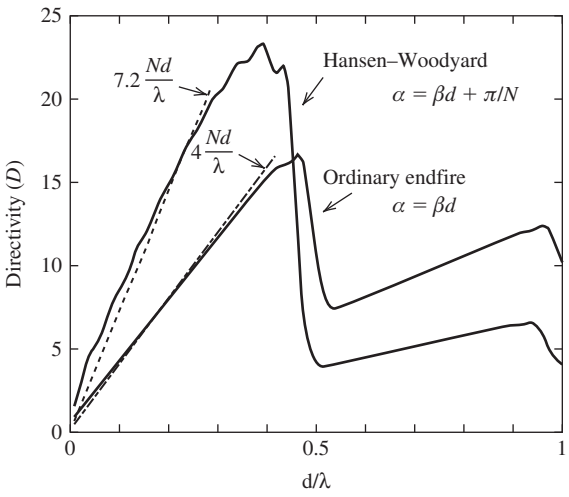

Figure 8-17 Comparison of directivities for two 10-element equally spaced, uniformly excited endfire arrays: ordinary endfire (dotted curve) and Hansen–Woodyard endfire (solid curve) calculated using (8-67). Also shown are straight line approximations using (8-70) and (8-71).

one-wavelength spacing. Note that (8-69) is exact for $d = \lambda/2$ because it equals N, as it should be based on (8-68).

The directivity of endfire arrays has trends similar to broadside arrays as illustrated by the graph in Fig. 8-17 which shows directivity versus element spacing for the case of 10 isotropic elements. Plotted are curves for both ordinary endfire and Hansen-Woodyard cases with phases given by (8-36*b*) and (8-38*b*), respectively. The results, again computed using (8-67), show that directivity increases with increasing element spacing until $d = \lambda/2$ is approached when a grating lobe begins to appear in the endfire direction opposite the main beam. Line-source theory results in (5-20) lead to the approximation

$$D \approx 4\frac{L}{\lambda} = 4\frac{Nd}{\lambda} \qquad \textit{ordinary endfire, UELA} \tag{8-70}$$

This straight-line approximation shown in Fig. 8-17 for 10 elements is an excellent fit.

There also is a straight-line approximate formula for the Hansen-Woodyard endfire case:

$$D \approx 7.2\frac{L}{\lambda} = 7.2\frac{Nd}{\lambda} \qquad \textit{Hansen-Woodyard endfire, UELA} \tag{8-71}$$

Constant values other than 7.2 can be found in the literature. But because the Hansen-Woodyard directivity curve does not follow a straight line as closely as does the ordinary endfire directivity curve, any linear fit would not be as accurate as the ordinary endfire straight line approximation in (8-70), which is within a few percent of the exact result. It is obvious from the Fig. 8-17 that more directivity is achieved with the Hansen-Woodyard array than with an ordinary endfire array of the same number of elements. In fact, the increase based on the ratio of (8-71) to (8-70) is $7.2/4 = 1.82 = 2.6$ dB. As an example, consider five-element endfire arrays similar to those in Examples 8-3 and 8-4. Exact directivity values for the ordinary and Hansen-Woodyard endfire cases from (8-67) are 5.88 and 9.41, respectively, while approximations (8-70) and (8-71) give 6.0 and 10.8.

The higher directivity associated with the Hansen-Woodyard array is due to the increased progressive phase (i.e., $\delta > 0$), which causes the peak of the main beam peak to move into the invisible region and narrows the visible main beam, reducing the beam solid angle and increasing directivity. It should be noted that the Hansen-Woodyard endfire array provides the highest directivity in most cases but not all. For spacings of isotropic elements much below a half-wavelength, the directivity can be increased somewhat by increasing the phase shift per element over that called for with Hansen-Woodyard operation. [2]

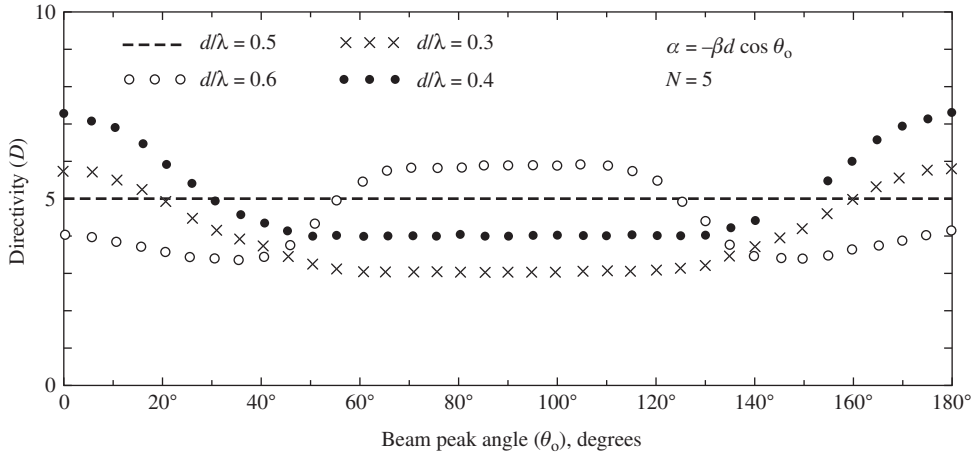

Figure 8-18 Variation of directivity with scan angle for five-element uniformly excited arrays of various element spacings. The elements are isotropic. Values were calculated using (8-67).

If the uniform excitation constraint is relaxed, it turns out that only a slight increase in directivity is possible, unless spacing is under a half-wavelength is permitted. [1] Non-uniformly excited arrays are discussed more fully in the next section.

Broadside and endfire represent the extreme beam scan directions. Fig. 8-18 plots directivity values at all scan angles for a uniform amplitude, five-element linear array of isotropic elements for various spacings. The $d = 0.5\,\lambda$ curve is a straight line equal to 5, which comes from (8-68), and demonstrates that directivity is independent of scan angle for $d = n\lambda/2$. The beamwidths calculated using (8-34) and (8-35) for broadside and endfire are 20.3° and 68.2°, respectively. While the beamwidth is much narrower for the broadside case, the pattern is an omnidirectional doughnut pattern in three dimensions (see Fig. 3-16 for a similar pattern). At endfire, there are two opposing broad, unidirectional beams as shown in Fig. 8-10*d*. It turns out that the beam solid angles, Ω_A, for the two vastly different patterns are the same, giving the same directivity. For the four cases shown in Fig. 8-18, the largest directivity in the broadside direction of $\theta_o = 90°$ is for the widest spacing of $d = 0.6\,\lambda$. As seen from Fig. 8-16, directivity continues to rise for spacings up to almost $d = 0.9\,\lambda$ in the $N = 5$ case. Fig. 8-18 shows that directivity remains constant over a wide range of scan angles around broadside; this will be explained in Sec. 8.9. The greatest directivity in the endfire scan cases ($\theta_o = 0°, 180°$) occurs for the largest spacing that satisfies the single main beam criterion of (8-36*a*), which is $d \leq 0.45\,\lambda$ as noted in Example 8-3. For the four cases considered, the largest spacing satisfying this single endfire beam condition is 0.4λ and, thus, has the greatest directivity at endfire as can be noted from Fig. 8-18.

There are only a few expressions available similar to (8-67) for the directivity of arrays with real elements (i.e., not isotropic) and directivity is usually found by integration using (2-142) in (2-144). The often-used formula that holds for uniformly excited linear arrays with elements that can be isotropic, collinear short dipoles, or parallel short dipoles is

$$D = \frac{\left|\dfrac{\sin(N\,\delta/2}{N\sin(\delta/2)}\right|^2}{\dfrac{a_0}{N} + \dfrac{2}{N^2}\displaystyle\sum_{m=1}^{N-1}\frac{N-m}{m\beta d}\,(a_1 \sin m\beta d + a_2 \cos m\beta d)\cos m\alpha} \tag{8-72}$$

where a_0, a_1, and a_2 are given in Table 8-1 for the element types. [3, 4] This formula reduces to (8-67) for isotropic elements. Directivity-versus-spacing plots based on this

Table 8-1 Parameters for Use in Computing the Directivity of Uniform Current Amplitude, Equally Spaced Linear Arrays; see (8-67)

Element Type	$\lvert g_a(\theta,\phi)\rvert^2$	a_0	a_1	a_2
Isotropic	1	1	1	0
Collinear short dipoles (Fig. 8-12)	$\sin^2\theta$	$\frac{2}{3}$	$\frac{2}{(m\beta d)^2}$	$\frac{-2}{m\beta d}$
Parallel short dipoles (Fig. 8-14)	$1-\sin^2\theta\cos^2\phi \quad =\sin^2\gamma$	$\frac{2}{3}$	$1-\frac{1}{(m\beta d)^2}$	$\frac{1}{m\beta d}$

formula are similar to Fig. 8-16 but the directivity values will, of course, be somewhat larger; see [1] for such plots. As an example, (8-72) yields $D = 12.2$ for an array of 10 collinear short dipoles spaced $0.6\,\lambda$ apart, whereas the same array but with isotropic elements has $D = 11.9$ from (8-67) or Fig. 8-16. In general, the directivity of long arrays $(L \gg \lambda)$ is primarily controlled by the array factor if the element pattern has low directivity and its major lobe is aligned with that of the array factor. In such cases, formulas based on isotropic elements like (8-69) to (8-71) can be used. Returning to the 10-element array of collinear short dipoles spaced $0.6\,\lambda$ apart, (8-69) gives $D = 12$, which is close to the exact value of $D = 12.2$.

The optimum (i.e., maximum directivity) array in most cases has uniform element amplitudes and linear phase shifts. For spacings under $\lambda/2$, the Hansen-Woodyard endfire array is close to optimum. Above $\lambda/2$ spacings, uniform amplitude, in-phase excitations are close to maximum with the spacing for peak directivity just under a wavelength and closer to a wavelength for larger numbers of elements. More is said on this topic in the next section.

There are several ways to estimate directivity for the purpose of quick approximate calculation. An approximate directivity formula for a UE, ESLA based on half-power beamwidth can be derived by substituting (5-19) into (5-12), giving

$$D \approx \frac{1.77}{\mathrm{HP}}\,\mathrm{rad} = \frac{101.5^\circ}{\mathrm{HP}_{\mathrm{deg}}} \tag{8-73}$$

For example, an ES, UELA of 10, half-wave spaced isotropic elements has $\mathrm{HP}_{\mathrm{deg}} = 20.3^\circ$ and (8-73) gives $D = 5$, which happens to be exactly correct from (8-68). For the example of 10 collinear short dipoles spaced 0.6λ apart, the beamwidth is 8.44° and then (8-73) gives 12.0 which is close to the correct value of 12.2. The formula also can be used with any omnidirectional antenna, but the following formula is more appropriate [5]:

$$D \approx \frac{101.5^\circ}{\mathrm{HP}_{\mathrm{deg}} - 0.0027\,\mathrm{HP}_{\mathrm{deg}}^2} \tag{8-74}$$

For example, a half-wave dipole which has a beamwidth of 78°, so (8-74) yields 1.65, which is close to the correct value of 1.64. The example of 10 collinear short dipoles spaced 0.6λ apart with a beamwidth of 8.44° has $D = 12.3$ from (8-74), and the correct value is 12.2.

The following simple formula can be found in the literature:

$$D \approx D_e D_i \tag{8-75}$$

where $D =$ directivity of the array, $D_e =$ directivity of one element in the array, and $D_i =$ directivity of the array with isotropic elements (i.e., directivity of the array factor). Application of this approximation is primarily to broadside, single main beam pattern

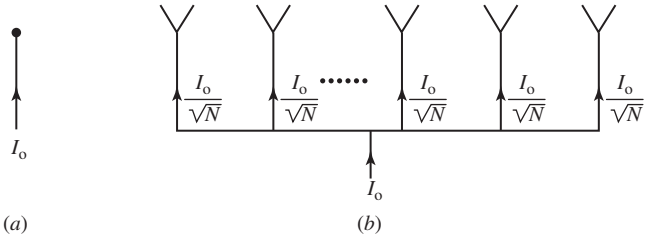

Figure 8-19 Array directivity is the ratio of the maximum radiation intensity of the array compared to that for an isotropic element with the same input power. (*a*) Reference isotropic antenna. (*b*) Array with the same total input power divided equally among the elements.

antennas (that is, grating lobes would not be accounted for). This formula is often presented without restriction, but, in fact, it must be used with caution, especially for linear antennas. [6] An alternate form of this formula that also can be found in the literature is $D \approx D_e N$. This form assumes the directivity of the array of isotropic elements equals the number of elements, $D_i = N$, which is only true for spacings equal to multiples of a half-wavelength (and for uniform current amplitudes), thus ignoring the effect spacing has on pattern and directivity. As an example, (8-75) applied to 10 collinear short dipoles spaced a half wavelength apart gives $D = D_e N = 1.5 \cdot 10 = 15$, which is way above the correct answer of 10.3. The directivity by (8-75) for 10 collinear half-wave dipoles spaced 0.75λ apart is $D = D_e D_i = 1.64 \cdot 14.5 = 23.8$, which again is much higher than the correct result obtained by integration of $D = 15.2$. On the other hand, (8-73) and (8-74) applied to this array, which has a pattern with $HP = 6.8^\circ$, give good results with directivity values of 14.9 and $D = 15.2$, respectively.

It is important to note that array directivity represents the increase in the radiation intensity in the direction of maximum radiation over that of a single element. Consider a single isotropic element and an array of N equally excited isotopic elements as shown in Fig. 8-19. The input power to the array is assumed to divide equally among the array elements, so the element powers are $1/N$ of the input power and the element currents are $1/\sqrt{N}$ of the input current. The radiation intensity U_o for the isotropic element is proportional to its input power, which in turn is proportional to the input current squared I_o^2. The maximum radiation intensity $U_{\max}$ of the array in Fig. 8-19*b* is a factor of D greater than that for a single isotropic element with the same input power.

8.6 NONUNIFORMLY EXCITED, EQUALLY SPACED LINEAR ARRAYS

We have seen that the main beam of an endfire array can be narrowed by changing the phase from that which is required for the ordinary endfire case. We can also shape the beam and control the level of the side lobes by adjusting the current amplitudes in an array. General synthesis procedures for achieving a specified pattern are presented in Chap. 10. In this section, a few simple techniques for controlling side lobe levels and beamwidth are introduced. Several examples are given that reveal the relationship between the array current distribution and the radiation pattern. The directivity for arrays with nonuniform excitation are also examined.

The array factor of (8-7) can be written as a polynomial in terms of $Z = e^{j\psi}$ as follows:

$$\text{AF} = \sum_{n=0}^{N-1} A_n e^{jn\psi} = \sum_{n=0}^{N-1} A_n Z^n \tag{8-76}$$

where the current amplitudes A_n are real and can be different for each n. It is a simple matter to investigate element current distributions using a computer to perform the array

factor summation. We present the results of several such calculations. The influence of the element current amplitudes will become apparent because we use the same five-element, broadside linear array with a half-wavelength element spacing throughout this section.

The pattern of a uniform array with all current amplitudes equal is plotted in linear, polar form in Fig. 8-20*a*, and the element currents are shown in Fig. 8-21*a*. If the element

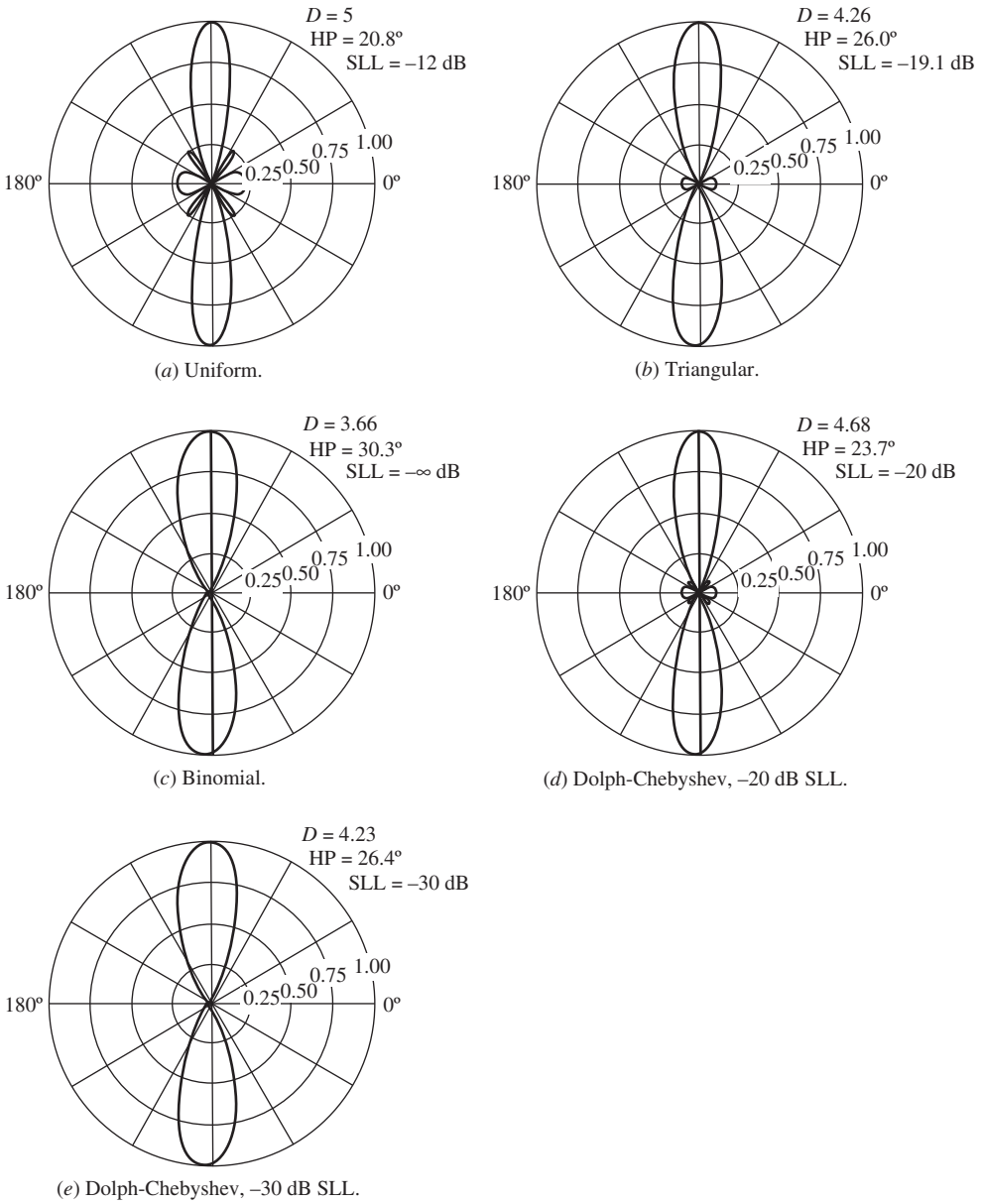

Figure 8-20 Patterns of several uniform phase ($\theta_o = 90^\circ$), equally spaced ($d = \lambda/2$) five-element linear arrays with various amplitude distributions. The currents are plotted in Fig. 8-21. (*a*) Uniform currents, 1:1:1:1:1. (*b*) Triangular current amplitude distribution, 1:2:3:2:1. (*c*) Binomial current amplitude distribution, 1:4:6:4:1. (*d*) Dolph–Chebyshev current amplitude distribution, 1:1.61:1.94:1.61:1, for a side lobe level of -20 dB. See Example 8-5. (e) Dolph–Chebyshev current amplitude distribution, 1:2.41:3.14:2.41:1, with a side lobe level of -30 dB.

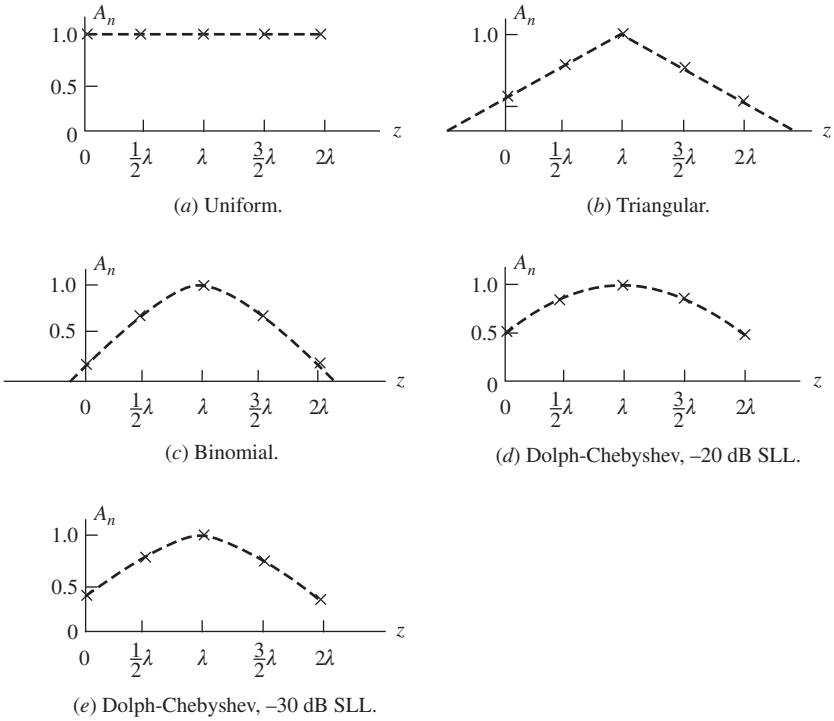

(*a*) Uniform. (*b*) Triangular.

(*c*) Binomial. (*d*) Dolph-Chebyshev, –20 dB SLL.

(*e*) Dolph-Chebyshev, –30 dB SLL.

Figure 8-21 Current distributions corresponding to the patterns of Fig. 8-20. The current phases are zero ($\alpha = 0$). Currents are normalized to unity at the array center.

current amplitudes form a triangle as shown in Fig. 8-21*b*, the radiation pattern of Fig. 8-20*b* results. Notice that the side lobes are considerably smaller than those of the uniformly illuminated array, but at the expense of increased beamwidth. This increased beamwidth (20.8–26.0°) is responsible for reduced directivity (from 5 to 4.26).

The side lobe reduction introduced by the triangular amplitude taper suggests that perhaps an amplitude distribution exists such that all side lobes are completely eliminated. Indeed, this is possible if the ratios of the currents are equal to the coefficients of the binomial series. To see how this comes about, first consider a two-element array with equal amplitudes and spacing d. The array factor from (8-76) is $\text{AF} = 1 + e^{j\psi}$ and can be written in terms of $z = e^{j\psi}$ as

$$\text{AF} = 1 + Z \tag{8-77}$$

If the spacing for this broadside array is less than, or at most equal to, a half-wavelength, the array factor will have no side lobes (see Fig. 3-16). Now consider an array formed by taking the product of two array factors of this type:

$$\text{AF} = (1 + Z)(1 + Z) = 1 + 2Z + Z^2 \tag{8-78}$$

This corresponds to a three-element array with the current amplitudes in the ratio 1 : 2 : 1. Since this array is simply the square of one that had no side lobes, the three-element array also has no side lobes. This process can also be viewed as arraying of two of the two-element arrays such that the centers of each subarray are spaced d apart. This leads to a coincidence of two elements in the middle of the total array, thus giving a current of 2. The total array factor is the product of the "element pattern," which is a two-element

subarray pattern, and the array factor that is again a two-element, equal amplitude array. Thus, the total array factor is the square of one subarray pattern. Continuing this process for an N element array, we obtain

$$\mathrm{AF} = (1+Z)^{N-1} \tag{8-79}$$

which is a binomial series; see (F-4). For $N = 5$,

$$\mathrm{AF} = (1+Z)^4 = 1 + 4Z + 6Z^2 + 4Z^3 + Z^4 \tag{8-80}$$

Therefore, the ratios of the current amplitudes are $1:4:6:4:1$. This current distribution is shown in Fig. 8-21*c* and the resulting pattern is shown in Fig. 8-20*c*. This pattern is broader than either the uniform or triangular distribution cases and has a lower directivity, but it has no side lobes.

From these five-element array examples, a trend is apparent: *As the current amplitude is tapered more from the center to the edge of an array, the side lobes decrease and the beamwidth of the main beam increases*. Many applications where interference/jamming concerns are important require low side lobes, but at the cost of reduced directivity due to the increased beamwidth. The tradeoff between beamwidth and side lobe level is a principle encountered frequently in antenna design that applies to both arrays and continuous distributions, and to slices containing the normal to two-dimensional apertures as well. An example is line sources with uniform and cosine tapered currents shown in Figs. 5-5*a* and 5-8*a*. The peak side lobe levels of the tapered distribution are 9.7 dB lower $(23-13.3)$ than the uniform case, but with a beamwidth that is a factor of 1.34 wider $(1.19/0.886)$, based on the data in Table 5-2.

The beamwidth/side lobe level tradeoff can be optimized. In other words, it is possible to determine the element current amplitudes such that the beamwidth is minimum for a specified side lobe level, or conversely to specify the beamwidth and obtain the lowest possible side lobe level. This array is referred to as a Dolph–Chebyshev array and it provides a pattern with all side lobes of the same level. The Dolph–Chebyshev array synthesis procedure is explained in detail in Sec. 10.4.1. For a five-element array with an element spacing of a half-wavelength and a specified side lobe level of -20 dB, the Dolph–Chebyshev current distribution is plotted in Fig. 8-21*d* and the corresponding pattern is shown in Fig. 8-20*d*. If the side lobe level for the Dolph–Chebyshev array is specified to be -30 dB, the distribution is that of Fig. 8-21*e* and the corresponding pattern is shown in Fig. 8-20*e*. Note that the main beam is slightly broader than in the previous case where the side lobe level was 10 dB higher.

The discussion of nonuniformly excited arrays thus far was for amplitudes that are tapered toward the ends of the linear array. If the amplitude distribution becomes larger at the ends of the array (called an inverse taper), we expect the opposite effect; that is, the side lobe level increases and the beamwidth decreases. Suppose, for example, that we invert the triangular distribution such that the amplitudes are $3:2:1:2:3$. The resulting pattern shown in Fig. 8-22 demonstrates the expected decrease in beamwidth and increase in side lobe level. Although the directivity for the inverse triangular tapered current is greater than that for the triangular taper of Fib. 8-20*b*, it is still not as large as that produced by the uniform distribution.

The directivity values were given for each of the examples in this section. We close this section by developing the directivity expression. With little additional complexity, we expand the treatment to include unequal element spacings as well as nonuniform excitation. The element positions along the z-axis are z_n and the element current amplitudes are A_n. If the element phases are linear with distance, then $\alpha_n = -\beta z_n \cos\theta_o$, where θ_o is the angle of the pattern maximum; the applications of this type of phasing are discussed in Sec. 8.9.1. The array factor of (8-53) is then appropriate and when normalized is

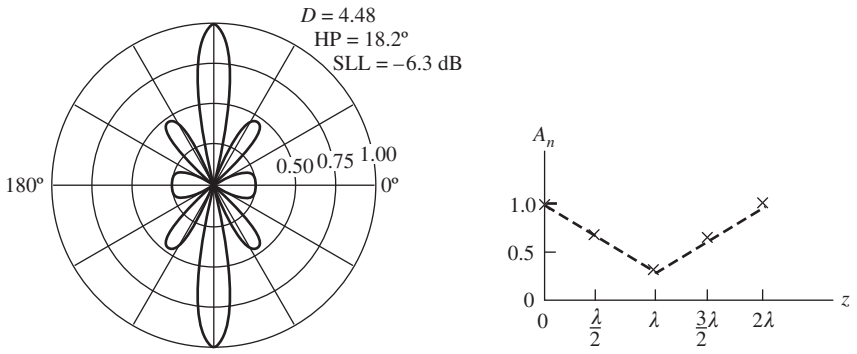

(*a*) The array factor. (*b*) The current distribution, 3:2:1:2:3.

Figure 8-22 The inverse triangular tapered, five-element linear array with $d = \lambda/2$ and $\theta_o = 90°$.

$$f(\theta) = \frac{\sum_{n=0}^{N-1} A_n e^{\,j\alpha_n} e^{\,j\beta z_n \cos\theta}}{\sum_{n=0}^{N-1} A_n} \tag{8-81}$$

The appropriate beam solid angle expression is

$$\begin{aligned}\Omega_A &= 2\pi \int_0^{\pi} |f(\theta)|^2 \sin\theta \; d\theta \\ &= \frac{2\pi}{\left(\sum_{k=0}^{N-1} A_k\right)^2} \sum_{m=0}^{N-1} \sum_{p=0}^{N-1} A_m A_p e^{j(\alpha_m - \alpha_p)} \int_0^{\pi} e^{j\beta(z_m - z_p)\cos\theta} \sin\theta \; d\theta\end{aligned} \tag{8-82}$$

Evaluating the integral in the above expression and applying the result to $D = 4\pi/\Omega_A$ yields

$$D = \frac{\left(\sum_{k=0}^{N-1} A_k\right)^2}{\sum_{m=0}^{N-1} \sum_{p=0}^{N-1} A_m A_p e^{j(\alpha_m - \alpha_p)} \dfrac{\sin[\beta(z_m - z_p)]}{\beta(z_m - z_p)}} \tag{8-83}$$

where $\alpha_n = -\beta z_n \cos\theta_o$ and the elements can have any positions z_n and current amplitudes A_n. This general result simplifies for a broadside, equally spaced array to

$$D = \frac{\left(\sum_{k=0}^{N-1} A_k\right)^2}{\sum_{m=0}^{N-1} \sum_{p=0}^{N-1} A_m A_p \dfrac{\sin[(m-p)\beta d]}{(m-p)\beta d}} \qquad \alpha_n = 0, \quad z_n = nd \tag{8-84}$$

As another special cases, when the spacings are a multiple of a half-wavelength, (8-83) reduces to

$$D = \frac{\left(\sum_{n=0}^{N-1} A_n\right)^2}{\sum_{n=0}^{N-1} (A_n)^2} \quad d = \frac{\lambda}{2}, \lambda, \ldots \tag{8-85}$$

Note that this is independent of scan angle θ_o, as indicated in Fig. 8-18 for $d = \lambda/2$. Also, if the amplitudes are uniform, (8-85) yields $D = N$ as given by (8-68). For a further example, consider the triangular excitation with the pattern of Fig. 8-20*b*. The directivity value from (8-85) is $[2(1)+ 2(2) + 3]^2/[2(1)^2 + 2(2)^2 + (3)^2] = 4.26$. Eq. (8-85) is a very instructive formula because it shows that directivity is a measure of the coherent radiation from the linear array. The numerator is proportional to the square of the *total* coherent field, whereas the denominator is proportional to the *sum* of the squares of the field from each of the elements.

There is no closed-form expression for directivity that includes element pattern effects in an array with weighted excitations that is analogous to (8-72), which is for uniformly illuminated linear arrays of simple element types. Instead directivity is found by integrating the pattern to find Ω_A and using $D = 4\pi/\Omega_A$. This is a relatively easy task with a math applications computer package.

Directivity can be increased without limit through close element spacings with extreme amplitude and phase changes across the array. As mentioned in Sec. 5.5, there are penalties with using superdirective antennas and they are not practical except for modest increases in directivity over that achieved with uniform excitation. For equally spaced, collinear arrays of half-wave dipoles that can have nonuniform amplitude excitations, the maximum directivity is only slightly larger than for uniform excitation up to a spacing of $0.7\,\lambda$ and is nearly identical to it for greater spacings. Hansen [H.8.11: Hansen] provides more details on superdirective arrays and superdirectivity in general.

8.7 MUTUAL COUPLING IN ARRAYS

Arrays so far have been treated as having non interacting elements and as being perfectly matched in impedance to the feed network. This allows the following further assumptions: (i) The element terminal currents are proportional to their incident signals, (ii) The relative current distributions across each element are identical (although they can be of different levels proportional to the excitations), and (iii) Pattern multiplication is valid. As might be expected, in a real array the elements interact with each other which alters the currents (and thus impedances). This interaction, called *mutual coupling*, changes the current magnitude, phase, and distribution on each element from their free-space values. As a consequence, the total array pattern is altered from the no-coupling case. In this section, we discuss the effects of mutual coupling on impedance and pattern, followed by methods to evaluate array element impedance and the array pattern in the presence of mutual coupling.

First, we present names and definitions for several terms used in the field of array antennas mainly following the classic work by Hannan [8], but other names appear in the literature for the same quantities. A *passive array* uses a single generator[2] followed by power dividers and phase adjustment devices. An *active array* has a separate generator at each element, which is the most common array model. The input impedance of an element that has been removed from the array and is isolated from all objects is called *isolated element impedance* or simply *antenna impedance*. Of course, the practical case is a fully active array with all elements excited to produce the desired beam shape, scan angle, and so on. The impedance of an element in its array environment with all elements

[2] Arrays are usually described for the transmit case, but the results apply to receiving arrays as well.

active is referred to as the *active impedance*, *driving impedance* or simply *input impedance*.[3] The active impedance for the elements will vary with position in the array and the excitations, including phasing for scan. Active impedance is difficult to measure because of the requirement for the array to be fully active, although simulations can be made for these conditions. In practice, element impedance behavior is characterized by exciting the one element and passively terminating all others, typically with nominal generator impedance or a reference load such as $50\,\Omega$. This is often called *passive impedance*. In most situations, passive impedance closely approximates active impedance because the coupling environment is identical and the terminating impedance conditions are nearly identical. Thus, it is more common to use the term active impedance in place of passive impedance and we will adopt this approach. To distinguish cases of fully active arrays, we use the term "active impedance in a fully active array."

8.7.1 Impedance Effects of Mutual Coupling

The three mechanisms responsible for mutual coupling are illustrated in Fig. 8-23*a*. First is direct space coupling between array elements. Second, indirect coupling can occur by scattering from nearby objects such as a support tower. Third, the feed network that interconnects elements in the array provides a path for coupling. In many practical arrays, feed network coupling can be minimized through proper impedance matching at each element. This permits each element in the array to be modeled with independent generators as in Fig. 8-23*b*, where the *m*th element has an applied generator voltage and terminal impedance given by V_m^g and Z_m^g. The voltage and current at the element terminals, V_m and I_m, include all coupling effects. An array of N elements is then treated as an N port network using conventional circuit analysis, giving

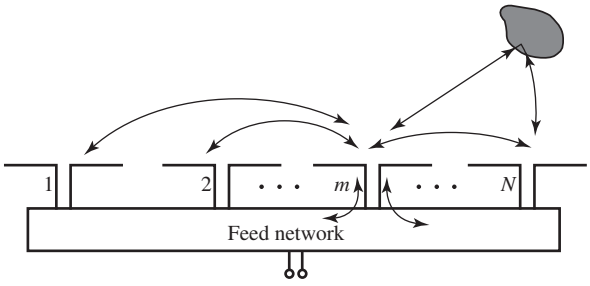

(*a*) Mechanisms for coupling between elements of an array.

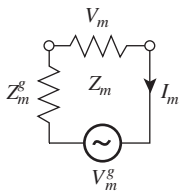

(*b*) Model for *m*th element in an array.

Figure 8-23 Mutual coupling in a fully excited array antenna.

[3] Some authors have used the term *scan impedance* in place of active impedance.

$$\begin{aligned} V_1 &= Z_{11}I_1 + Z_{12}I_2 + \cdots + Z_{1N}I_N \\ V_2 &= Z_{12}I_1 + Z_{22}I_2 + \cdots + Z_{2N}I_N \\ &\vdots \\ V_N &= Z_{1N}I_1 + Z_{2N}I_2 + \cdots + Z_{NN}I_N \end{aligned} \tag{8-86}$$

where V_n and I_n are the impressed current and voltage in the nth element, and Z_{nn} is the *self-impedance* of the nth element when all other elements are open-circuited. The *mutual impedance* Z_{mn} ($= Z_{nm}$ by reciprocity) between the two terminal pairs of elements m and n is the open circuit voltage produced at the first terminal pair divided by the current supplied to the second when all other terminals are open-circuited; that is,

$$Z_{mn} = \left.\frac{V_m}{I_n}\right|_{I_{i=0}} \quad \textit{for all } i \textit{ except } i = n \tag{8-87}$$

For example, $Z_{12} = Z_{21} = V_2/I_1$ with port 2 open circuited.

Mutual impedance is, in general, difficult to compute or measure. However, wide availability of commercial simulation codes based on moment methods discussed in Chap. 14 have made the evaluation of mutual impedance values for wire antennas relatively easy. Before showing simulation results, we discuss how mutual impedance between two antennas is measured, and the results are easily generalized for the determination of mutual impedance between any two elements of an arbitrary array, Z_{mn}. An antenna when isolated in free space with voltage V_1 and current I_1 has an input impedance of

$$Z_{11} = \frac{V_1}{I_1} \quad \textit{single isolated element} \tag{8-88}$$

If a second antenna is brought into proximity with the first, then radiation from the first antenna induces currents on the second, which in turn radiates and also influences the current on the first antenna. The second antenna can either be excited or unexcited (parasitic), but in any case it has terminal current I_2. Then the total voltage at the first antenna is

$$V_1 = Z_{11}I_1 + Z_{12}I_2 \tag{8-89}$$

Similarly, the voltage at the terminals of the second antenna is expressed by

$$V_2 = Z_{21}I_1 + Z_{22}I_2 \tag{8-90}$$

Note that (8-86) is a generalization of (8-89) and (8-90).

Now suppose the second antenna has a load impedance Z_2^g across its terminals ($V_2^g = 0$) such that $V_2 = -Z_2^g I_2$. We can write (8-90) as

$$-Z_2^g I_2 = Z_{21}I_1 + Z_{22}I_2 \tag{8-91}$$

Solving for I_2 and using $Z_{21} = Z_{12}$, we obtain

$$I_2 = \frac{-Z_{21}I_1}{Z_{22} + Z_2^g} = \frac{-Z_{12}I_1}{Z_{22} + Z_2^g} \tag{8-92}$$

Substituting this into (8-89) and dividing by I_1, we find that

$$\frac{V_1}{I_1} = Z_1 = Z_{11} - \frac{(Z_{12})^2}{Z_{22} + Z_2^g} \tag{8-93}$$

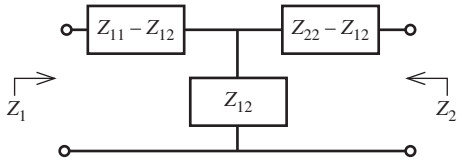

Figure 8-24 Network representation of the coupling between two antennas.

This expresses the input impedance in terms of the two self-impedances (Z_{11} and Z_{22}), the mutual impedance Z_{12}, and the load Z_2^g at the unexcited terminals of antenna 2.

The above discussion suggests the equivalent circuit of Fig. 8-24 for the coupling between two resonant antennas. For a single isolated antenna (i.e., antenna 2 very far away), $Z_{12} = 0$, and (8-93) gives the input impedance equal to the self-impedance, $Z_1 = Z_{11}$. If antenna 2 is open-circuited, then $Z_2^g = \infty$ and (8-93) gives $Z_1 = Z_{oc} = Z_{11}$. Open circuiting implies that the current all along antenna 2 is reduced to zero. This occurs for antennas such as half-wave dipoles, where resonant behavior is eliminated by open circuiting. In other antennas (such as full-wave dipoles), even with an open circuit there will be current induced on the antenna. In this case, the second antenna should be removed.

The general procedure for determining mutual impedance from open-circuit and short-circuit measurements involves the following steps. [H.6: Hansen, Vol. II, pp. 157–160]:

1. Open circuit (or remove) antenna 2. Measure $Z_{oc} = Z_{11}$ at the terminals to antenna 1. For identical antennas, $Z_{22} = Z_{11}$.
2. Short circuit antenna 2. Measure Z_{sc} at the terminals to antenna 1.
3. Compute Z_{12}, using

$$Z_{12} = \sqrt{Z_{oc}(Z_{oc} - Z_{sc})} \tag{8-94}$$

This follows from (8-93) with $Z_2^g = 0$.

The proper sign must be chosen with (8-94). This is aided by examining variations with spacing in the limit of small spacing and maintaining continuity through zero crossings [9]. Good agreement between simulations are experimental results based on this method is reported in [9].

Mutual impedance is computed by placing a generator on the input of one antenna, finding the voltage appearing at the input terminals of the second antenna, and then taking the ratio of the voltage to the current. Results of simulations using a moment method code based on principles in Chap. 14 for two free-space resonated half-wave dipoles that are oriented parallel to each other as a function of separation distance is plotted in Fig. 8-25. Similar results are presented in Fig. 8-26 for dipoles that are collinear. The mutual impedance values decrease with increasing separation distance in both dipole orientation cases. The general trends for mutual coupling in arrays are as follows [H.6: Rudge et al., Vol. II, Sec. 10.3]:

a. The magnitude of mutual impedance decreases with spacing distance d, in many cases decaying as $1/d^2$ [H.8.2: Hansen, "Phased Array Antennas," 2nd ed., p. 225].
b. The far field pattern is an indicator of coupling between elements, although the coupling mechanism is a near-field, not far-field, effect. Coupling is proportional to the element pattern level in the array plane (or surface). And, elements with a narrow pattern will have lower coupling than a elements with a broad beam.
c. Elements with polarizations (i.e., electric field orientations) that are parallel couple more than when collinear.
d. Larger elements have smaller coupling.

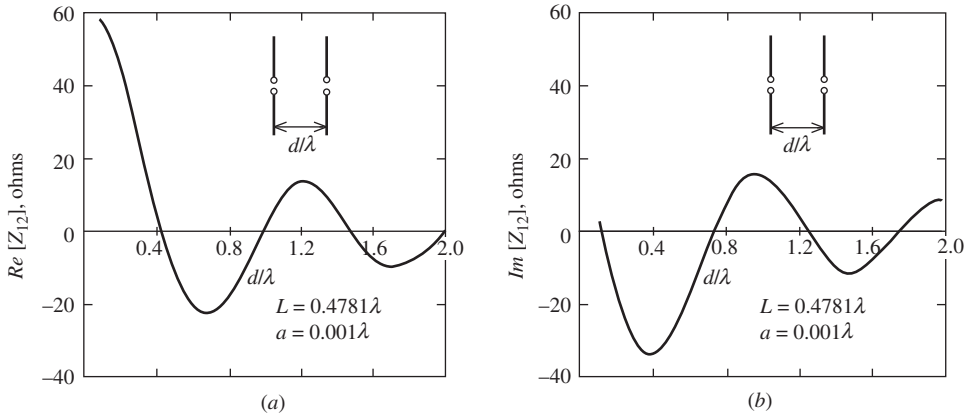

Figure 8-25 The mutual impedance between two resonant parallel dipoles as a function of their spacing relative to a wavelength. (*a*) The real part. (*b*) The imaginary part.

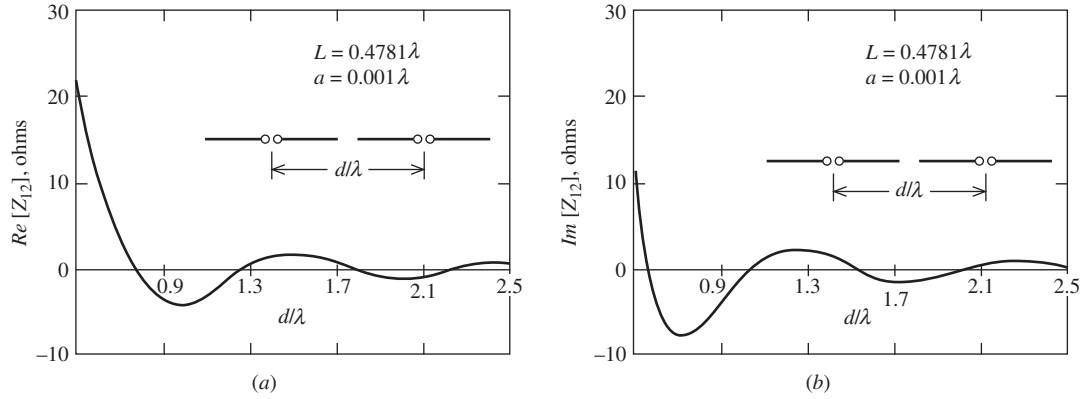

Figure 8-26 The mutual impedance between two resonant collinear parallel dipoles as a function of their spacing relative to a wavelength. (*a*) The real part. (*b*) The imaginary part.

Figs. 8-25 and 8-26 demonstrate these trends. Trend (a) is clear, and trends (b) and (c) are evident when comparing the parallel and collinear dipole results.

A second way to quantify coupled arrays in addition to the mutual impedance approach is to use the scattering parameter method that is commonly used in radio-frequency circuit analysis. For an N-element array, the scattering approach consists of incident voltage wave with an $N \times 1$ column matrix $[a]$ and reflected voltage wave $N \times 1$ column matrix $[b]$ that are related by an $N \times$ N square *scattering matrix* $[S]$ through the matrix equation $[b] = [S][a]$. The voltage wave matrix and scattering matrix entries (called *scattering parameters* or *scattering coefficients*) are complex valued, and carry magnitude and phase information. The scattering parameter S_{mn} is the ratio of the output voltage wave amplitude at port m (b_m) due to the input voltage wave amplitude at port n (a_n) with all other ports not excited. The scattering parameters are popular because they relate directly to measurements, and network analyzers output the values. The scattering matrix diagonal entries are the reflection coefficients at each port, so

$$S_{nm} = \Gamma_m \tag{8-95}$$

Just as with the impedance matrix, the scattering matrix is symmetric for a reciprocal device and $S_{nm} = S_{mn}$. The off-diagonal entries represent the coupling between ports. So the coupling between ports m and n in dB, C_{mn}, is

$$C_{mn} = 20\log|S_{mn}| \qquad [\text{dB}] \tag{8-96}$$

The scattering matrix entries can be found from the impedance matrix entries, Z_{mn}. For element one of a two-element array with all connecting transmission lines of characteristic impedance Z_o:

$$S_{11} = \frac{(Z_{11} - Z_o)(Z_{22} + Z_o) - Z_{12}^2}{(Z_{11} + Z_o)(Z_{22} + Z_o) - Z_{12}^2} \tag{8-97}$$

$$S_{12} = \frac{2Z_oZ_{12}}{(Z_{11} + Z_o)(Z_{22} + Z_o) - Z_{12}^2} \tag{8-98}$$

We can perform some simple reality checks on these equations. For no mutual coupling ($Z_{12} = 0$), (8-97) gives $S_{11} = \Gamma_1 = (Z_{11} - Z_o)/(Z_{11} + Z_o)$, which is the conventional one-port reflection coefficient formula. Also, for no mutual coupling (8-98) yields $S_{12} = 0$, as should be the case.

To illustrate how mutual coupling values are used to calculate coupling, consider the two-element array of parallel half-wave dipoles with a spacing of $0.6\,\lambda$. Fig. 8-25 gives $Z_{12} = -23 - j17\,\Omega$ and using a matched condition with $Z_{11} = Z_o = 70\,\Omega$, (8-98) in (8-96) yields a coupling level of $C_{11} = -13.7$ dB. As we indicated earlier, coupling levels vary widely as dipole spacing and orientation are changed. Microstrip elements on a common substrate have coupling levels that decrease monotonically from -15 to -40 dB as element spacing is increased from about 0.5 to $1.5\,\lambda$ in the H-plane and from -20 to -30 dB in the E-plane. [H.8.4: Bancroft, p. 175] Prob. 8.7-4 addresses mutual impedance calculation using simulations.

The input impedance of an element in the array can now be computed using the mutual impedance values. For the mth element, the input impedance is found using (8-86) as

$$Z_m = \frac{V_m}{I_m} = Z_{m1}\frac{I_1}{I_m} + Z_{m2}\frac{I_2}{I_m} + \cdots + Z_{mN}\frac{I_N}{I_m} \tag{8-99}$$

This is the input impedance in the presence of all elements; i.e., the *active impedance* in a fully excited array. All coupling effects are included via the mutual impedances found from numerical simulations or from measurements using (8-94). The formula clearly shows the dependence of the input impedance on not only the mutual impedances, but also on the terminal currents of each element. Of practical significance is that input impedance is affected by the phase of the terminal currents as it is adjusted to phase-scan the pattern. Thus, the input impedance of all elements in an array will change with scan angle.

8.7.2 Array Pattern Evaluation Including Mutual Coupling

In addition to the element impedances, mutual coupling influences the radiation properties of an array as will be discussed in this section. Complete analysis using simulations or measuring the parameters of each embedded element antenna can be used for full characterization of the array, but this is tedious and rarely done. Instead, approximate techniques for including mutual coupling effects are employed, as we will present. Arrays can be modeled using all mutual impedances explicitly, or by absorbing coupling effects into the currents (isolated-element pattern approach) or into the element pattern (active-element

pattern approach), which is the approach we take here. [H.6: Hansen, Vol. II, Chap. 3; H.8.2: Mailloux, 2nd ed., Sec. 2.1].

In the isolated-element pattern approach, all coupling effects in the total array pattern are accounted for in the excitations:

$$F_{\text{un}}(\theta, \phi) = g_i(\theta, \phi) \sum_{m=1}^{N} I_m e^{j\xi_m} \tag{8-100}$$

where ξ_m is the total phase contribution (usually referenced to the center of the array) due to spatial phase delay. It is the classical array pattern approach of Sec. 8.4 consisting of the product of an *isolated-element pattern* $g_i(\theta, \phi)$ and an array factor. Without coupling effects, the currents $\{I_m\}$ vary in proportion to the excitation voltages. Coupling effects are included using the simple circuit model of the mth element in Fig. 8-23*b*:

$$I_m = \frac{V_m^g}{Z_m^g + Z_m} \tag{8-101}$$

This is called "free excitation" because the element terminal voltage will change with scan angle. Instead of a constant-voltage feed, it is a constant-incident (available) power feed as is the case in Fig. 8-19. For an infinite array of identical elements in a uniform grid where all elements have same coupling, each element "sees" the same environment and the active impedances are identical, so that all $\{Z_m\}$ equal Z_A. Then the currents are proportional to the voltages across the element terminals:

$$I_m = \frac{V_m^g}{Z^g + Z_A} \propto V_m \tag{8-102}$$

This situation applies to large, equally spaced arrays. It must be pointed out that the common implementation of (8-100) for finite arrays uses the approximation of (8-102), thereby ignoring terminal current variations due to mutual coupling and only including generator voltage variations. It is difficult to obtain accurate current information so that (8-100) can be evaluated, and the active-element pattern method is usually employed; this method is discussed next.

In the active-element pattern approach, all coupling effects are accounted for through the active element. The *active-element pattern* $g_{\text{ae}}^n(\theta, \phi)$ is obtained by exciting only the nth element and loading all other elements with the generator impedance Z^g. The active-element pattern arises from direct radiation from the nth element combined with fields reradiated from the other elements, which in turn receive their power through spatial coupling from the element n. The array pattern in this formulation is

$$F_{\text{un}}(\theta, \phi) = \sum_{n=1}^{N} g_{\text{ae}}^n(\theta, \phi) I_n e^{j\xi_n} \tag{8-103}$$

Here, the currents $\{I_n\}$ are proportional to excitation voltages $\{V_n\}$ as in (8-102). All mutual coupling effects are incorporated into the active-element patterns $g_{\text{ae}}^n(\theta, \phi)$, which depend on the element characteristics and the array geometry. To represent the possibility of gain variations, the active-element pattern levels are relative to a reference element near the center of the array.

It would be tedious to measure active-element patterns for each element in an array. Fortunately, this is usually not necessary. For a large array of identical elements in an equally spaced array, each element sees the same environment of nearest neighbors, except for the edge elements. The appropriate approximation is to factor (8-103) using an *average active-element pattern,* $g_{\text{ae}}(\theta, \phi)$, which is the normalized pattern for a typical central element in the array:

$$F_{\text{un}}(\theta,\phi) = g_{\text{ae}}(\theta,\phi)\sum_{n=1}^{N} I_n e^{j\xi_n} \tag{8-104}$$

The advantage of this approach is that the summation in this equation is the array factor based on simple theory without mutual coupling. All coupling effects are contained in the average active-element pattern, which is found by a single pattern measurement of a central element in a large array.

The normalized form of (8-104) gives the important approximate result:

$$\boxed{F(\theta,\phi) = g_{\text{ae}}(\theta,\phi) f(\theta,\phi)} \tag{8-105}$$

where

$g_{\text{ae}}(\theta,\phi)$ = average active-element pattern
$f(\theta,\phi)$ = array factor
$F(\theta,\phi)$ = array pattern

This is of the same form as the pattern multiplication formula of (8-54), but mutual coupling effects are included. This approximation is widely used in practice. The average active-element pattern also plays an important role in array construction. The pattern of a single active element surrounded by several passively terminated elements is measured and evaluated before the fully active large array is built and tested. If the active-element pattern is not well formed, the full array will not be either. It has been shown that the active input impedance can be obtained from the active-element pattern data. [10]

The isolated-element pattern will differ from the active-element patterns of the elements in the array. But, for a sufficiently large array, the average-element pattern is representative of the majority of the active-element patterns in the array. How large an array has to be before (8-105) can be applied is an important question that is addressed through guidelines and examples. As array size becomes large (ideally, an infinite number of elements), the active-element patterns for the individual elements converge toward being identical and being equal to the average-active element pattern. Elements near the edge of a finite array have patterns that deviate from the pattern of central elements, which should be close to the average-element pattern. This is illustrated by the patterns in Fig. 8-27 that shows the active element patterns for each element in an array of eight microstrip patch antennas spaced 0.57λ apart. The polar-dB patterns shown for selected elements were measured for that element excited and all others match loaded. The patterns for elements 2 through 7 (only pattern 5 is shown) are nearly identical and are symmetric. The edge element patterns (1 and 8) are distorted due to the asymmetric array environment and due to the finite ground plane edge effects. Note that most pattern distortion is on the side away from the array. Similar results have been reported for dipoles in front of a ground plane. [H.3: Milligan, Sec. 12.5; H.8.2: Haupt, Sec. 6.4] The topic of a representative element pattern in a finite array is revisited in Sec. 8.9.1.

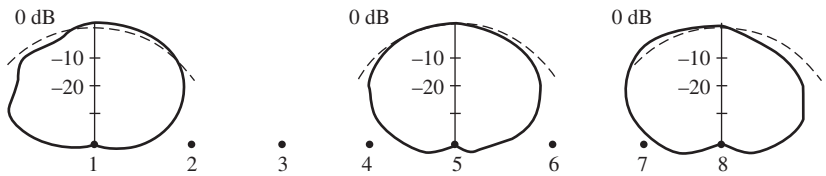

Figure 8-27 Measured active-element patterns for three elements, an interior element (5) and the end elements (1 and 8), of a linear array of eight microstrip patch elements spaced 0.57λ apart.

The full array pattern is, of course, affected by mutual coupling within the array. Arrays are modeled with voltage generator excitations based on a desired set of terminal currents. In the absence of mutual coupling, the terminal currents are proportional to the excitation voltages, (8-102) applies, and the desired pattern is realized. With coupling present the pattern is distorted, but it often turns out that the terminal currents can deviate rather far from the desired excitations and the pattern is not greatly affected. A linear array of 12 half-wave spaced, parallel, half-wave dipoles with excitation voltages designed to steer the beam 45° off broadside has a pattern in Fig. 14-27 (dashed curve) that does not differ much from the ideal no-coupling excitation case (solid curve). The beam is steered correctly as well. Although the element currents and impedances are not close to the desired values (see Table 14-1), the integrating effect of the pattern tends to smooth out the variations; also see [11]. In addition to pattern, the gain and polarization of the total array pattern are affected by mutual coupling. Guidelines similar to those used for impedance in Sec. 8.7.1 also apply to radiation from arrays.

Techniques are available to compensate for mutual coupling effects. Mutual coupling does not change the current distribution on elements in the array but does change the complex terminal currents. Compensation schemes essentially anticipate how the terminal currents will be altered by mutual coupling and change the excitation voltages to produce the desired currents. [H.3: Milligan, Sec. 3.11; 12] There are also physical means to reduce mutual coupling directly such as inserting conducting baffles (i.e., fences) between elements. [H.8.3: Haupt, Sec. 6.8].

8.8 MULTIDIMENSIONAL ARRAYS

Linear arrays have a number of limitations. For instance, they can be phase-scanned in only a plane containing the line of the elements' centers. The beamwidth in a plane perpendicular to the line of element centers is determined by the element beamwidth in that plane. This usually limits the realizable gain. Thus, multidimensional arrays are used for applications requiring a pencil beam, high gain, or main beam scanning in any direction. With advances in fabrication and integrated feed electronics, the costs of large multidimensional arrays are affordable in many situations. Multidimensional arrays are classified by three characteristics: The geometric shape of the surface on which the element centers are located, the perimeter of the array, and the grid geometry of the element centers. The surface on which elements are placed can be linear, circular, planar, etc. The perimeter of planar arrays is usually circular, rectangular, or square in shape. Fig. 8-28 illustrates a planar array with a rectangular perimeter. The array grid (or lattice) can have equal or unequal row and column spacings. A planar array with equal element spacings of d_x and d_y in the principal planes such as in Fig. 8-28 is referred to as having a rectangular grid. If $d_x = d_y$, the grid is said to be square. A triangular grid is also widely used. When the array conforms to a complicated surface such as the fuselage of an aircraft, the array is

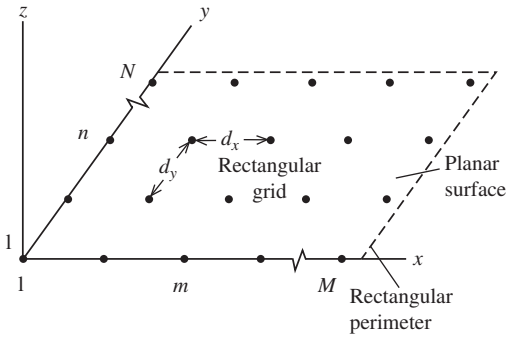

Figure 8-28 Geometry of a planar array.

said to be conformal. In this section, we present techniques for analyzing arrays of arbitrary geometry as well as a few important special case geometries.

The pattern multiplication principles developed in Sec. 8.4 for linear arrays apply to arrays of any geometry as long as the elements are similar. That is, if the elements are identical and oriented in the same direction, the total array pattern is factorable as in (8-105), which includes mutual coupling effects. This is the usual situation and permits us to confine attention to the array factor $f(\theta, \phi)$ when studying multidimensional arrays. In this section, we develop the array factor for an arbitrary geometry.

The elements for an arbitrary three-dimensional array are located with position vectors from the origin to the *mn*th element:

$$r'_{\text{mn}} = x'_{\text{mn}}\hat{\mathbf{x}} + y'_{\text{mn}}\hat{\mathbf{y}} + z'_{\text{mn}}\hat{\mathbf{z}} \tag{8-106}$$

The array factor is then

$$\text{AF}(\theta, \phi) = \sum_{n=1}^{N} \sum_{m=1}^{M} I_{\text{mn}} e^{j(\beta \hat{\mathbf{r}} \cdot \mathbf{r}'_{\text{mn}} + \alpha_{\text{mn}})} \tag{8-107}$$

which, when normalized, is $f(\theta, \phi)$. This equation is general but is directly applicable to the common situation of an array on a surface. The double summation is useful in geometries that employ "rows" and "columns." The phase term α_{mn} is that portion of the excitation current phase used to scan the main beam and is shown explicitly. A common geometry for phased arrays is planar. The array factor for a planar array in the *xy*-plane, as in Fig. 8-28, follows from (8-107) as

$$\text{AF}(\theta, \phi) = \sum_{n=1}^{N} \sum_{m=1}^{M} I_{\text{mn}} e^{j\alpha_{\text{mn}}} e^{j\xi_{\text{mn}}} \tag{8-108}$$

where

$$\xi_{\text{mn}} = \beta \hat{\mathbf{r}} \cdot \hat{\mathbf{r}}'_{\text{mn}} = \beta[x'_{\text{mn}} \sin\theta \cos\phi + y'_{\text{mn}} \sin\theta \sin\phi]$$

$$\alpha_{\text{mn}} = -\beta[x'_{\text{mn}} \sin\theta_o \cos\phi_o + y'_{\text{mn}} \sin\theta_{\text{o}} \sin\phi_o]$$

$\theta_o, \phi_o =$ main beam pointing direction

This formulation is a generalization of that for a linear array. Note that the *z*-axis is normal to the plane of the array, whereas in our treatment of linear arrays the *z*-axis is along the array. If all rows parallel to the *x*-axis, have the same current distribution, and if all columns have identical current distributions, then the current is separable (e.g., $I_{\text{mn}} = I_{\text{xm}} I_{\text{yn}}$) and (8-108) reduces to

$$\text{AF}(\theta, \phi) = \sum_{m=1}^{M} I_{\text{xm}} e^{j\xi_{\text{xm}}} \cdot \sum_{n=1}^{N} I_{\text{yn}} e^{j\xi_{\text{yn}}} \tag{8-109}$$

where the phase of the current for beam steering is not shown explicitly and

$$\xi_{\text{xm}} = \beta x'_m \sin\theta \cos\phi \qquad \text{and} \qquad \xi_{\text{yn}} = \beta y'_n \sin\theta \sin\phi$$

This is a product of two linear array factors associated with the row and column current distributions. The patterns in the principal planes ($\phi = 0^\circ, 90^\circ$ and called the cardinal planes) are those of the corresponding linear arrays (row, column). Planar arrays normally have separable current distributions, so linear array analysis can be applied directly to find the principal plane patterns.

For planes off the principal planes, called the intercardinal planes, the pattern is the product of the row and column linear array patterns if the current distribution is separable. In the 45°-plane, the side lobes will be very low because they are a product of the side lobe levels in the principal planes; Fig. 9-7 illustrates this point using a continuous planar

aperture distribution. A technique for finding the pattern of a planar array in any cut-plane is the *projection method*, or method of collapsed distributions, for finding the array factor. The element locations are projected onto the cut-plane along with the current weighting for the elements along the projection line. The projection line contains the elements in the equivalent linear array. The weightings for coincident projections are added together. The current distribution in the original array need not be separable and the grid need not be regular. For an example of the projection method, a 4×4 planar array of elements spaced 0.5λ apart and uniformly excited has an equivalent array in the 45°-plane of seven elements spaced 0.354λ apart with the following weightings: $1:2:3:4:3:2:1$. Prob. 8.8-5 shows that pattern of the projected linear array is identical to the planar array pattern. See [H.3: Elliott, Sec. 6.10] for more examples. The method can be used for a variety of geometries, such as finding the equivalent linear array for a circular array.

Planar arrays are used to create a highly directive beam, often with scan capability as discussed in the next section. Here we present directivity calculation methods. First consider a cell of an array, which is the area surrounding an element. The maximum possible directivity for one cell based on (4-23) and using the physical area of a cell as the maximum effective aperture, A_{em} is

$$D_{\text{MaxCell}} = \frac{4\pi}{\lambda^2} A_{\text{Cell}} \tag{8-110}$$

This formula assumes radiation into the half-space on one side of the array face. It provides an upper bound on the directivity of one element embedded in an array. For a half-wavelength spaced square-grid planar array, the cell area is $A_{\text{Cell}} = d_x d_y = (\lambda/2)(\lambda/2) = \lambda^2/4$ and (8-110) yields $D_{\text{MaxCell}} = \pi$. Finite arrays of dipoles in a $\lambda/2 \times \lambda/2$ square grid and backed by a ground plane have a maximum element gain (see Sec. 8.9.1) somewhat above or below the maximum cell area directivity from (8-110) of 3.14, depending on the number of elements and ground plane distance. [13]. The directivity of a full array is found from a similar formula using the physical area of the full array, A_p:

$$D_{\text{MaxArray}} = \frac{4\pi}{\lambda^2} A_p = \pi D_x D_y \tag{8-111}$$

which is also given in (9-67) for aperture antennas. The second part of this formula comes from using $A_p = L_x L_y$ and introducing the directivities of uniform line sources in the x and y directions of a planar array in the xy-plane from (5-19): $D_x = 2L_x/\lambda$ and $D_y = 2L_y/\lambda$.

This formula also can be found based on (8-75) as $D_{\text{MaxArray}} = \text{Max}\{D_e D_i\} = D_{\text{MaxCell}} N = (4\pi/\lambda^2) A_{\text{Cell}} N = (4\pi/\lambda^2) A_p$ where N is the total number of elements in the array. Forman [14] gives the range of spacing values in a square grid array for which (8-111) equals the correct directivity for a few element types, but the ranges are small and (8-111) should used only as a guideline. In general, the directivity of planar arrays increases with element spacing similar to that for linear arrays until grating lobes begin to appear and directivity decreases. King and Wong [15] note this effect, and that directivity becomes asymptotic to ND_e, where D_e is the directivity for actual element, for spacing values around $1\,\lambda$ depending on the element pattern. Formulas are available in the literature [14] for calculating the directivity of planar arrays with simple element types, although they tend to be complicated and have restrictions on their application. But such formulas are useful for checking computer programs based on pattern integration to find directivity. Forman found that (8-111) is close to the actual array directivity for an element pattern of $\cos^{0.5}\theta$; the following example demonstrates this.

EXAMPLE 8-8 *Directivity of Planar Arrays*

In this example, we examine the exact and approximate methods for calculating the directivity of a square-grid (5×5) planar array in the xy-plane. The 25 elements have the pattern

$g_a(\theta) = \cos^{0.5}\theta$ (for $\theta < 90°$ and zero otherwise). We consider two approximate directivity formulas. The first, which was mentioned in association with (8-75) for linear arrays, depends only on the element type and not the spacing:

$$D_{\text{ApraxArray}} = ND_e = 25 \cdot 4 = 100 = 20\,\text{dB} \tag{8-112}$$

where the element directivity was obtained by pattern integration. The second approximation is that of (8-111):

$$D_{\text{MaxArray}} = \frac{4\pi}{\lambda^2}A_p = \frac{4\pi}{\lambda^2}(N_x d_x)(N_y d_y) = 4\pi N\frac{d_x}{\lambda}\frac{d_y}{\lambda} \tag{8-113}$$

First consider spacings of $d = d_x = d_y = 0.5\,\lambda$. The maximum directivity from (8-113) is 19 dB. Evaluating the directivity by pattern integration gives 18.3 dB for isotropic elements and 18.98 dB for square-root cosine element patterns. Increasing the spacing to $d = 0.8\,\lambda$ increases the directivity from (8-113) to 23 dB and the directivity by numerical integration to 21.6 and 22.4 dB for isotropic and square-root cosine element patterns, respectively. From these calculations we see that (8-112) is not reliable, and (8-113) and its general form (8-111) provide a good upper bound directivity prediction for the square-root cosine element pattern array.

To produce radiation in only one hemisphere, arrays are often operated with a conducting ground plane backing the elements. The same principle applies to the single element case illustrated in Fig. 3-20. For example, a linear array backed by a ground plane can be analyzed by removing the ground plane and introducing images of the elements, forming a planar array; Probs. 8.8-2 and -3 are arrays of this type. The patterns of planar arrays can be found using sequential linear array analysis if sufficient symmetry exists. One row is considered as an "element" and its array pattern is multiplied by that of a column, considered as a linear array; Prob. 8.8-4 is an example. Grids other than rectangular are used. The triangular grid can offer similar pattern performance but requiring fewer elements; Prob. 8.8-6 compares a square grid to a triangular one of the same array area.

There are many applications for non-planar arrays such as a *conformal array* that conforms to an aircraft surface, to the superstructure of a ship, or to the skin of missile. The techniques used in this section can be used to find the radiation pattern for conformal arrays.

Directivity usually must be found by numerical integration. More examples and details on analysis techniques are available in [H.8.2: Haupt, Chap. 5] and [H.8.2: Visser, Chap. 10]. An interesting array configuration is one that uses linearly polarized elements to produce circularly polarized radiation. The planar array is made of 2×2 subarrays of four linearly polarized elements with angular orientations of 0°, 90°, 180°, and 270°, and phased in the same way. This array is preferred over one using circularly polarized elements because circularly polarized elements require more complicated feed hardware, leading to more loss, weight, and cost.

The largest antennas found in practice are arrays and are used to achieve high directivity or narrow beamwidth. Arrays are preferred to a single large continuous aperture antenna, such as a reflector, because of its large physical size and corresponding weight, complexity, and cost. Radio astronomy applications have several very large arrays in use or in the planning stages made up of thousands of elements and some have element separations of many kilometers. There are also many radars employing arrays, as will be discussed in the next section.

8.9 PHASED ARRAYS AND ARRAY FEEDING TECHNIQUES

It is often required that the antenna main beam pointing direction be varied with time, which is referred to as scanning. Scanning can be accomplished mechanically or electronically. Mechanical scan is achieved by slewing the entire antenna, which can be any

type of antenna but most often is a reflector antenna or a fixed-phase array. However, mechanical scan requires a positioning system that can be large and costly, and mechanical scan is often too slow. The alternative is to use a **phased array**, which is an array whose phase (or time delay) at each element is controlled to steer the pattern in angular space. Phased arrays offer the advantage of electronic-speed, inertia-less scanning with the ability to track multiple targets (users) simultaneously. In general, the magnitude and phases of elements can be controlled for low side lobes or to shape the main beam. Phased arrays find applications in radar, sensing, and communications. In radar, targets can be tracked to obtain their angular coordinates for surveillance. In communications, the array radiation pattern can be adjusted for varying traffic conditions such as mobile users changing location. In this section, we review electronic scanning principles along with practical constraints. This is followed by the topics of feed networks and associated enabling technologies, and operational phased arrays—past, present, and future.

8.9.1 Scan Principles

The simple formulas developed in Sec. 8.3.2 for calculating the linear phase taper across an array required to steer the pattern main beam to a desired angle holds for all linear arrays and is easily extended to other array geometries. The element phases are adjusted to form a phase front that is planar and oriented to steer the main beam in a direction normal to the formed planar wavefront.

The array factor for a linear array in (8-53) can be generalized to include element phases with a linear portion $\{\alpha_n\}$ and a nonlinear portion $\{\delta_n\}$, and to include arbitrarily positioned elements:

$$\mathrm{AF}(\theta) = \sum_{n=0}^{N-1} I_n e^{j\xi_n} = \sum_{n=0}^{N-1} A_n e^{j(\alpha_n+\delta_n)} e^{j\xi_n} \tag{8-114}$$

The spatial phase for the nth element located on the z-axis at z_n is

$$\xi_n = \beta z_n \cos\theta \tag{8-115}$$

The current for the nth element has magnitude A_n and phase $\alpha_n + \delta_n$. The phases $\{\alpha_n\}$ vary linearly with position in the array and determine the main beam maximum direction from

$$\alpha_n = -\beta z_n \cos\theta_o \tag{8-116}$$

and are referred to as *linear phase*, or *uniform progressive phase*. For an equally spaced array, $z_n = nd$ and $\alpha_n = n\alpha$ where $\alpha = -\beta d \cos\theta_o$ as in (8-25). Nonlinear phases $\{\delta_n\}$ can be used for pattern shaping (see Chap. 10).

As the pattern of an array is scanned off broadside, the main beam widens. This effect is called *beam broadening*. We illustrate this for a linear array of five isotropic elements spaced 0.4λ apart. Fig. 8-29 shows a series of patterns for increasing off-broadside scan angles. Notice the increase in the beamwidth of the main beam with scan off broadside. The full pattern for this array is obtained by rotating the pattern about the z-axis. Two examples of three-dimensional patterns are shown in Figs. 8-29*b* and 8-29*f*. As the main beam is scanned away from broadside, the increase in beam solid angle of the main beam is just about compensated for by the reduced solid angle of the total pattern (formed by rotation of the pattern about the array axis). Thus, directivity of the array factor remains relatively constant, with scan for spacings less than a half-wavelength and for scan angles not close to endfire; see Fig. 8-18. For spacings slightly greater than a half-wavelength, a grating lobe begins to appear for scan angles near endfire and the directivity decreases; again, refer to Fig. 8-18. Since isotropic elements were assumed, these remarks apply to

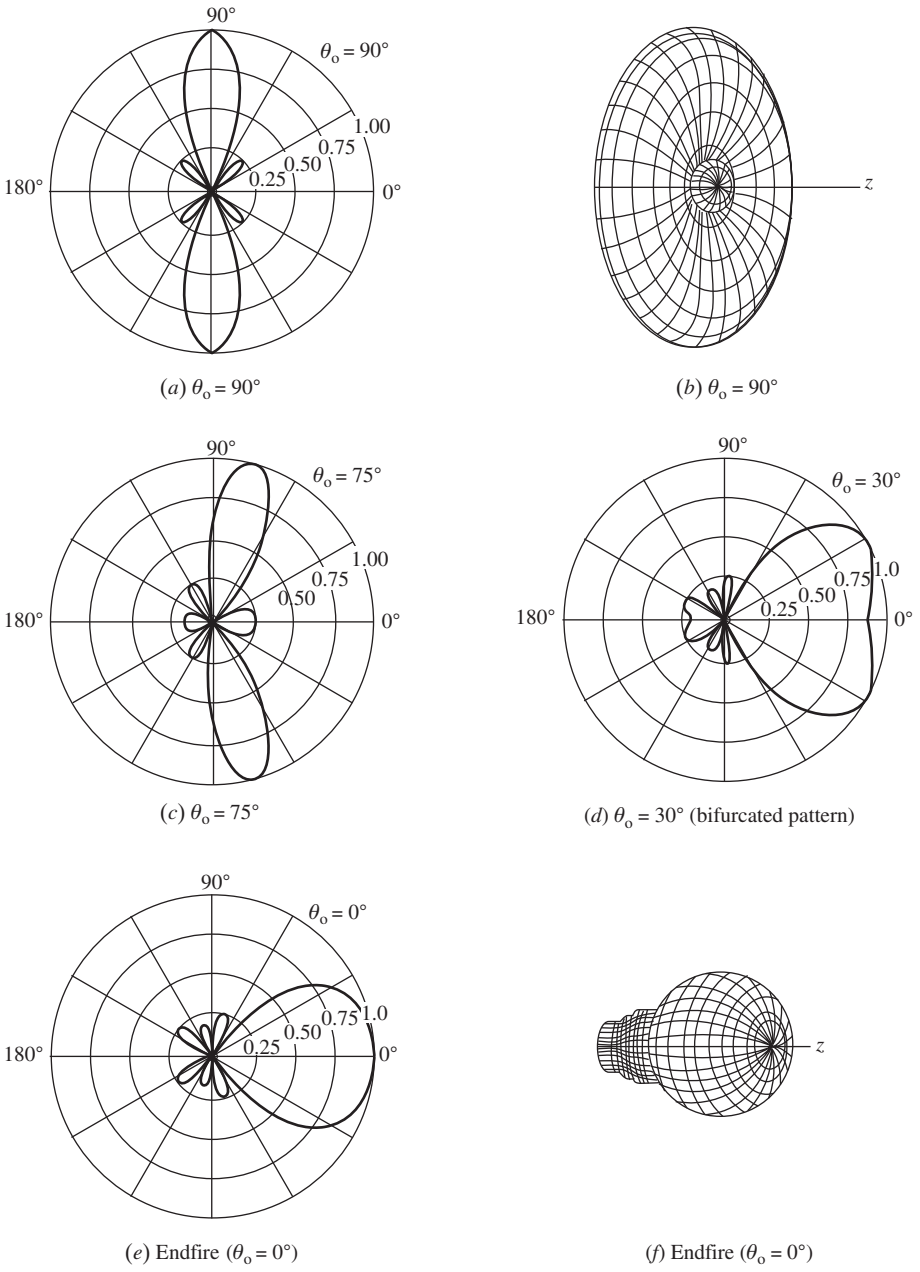

Figure 8-29 Example of phase-scanned patterns for a five-element linear array along the z-axis with isotropic elements equally spaced at $d = 0.4\lambda$ and with uniform current magnitudes for various main beam pointing angles θ_o.

array factors. When the element pattern effects are included for the case of a directive, broadside element pattern, directivity will decrease with scan angle.

As we noted in Sec. 8.2, for half-wavelength spacings there is exactly one period of the array factor in the visible region and no grating lobe will be visible, except for endfire operation that produces two endfire beams. For spacings larger than a half-wavelength, part or all of a grating lobe may be visible depending on scan angle. For one wavelength

spacing or more, there will be visible grating lobes. When spacings of several wavelengths are used, many grating lobes are visible (see Fig. 8-3 for a simple example) and the array is called an **interferometer**. Each major lobe has a narrow beamwidth but there are many of them. Large element spacings, however, permit electrically large elements with relatively narrow beamwidth patterns that act to decrease the size of the grating lobes. In normal applications, grating lobes limit the performance of phased arrays and are to be avoided. Grating lobe peaks will be not appear in the visible region if element spacings are restricted as follows:

$$d < \frac{\lambda}{1 + |\cos\theta_o|} \quad \textit{to avoid grating lobes} \tag{8-117}$$

where θ_o is the main beam pointing angle with respect to the line of the array corresponding to the largest scan angle off broadside. This relation is derived by solving (8-27) for the first grating lobe at $\psi = 2\pi$, where $\theta = 0^\circ$. For broadside operation, $\theta_o = 90^\circ$ and (8-117) gives $d < \lambda$. If scanning to endfire ($\theta_o = 0,\ 180^\circ$) is desired, then $d < \lambda/2$. This result is based on an omnidirectional element pattern in the plane of scan. Larger spacings are permitted for directive element patterns since they diminish the effect of grating lobes.

The principles required of scanning multidimensional arrays were covered in the previous section. The expression for determining the phases of the *mn*th elements located at positions $(x'_{mn}, y'_{mn}, z'_{mn})$ needed to steer the beam peak of the array factor to the angle (θ_o, ϕ_o) is given in (8-108). For planar arrays, the orientation of the array that provides the most convenient mathematical formulation is for element centers located in the *xy*-plane. This makes the direction broadside to the array the *z*-direction, and then the angle θ is the angle off broadside. In contrast, for linear arrays we placed elements along the *z*-axis, making θ the angle relative to endfire, not broadside. In the remainder of this chapter, the *z*-axis is normal to the array, and *scan angle* refers to the angle the beam peak is scanned away from broadside.

The complete pattern of a phased array is found by multiplying the array factor by the element pattern as in (8-54). The important subtlety in pattern multiplication is that while the array factor scans with phase change the element pattern remains fixed. *As a phased array is steered, the peak of the total array pattern follows the element pattern shape*. Fig. 8-30 shows a linear array operated for a broadside beam and for scan to 30° off broadside. The array is four 0.7-λ spaced elements that have uniform current magnitudes and phases as required to steer the array factor. The element pattern (dashed curve), $\cos^2\theta$, is unaffected by the scan angle, which has several effects on the total array pattern (solid curve). First, the peak of the main beam is reduced by the level of the element pattern at the angle of interest. In this case, the scanned beam peak is reduced to 0.77, for a 2.3-dB scan loss. Second, the beam peak direction does not go to the desired angle of 30° off broadside. Instead, the actual scan angle is a few degrees less than desired. The final effect on the scanned pattern is the altering of the whole pattern from the array factor shape. But this distortion can actually be an improvement. In the example in Fig. 8-30*b*, the side lobe at $\theta = -50^\circ$ is a remnant of a full grating lobe the array factor has at -68°. So the element pattern acts to greatly reduce grating lobes in scanned patterns. These are general trends in array scanning. Mutual coupling effects can be included for scanned patterns using (8-105), where the mutual coupling effects are included in the average active-element pattern. The array grid of planar arrays controls the grating lobes. The scan performance of a rectangular-grid array behaves like the projected linear array in the scan plane.

The pattern and the element impedances of phased arrays vary with scan angle because the mutual coupling changes. The input impedance influence is evident in (8-99) because as the phases of the currents $\{I_n\}$ are changed to scan the beam the summation of mutual impedances weighted by the currents changes. The most serious effect is *scan blindness,* which is manifested by a dramatic reduction in radiated power due to high reflection

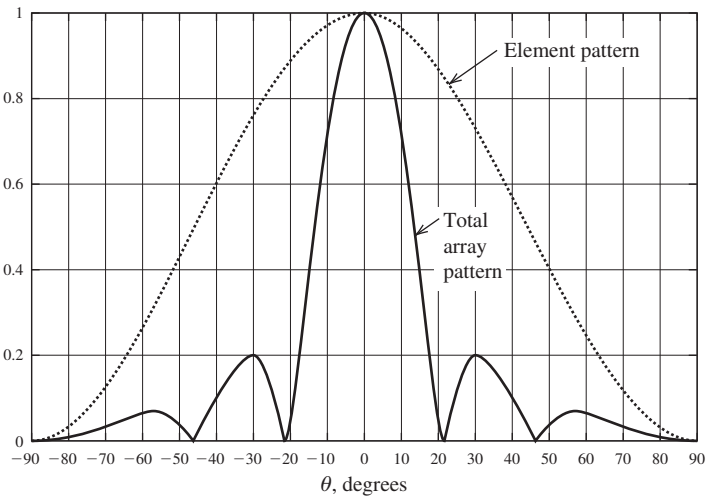

(*a*) Brodside case.

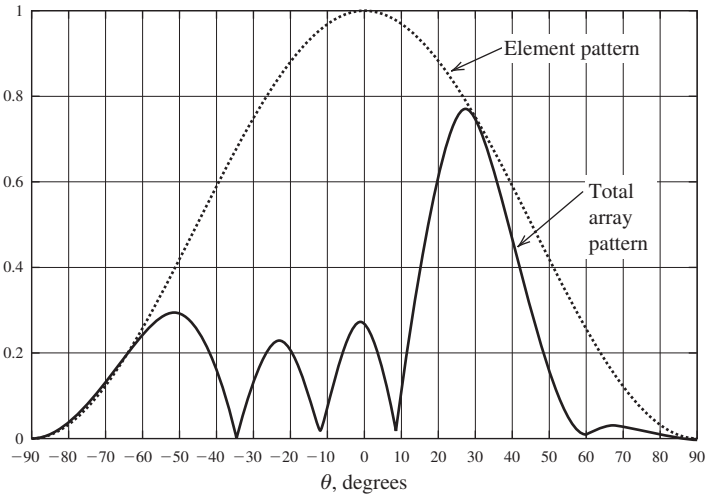

(*b*) Phased to scan to 30°.

Figure 8-30 The total array pattern (solid curve) for a four-element linear array that has 0.7 λ spacings, uniform excitation magnitudes, and excitation phases for (*a*) broadside operation and (*b*) scanned 30° off broadside. The element pattern (dashed curve) is $\cos^2\theta$. Note that the element pattern remains stationary during scan.

when the array is scanned to a blindness angle. In the transmitting case, when the feed network is configured to steer the beam to a blind scan angle there is power reflected back into the transmitter, which can cause damage. If $\Gamma_m(\theta_o, \phi_o)$ is the *active reflection coefficient* of the *m*th element in a fully excited phased array, the power delivered to that element is

$$P_m(\theta_o, \phi_o) = P_{inc}\left[1 - |\Gamma_m(\theta_o, \phi_o)|^2\right] \tag{8-118}$$

where (4-41) was used and P_{inc} is the incident power. From this we can find the gain of the *m*th element operating in presence of the other elements [16], called an *element-gain pattern*:

$$G_{\mathrm{EG}}^{m}(\theta_o, \phi_o) = G_i(\theta_o, \phi_o)\left[1 - |\Gamma_m(\theta_o, \phi_o)|^2\right] \tag{8-119}$$

where $G_i(\theta_o, \phi_o)$ is the gain pattern of an isolated element, that is, $G_i \ |F(\theta, \phi)|^2$. It is a realized gain because impedance mismatch effects due to mutual coupling are included, although feed network impedance matches are not. It is proportional to the active element pattern, so (8-119) is essentially an active element-gain pattern. In an infinite array, all element patterns are identical. In a large array with small edge effects (to be discussed shortly), the element-gain patterns of all elements except those near the edge are nearly identical and an *average element-gain pattern* (developed similarly to the pattern expression of (8-105)) can be used in (8-119) to give:

$$G_{\mathrm{EG}}(\theta_o, \phi_o) = G_i(\theta_o, \phi_o)\left[1 - |\Gamma(\theta_o, \phi_o)|^2\right] \tag{8-120}$$

where $\Gamma(\theta_o, \phi_o)$ is the reflection coefficient of a central element in the array. Usually an array is nearly matched at broadside, so $\Gamma(0, 0) = 0$, and impedance mismatch increases with scan angle.

In an infinite array, a complete mismatch occurs at the blindness angle, if it exists, when $|\Gamma(\theta_o, \phi_o)| = 1$. Then (8-120) shows that the average element-gain pattern goes to zero. In finite arrays, the blindness effect does not yield complete mismatch, but there can still be significant mismatch in large arrays. Scan blindness is associated with surface wave–like phenomena and usually occurs for spacing values less than a wavelength and at a scan angle less than that for which grating lobes occur in (8-117), and thus is often the factor limiting the scan range of a phased array. Scan blindness varies with the scan plane. In planar arrays of dipoles mismatches are larger for scan in the *E*-plane than in the *H*-plane. This is illustrated in Fig. 14-28, which plots the input impedance of a central element in a planar array of dipoles as a function of scan angle. The real part of the input impedance approaches zero in the *E*-plane, but not in the *H*-plane. In the *E*-plane, the dipole creates an electric field component perpendicular to the ground plane that can set up a surface wave, whereas in the *H*-plane the electric field from the dipole traveling along the array face is parallel to the ground plane and is shorted out. For arrays printed on a dielectric substrate, the blindness angle moves toward broadside as dielectric thickness is increased. [13] If the feed network resides on a common dielectric substrate, an additional blindness effect, called "feed blindness," can occur which has behavior opposite that of surface-wave blindness. The feed blindness scan angle moves toward endfire rather than broadside as dielectric loading increases. [17] The best way to avoid scan blindness effects is to use small element spacing, typically under a half-wavelength. Blindness effects can also be reduced by using subarrays, which are clusters of neighboring elements fed with the same excitation. [18] But subarraying introduces additional grating lobes.

Reducing the mutual coupling will help reduce blindness effects. Adding conducting fences between elements helps, as mentioned in Sec. 8.7.2. Placing elements in cavities has been used to reduce surface waves and improve blindness. [19] For more details on scan blindness and its mitigation see [H.6: Hansen, Vol. II]. Pozar [13] recommends using array designs that limit the maximum scan angle to about 10° less than the scan blindness angle.

Techniques are available for analyzing infinite arrays that take advantage of the unending periodicity. [H.6: Hansen, Vol. II, Chap. 3; Haupt: H.8.2, Sec. 6.5] An infinite array with a regular grid presents the same operating environment to each element. So the active element patterns, reflection coefficient, and input impedance for each element are identical. The pattern of the full infinite array is in theory an impulse function (giving infinite directivity) which traces out the element pattern as scan angle is varied. Infinite array analysis is useful in determining element performance of the central elements of a finite array of the same type. As with linear arrays discussed in Sec. 8.7.2, the patterns of elements near the edge of an array differ from that for centrally located elements.

As array size increases, the array pattern becomes more accurately predicted from the pattern multiplication formula of (8-105) using the average active-element pattern and array factor. The array size for which this formula is acceptable depends on the element type, array geometry, and other factors. An experimental study with microstrip elements found that a 7×7 array is sufficiently large. [20] For a planar array of half-wave spaced printed dipoles, an array size of 19×19 was found to be large enough for the active reflection coefficient to behave similar to being in an infinite array. [13] This is consistent with the general guideline of $10\,\lambda$ per side. [H.8.2: Mailloux, 2nd ed., p. 71].

Array size is usually driven by the requirements on resolution (width of the main beam) or gain (directivity reduced by efficiencies), which is also affected by element spacing. It is desirable to have wide element spacing (approaching a wavelength), which reduces the number of elements and the associated costs for elements and the feed network. However, the maximum scan angle limits how far apart elements can be in order to avoid grating lobes as given by (8-117) and to avoid scan blindness.

8.9.2 Feed Networks and Array Technology

As mentioned in Sec. 8.1, phased arrays offer the unique advantages of electronic-speed beam scanning without mechanical motion. Additional unique features are the capability of tracking multiple targets (or users) that are in different directions, dynamic pattern control, and graceful degradation as elements fail. In addition, beam nulls can be formed to cancel jamming signals (or interference). Design for low radar cross section (see Sec. 4.6) is possible by redirecting an enemy jamming signal away from the direction back toward the threat. The many attractive features of arrays come with the penalty that each element of an array must have a transmission path to the receiver (or transmitter). In addition, a phased array requires hardware and software to control the phase of the elements. The usual choice that is faced when deciding on a high-gain antenna is between a reflector with a simple feed system but with a large steering mechanism and a phased array with low-weight electronic scanning but a large feed network.

The possible array feed network architectures are shown in Fig. 8-31. The parallel and series feeds follow directly from circuit concepts. The *parallel feed* shown in Fig. 8-31*a* is the network form that we have assumed thus far and is the most common. It is also called a corporate feed that looks like the organizational diagram of a corporation. It has the desirable characteristic of equal line length to each element, making the network symmetric that helps with balancing mutual coupling effects. Most important, the signal phase and amplitude to each element is naturally identical, as often used in practice. The equal line lengths also make the network frequency independent, and thus wide bandwidth. The *series feed* of Fig. 8-31*b* offers advantages of simple construction a compact structure. A waveguide slot array is a popular series-fed array; example slots are shown in Fig. 8-35*b*. A disadvantage of the series feed is that the common feed line attenuates the signal to successive elements, causing loss and complicating the design. Series-fed arrays offer the possibility of *frequency scanning* by changing frequency which changes the electrical line length between elements, and thus the phase. One realization of a series feed is the "serpentine" waveguide feed which is a waveguide bent into a serpentine similar to the shape in Fig. 8-31*b* with radiating elements, usually dipoles, with probes tapped into the waveguide. Phase shifters can be inserted into the connecting series transmission lines or in the individual element feed lines. A series feed introduces dispersion that distorts short pulses and limits bandwidth.

The preceding feeds are sometimes referred to as "constrained" feeds because of the physical constraint of continuous connectivity from the feed to the elements. In contrast, the *space feed* uses a primary antenna illuminating a separate unit (sometimes called an "active lens") consisting of pickup elements connected to a secondary radiating array face, as illustrated in Fig. 8-31*c* for the transmitting case. Typically only used for large phased arrays, the space feed array takes advantage of the free space environment

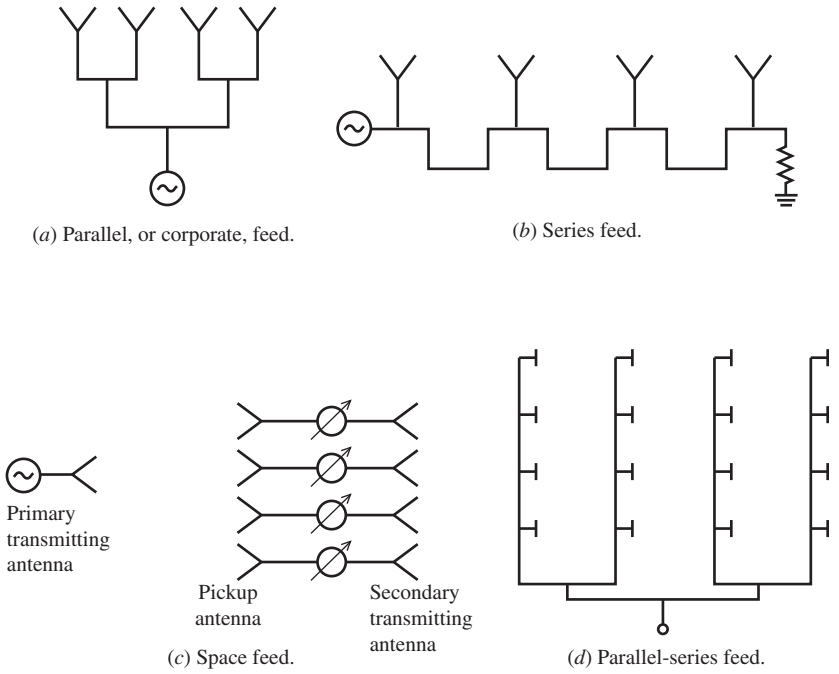

Figure 8-31 Types of array feed networks.

between the primary feed and the pickup array, leading to size, weight, and cost reduction compared to a fully connected feed network. The amplitude distribution of the array is determined by the primary feed pattern and the pickup array element placements. The phase introduced by the different path lengths from the primary feed to each pickup element is compensated for by the phase shifters on the radiating elements, which also are used for beam scanning. Just as with a reflector antenna, there is spillover loss associated with the primary feed power missing the pickup array. It is common to taper the amplitude distribution across the secondary radiating array to reduce side lobes by "thinning" the array by not connecting some elements. The elements are not removed but are dummy loaded to present a regular impedance environment to the active elements. This is called *density tapering*. The primary feed is often configured with a central feed antenna, usually a horn, surrounded by two pairs of horns, one pair in each plane, for producing difference patterns with a null on axis for direction finding in the vertical and horizontal planes. A related feed method is the *reflectarray*, which has a primary feed illuminating an array which receives, processes, and transmits a formed beam back in the direction of the feed, appearing to reflect the signal. [H.6: *Ant. Eng. Hdbk.*, 4th ed., Chap. 35] Scanning is possible by including phase shift functionality into the array.

The three feed architectures were illustrated as linear arrays, but the concept is easily extended to multidimensional arrays. The corporate feed network will become very large for arrays with many elements. The space feed is an alternative, but the *hybrid feed* of Fig. 8-31*d* is more commonly used. It is shown as a parallel-series hybrid with the rows fed in parallel and the columns series fed. By inserting phase shifters in the legs of the parallel feed the pattern can be steered in the azimuth plane (left-right as shown). The parallel-parallel hybrid feed facilitates the use of subarrays that have the same amplitude and/or phase in each element of the subarray.

Physical construction of the feed network and its associated components behind the array face is in one of two forms, brick or tile. [H.8.2: Mailloux, 2nd ed., p. 46] In *brick* construction, the complete feed hardware modules for one element (or a few elements),

often including the element itself and all in a monolithic or hybrid integrated circuit, is placed perpendicular to the array face. A brick can be as small as a single module connected to a single element. *Tile* construction consists of several parallel layers with each layer containing the same components performing the same function. For example, there could be separate layers for the elements, phase shifters, and amplifiers. Tiles are more compact than bricks but may have thermal management issues.

Beam scanning is implemented using one of the following methods. The term "phase shifter" often includes any of these means for changing the phase. For more details see [H.8.2: Mailloux, 2nd ed., Sec. 1.3], [H.6: Balanis, Ed., Chap. 25].

Phase shift — The use of phase shifter devices to adjust element phases for beam scanning is the most popular method. Phase can be changed by altering the permeability using a ferrite phase shifter or by changing permittivity (dielectric constant) such as with a ferroelectric phase shifter. Phase shifters are narrow band.

Time delay — Phase shift in time-delay devices is accomplished by adjusting line length, usually by switching in various sections of transmission line.

Hybrid (usually phase-time delay) — Time-delay lines are generally larger than conventional phase shifters, so in applications where time delay is required, time delay and phase shift are combined. This will reduce the spreading of a pulse when the beam is scanned compared to a phase-only feed. [21].

Frequency scanning — Phase is changed by changing frequency, which changes the electrical length of the interconnecting lines and is used with series feeds. Frequency scanned arrays are found in practice, mostly in radars rather than communications where frequency is usually required to be fixed. An example of a series-fed array is a waveguide with slots milled in one wall that act as radiating elements.

Beam switching — Beam scanning could be accomplished by switching between separate antennas pointed in different directions, but the system would be large and complex. Instead, a *beamforming network* (*BFN*) is used to form multiple beams. A BFN that forms N beams has N input ports, one for each beam. By adding a $1 \times N$ switch to the input, beams can be selected by controlling the switch.

Digital beamforming — Beamforming can be achieved in the digital domain by sampling the RF signal at the element level and routing to a digital processor unit for complex weighting (i.e., amplitude and phase control) and summing to form the beam. Multiple simultaneous beams and adaptive features such as interference rejection are possible as well.

Most phase-shifter technologies can be realized in digital as well as analog (allowing adjustment to any phase value) form. An M-bit digital phase shifter provides phase increments in multiples of $360/2^M$ degrees. For example, a 3-bit phase shifter has phase states of 0°, 45°, 90°, 135°, 180°, 225°, 270°, and 315°. These settings are the cumulative phases of the three bits in series in all possible on/off states where the "off" states are 0° and the "on" states are 45°, 90°, and 180°. Arrays in practice typically use from 3 to 7 bits of phase shift. Quantization effects result from using the nearest digital phase state rather than the exact phase, with the main issue being an increase in side lobes. [H.6: Rudge, Vol. 2, Sec. 9.2.4] Similar high-side lobe problems develop when using subarrays with the same phase supplied to all elements in the subarray. [H.8.2: Mailloux, 2nd ed., Sec. 7.3] Also, digital phase shifters will place beams at discrete locations rather than directly toward a user as is possible with analog phase steering. Hybrid use of both digital and analog phase shifters may provide an optimum feed network. [H.6: Balanis, Ed., Sec. 25.5.3]

Delay line phase shifting can be realized by electromechanical adjustment of a "line stretcher," variable length transmission line. However, most time delay phase shifting is done by switching in (or bypassing) fixed-length sections of line. The phase shift in time

delay devices is proportional to frequency just as in a transmission line, leading to wide bandwidth. The frequency proportionality follows from (8-116), where the phase shift for the nth element of a linear array on the z-axis is $\alpha_n = -(2\pi/c)fnd\cos\theta_o$. A delay line with this phase will give a beam peak in the direction θ_o for all frequencies. Time delay is preferred in pulse radar to preserve the pulse shape as the scan angle is changed.

So far we have modeled arrays using unspecified phase shifters and will now discuss how they are implemented. [H.8.2: Mailloux, 2nd ed., Sec. 1.3] Although intrinsically analog, ferrite phase shifters are usually configured as digital phase shifters. Ferrite phase shifters operate by changing the permeability of ferrite material that the wave propagates through. They are often constructed in waveguide and can handle high power levels needed in phased array radars. Due to their large size and weight, they are not often used in space applications and large airborne systems. Diode phase shifters can also be analog or digital. Analog diode phase shifters are realized with Schottky barrier or varactor diodes. Digital diode phase shifters operate by using diodes (PIN, Gallium-Arsenide-based devices, and others) to switch delay lines. Also, MEMS (micro-electromechanical systems) switches are used to switch in fixed sections of line length to give the proper number of bits of phase. In addition to the foregoing through-line devices, phase shifting is also realized in devices configured for reflection from a shorted load. Ferroelectric phase shifters operate by changing the material permittivity via an applied DC voltage. When fully developed they will find wide acceptance because of their desirable characteristics of low weight and low power draw due to being voltage actuated, unlike MEMS-based units. Photonic technology is also employed in array feed networks. [H.8.2: Hansen, 2nd ed., Sec. 6.4] Using open optical beams or fiber optic cables to distribute signals reduces the size and weight of the network compared to conventional metallic feeds. Immunity to RF interference is an added advantage. However, the required converters between optical and RF frequencies are lossy and non-reciprocal.

Beamforming networks are constructed using conventional network techniques or using quasi-optical lenses. [H.8.2: Hansen, 2nd ed., Chap. 10] Conventional constrained networks can be as simple as a series of power dividers that include phase shifters if scanning is required. For example, in Fig. 8-31*a* two-way power dividers are located at the tee junctions, or one four-way power divider could be used. A power divider based network, however, becomes excessively large for more than a moderate number of elements in the array. One of the most popular conventional-network BFNs is the *Butler matrix*, which was introduced in 1961. [22] Compact Butler matrix units are available commercially and find application in smart antennas to be discussed in Sec. 12.4. The Butler matrix essentially performs a fast Fourier transform, radiating a set of beams that are orthogonal so that the signals into one port only appear in the beam associated with that port. A Butler matrix connects a 2^n element array to n input ports that are inputs to the beams. Fig. 8-32 shows a functional diagram of a four-beam Butler matrix. Operation is illustrated for Beam 2 using the highlighted portion of Fig. 8-32. The signal passes through two quadrature hybrid power dividers, denoted "H," each with two input ports on the bottom and two output ports on the top that have equal power outputs that are in-phase (90° out of phase) from the same-side (opposite-side) input ports. Fixed phase shifters of $-45°$ are also used. The resulting outputs of the matrix have equal amplitude and a progressive 45° interelement phase shift. The patterns are shown for half-wavelength element spacing and a $\sin\theta$ element pattern (array along the z-axis). In the isotropic element case, the direction of one beam peak is in the null direction for the other beams, which is the orthogonality property. This is approximately true for the array of Fig. 8-32. The beam peaks are 14.5° and 48.6° off broadside for the isotropic element case and 13.5° and 41° for the $\sin\theta$ element pattern. The beam crossover points at angles 0° and 30° off broadside are 3.7 dB below the beam peaks, which is the same for the $\sin\theta$ element case, except the crossover level is lower at 30° off broadside. Higher-order Butler matrix BFNs behave similarly: An 8×8 matrix for eight beams with a

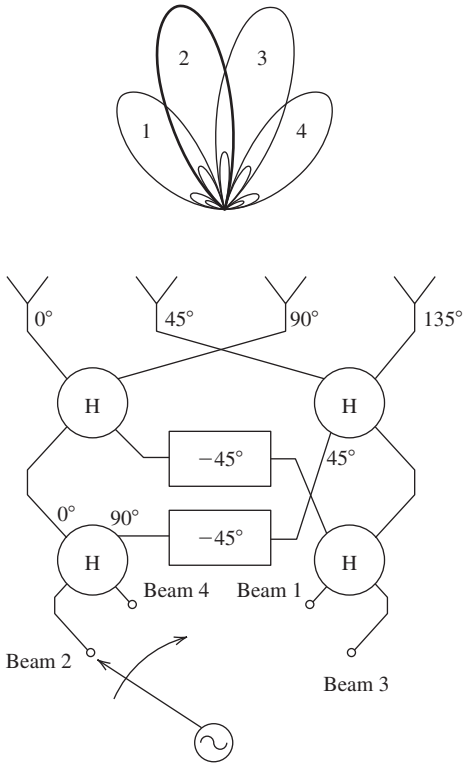

Figure 8-32 Functional diagram of a four-beam Butler matrix beamformer. "H" represents a quadrature hybrid power divider; the input ports are on the bottom, and the two output ports on the top have equal power outputs that are in-phase (90° out of phase) with the same-side (opposite-side) input port. The patterns shown are for half-wave spaced elements with $\sin\theta$ patterns (array on the z-axis). Beam 2 is active and its pattern is shown as bold.

crossover level of −3.9 dB. [H.8.3: Milligan, 2nd ed., p. 595] A BFN can be used in a *multiple beam array*, taking advantage of the orthogonal beam property where simultaneous beams can be processed separately for multiple user (target) tracking or beams can be combined and weighted for special beam shaping.

A second BFN is the *Blass matrix*, which uses transmission lines of the proper lengths to produce time-delay phasing and directional couplers to produce multiple beams. Although not as compact as the Butler matrix, it is inherently wideband. [H.8.2: Mailloux, 2nd ed., Sec. 8.1.3] Quasi-optical beamformers find use in applications calling for wide bandwidth, where the Butler matrix falls short; however, they are generally bulky and heavy. Here we mention two prominent examples, and a more detailed treatment is found in [H.8.2: Hansen, 2nd ed., Sec. 10.2.2]. The *Luneberg lens* is a spherical dielectric with relative permittivity that decreases from 2 at the center to unity at the surface. This yields the unique property that an incident signal (implemented with a small horn antenna) on the surface produces an output beam directly opposite. Multiple feeds produce multiple radiated beams. Functioning in similar fashion to the Luneberg lens is the *Rotman lens*, constructed with parallel plate waveguide, stripline, or microstrip media. Finally, we mention *parasitic beamforming*, in which only a few elements in an array are active while others are passive but have controlled loads. [H.9.1: Thiel and Smith] For example, an active monopole with parasitic monopoles on each side can be beam-steered 180° by switching between two parasitic monopole states of first having the left one shorted and the right one open loaded, and second reversing these load conditions.

The most flexible array is a *fully distributed array* (also called an *active aperture*) in which all RF functions (phase shift, up conversion, amplification in the transmit chain, and low noise amplifier and down conversion in the receive chain) are present for each element. This architecture is used in *digital beamforming*, which is the application of

digital technology to array antenna technology.[4] A digital beamforming array consists of array elements followed by transceivers that down convert and digitize signals that then stream into a digital signal processor unit. This unit supplies amplitude and phase weights to each element, which permits beam shaping, beam steering, multiple beamforming, and adaptive beamforming (which is used in smart antennas, discussed in Sec. 12.4). These features are possible because the digital signal processor unit has all array element output information available, in contrast to a conventional analog beamformer that outputs a weighted sum of the element signals.

Feed network construction usually employs the same technology as the element uses. For example, microstrip elements are fed by microstrip feed lines, and horn or open-ended waveguide elements are connected to waveguide phase shifters. For small arrays, coaxial cables are often sufficient for the feed. Modern phased arrays make use of transmit-receive (T/R) modules that provide full duplex (simultaneous transmit and receive functions). The critical components in T/R modules are a low-noise amplifier on receive and a power amplifier in the transmit path, both usually constructed in MMIC (monolithic microwave integrated circuits). [H.8.2: Fourikis, Sec. 4.6] In digital beamformers, analog-to-digital converters are also included.

8.9.3 Operational Array Examples and the Future of Arrays

Radars made early use of arrays. The SCR-270 radar was a fixed-phase array in an 8×4 element configuration (horizontal $\times$ vertical) that was mechanically rotated in azimuth and operated at about 110 MHz. One of SCR-270 radars detected the planes approaching Hawaii in December 1941, but there was no military response, resulting in the attack on Pearl Harbor. Prompted by military preparedness concerns, phased array development programs started in the 1930s, resulting in the first phased array in 1937. Since that time there have been many technology developments that expanded capability, improved performance, and lowered cost, including RF electronics (transmit/receive active devices), feed network components (power dividers, phase shifters, etc.), signal processing units, and antenna elements (discussed in the next section). Further history of phased arrays can be found in [H.8.2: Visser, Chap. 2].

Now we consider some examples of operational arrays; more examples are found in [H.8.2: Fourikis, Chap. 1]. Arrays are used for land, sea, air, and space applications. Here we present two arrays in some detail. The first is a small flat-plate array, the AN PPS-18 radar, and the second is the large airborne AWACS phased array. The PPS-18 is mounted with the array face vertical and rotated mechanically to locate moving personnel by Doppler radar techniques. Azimuth angle is read off the mechanical positioner, and the range in steps of 25 m is determined out to 3 km from radar return delay time. The antenna consists of 256 bow-tie elements built up from 2×2 subarrays fed in parallel. Fig. 8-33 shows the top of the substrate along the other halves of two elements on the bottom of the substrate. The operating band is 9 to 9.5 GHz ($f_c = 9.25$ GHz and $\lambda_c = 3.24$ cm) so the element spacing of 2 cm in both dimensions is $d = 0.61\,\lambda_c$. The array area is $A_p = 32 \cdot 32 = 1{,}024\,\text{cm}^2$. Using the stated beamwidth in both principal planes of 6° in (4-57) gives $G_{\text{app}} = 26{,}000/36 = 28.6$ dB, which compares to the specified gain of 27 dB. From $G = \varepsilon_{\text{ap}}(4\pi/\lambda^2)\text{A}_\text{p}$ in (9-78), the aperture efficiency is found to be $\varepsilon_{\text{ap}} = 41\%$.

The Airborne Warning and Control System (AWACS) is an impressive example of an airborne phased array that has been in operation since 1977. The antenna is inside a rotating radome mounted on top of a U.S. Air Force E-3 (Boeing 707) airplane, shown in Fig. 8-34*a*. The array is the waveguide slot array with over 4,000 slots shown in

[4] Sometimes feed networks that use digital phase shifters are also referred to as digital beamformers.

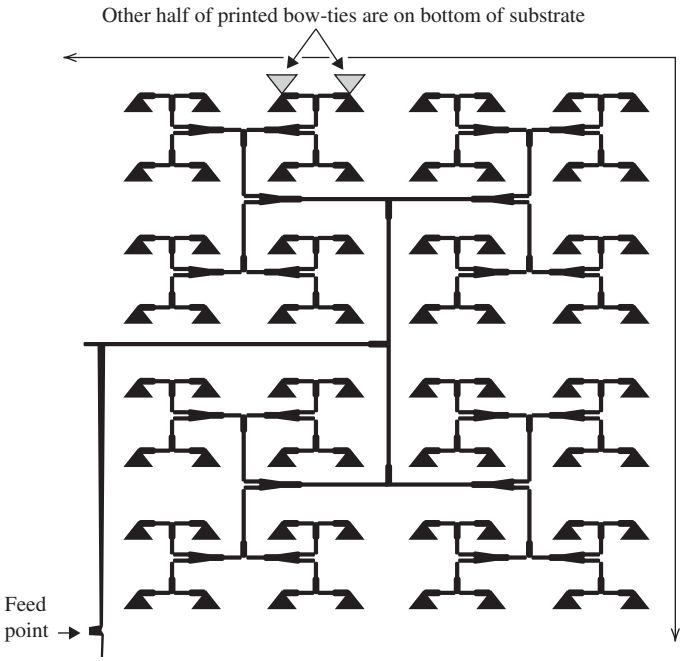

Figure 8-33 The upper right quadrant of the AN/PPS-18 Doppler radar flat-plate array. The full array has 256 bow-tie elements. The other half of the bow-tie elements (shown as dotted for two) are on the bottom of the substrate.

Fig. 8-34*b*; slot arrays are discussed in the next section. It is a hybrid parallel-series array of the type in Fig. 8-31*d*. The waveguides with series-fed slots go out in both horizontal directions from the center feed. In the vertical direction, the 28 waveguides are fed in parallel, each with a phase shifter for scanning in elevation. The entire array rotates 10 revolutions per minute for azimuth coverage. Side lobes below -40 dB are needed to distinguish low-flying aircraft targets from clutter as far as 400 km away.

In the field of antennas, the future is probably most promising for arrays. Array technology is evolving toward integration of transmit/receive modules and associated controllers, which, when affordable, enable many applications. Traditionally an antenna has been treated as a stand-alone device, but antennas are evolving into subsystems. This is especially true for digital arrays where, in fact, it is hard to even identify where the antenna is because many of its functions are embedded in software and digital processing. Arrays offer the opportunity for combining several separate functions in a single antenna using a *multifunctional antenna*. For example, the many antennas protruding from a vehicle will be replaced by one multifunctional array conforming to the surface of the vehicle. A complete multifunctional antenna performs tasks of communications over several bands and waveforms, as well as radar, sensing, and countermeasure tasks. Antennas of the future will be fully distributed digital beamforming arrays that are wideband covering more than 10 : 1 bandwidth and will support multiple polarizations. To make this possible, the enabling technologies must continue to develop by lowering the size and cost of components. There is a need for fabricating feed hardware, including several radiating elements, into a single transceiver-antenna element unit affordably. Also needed are commercial products of ferroelectric phase shifters and of MEMS switches for reconfigurable arrays. Photonic feed networks may find wider use also. As arrays develop in this fashion, reflector antennas and complex analog arrays will give way to digital beamforming arrays.

(*a*) The Boeing 707 showing the radome containing the antenna.
(Courtesy of The Boeing Company. Used with permission.)

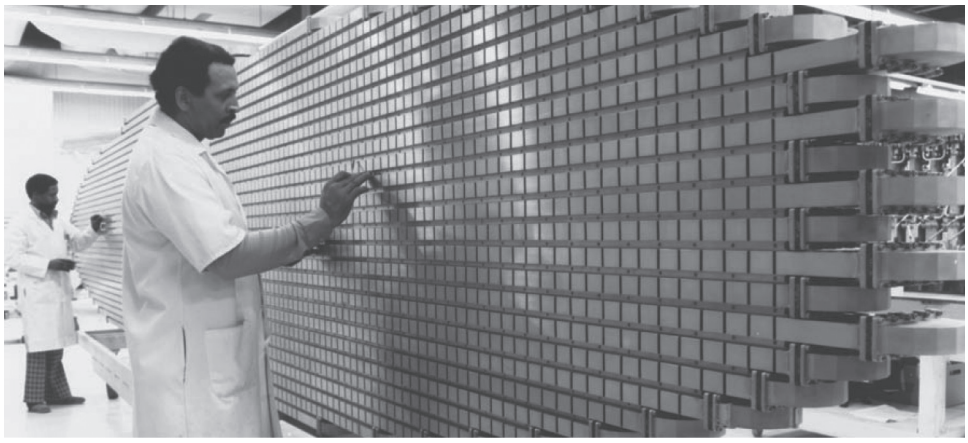

(*b*) The waveguide slot phased array antenna.
(Courtesy of Northrop Grumman Corporation. Used with permission.)

Figure 8-34 The AWACS surveillance system.

8.10 ELEMENTS FOR ARRAYS

Array elements are selected based on the application for the array. An array can be a *fixed-phase array*, also called a *flat-plate array*, or a phased array. Fixed-phase arrays do not have a means to adjust the phase to the elements and thus have a pattern that is fixed in space. They are often used as replacements for reflector antennas and offer the advantage of a thinner, more appealing appearance. Flat-plate arrays are used in many parts of the world for reception of television programming via satellite or terrestrial signals. Some military radars use flat-plate arrays that are mechanically steered in the azimuth plane (i.e., parallel to the ground), such as in Fig. 8-33. Fixed-phase arrays also permit the use of narrow beam elements of moderate gain such as helix, Yagi-Uda, and horn antennas. These elements, of course, are not appropriate for use in a flat-plate array because they are long, making the array a deep structure. Wide element spacing is possible because grating lobe effects are minimized by the broadside-only operation and the narrow element pattern. Widely spaced element arrays allow the use of fewer elements for lower weight and cost. They are often used in mechanical-tracking satellite Earth terminals. As material costs decrease, flat-plate arrays will find more applications.

Phased array elements must support the desired angular range of electronic scan. Most importantly the element pattern needs to be wide enough to avoid significant gain loss with scan angle; the scan loss effect is illustrated by example in Fig. 8-30. Secondly, the element spacing should be small enough to avoid grating lobes as guided by the limit in (8-117). Third, impedance match will vary with scan angle, and the array element and array geometry should be selected to avoid scan blindness, which was discussed in Sec. 8.9.1. These considerations generally lead to the guideline that increasing scan angle requires closer element spacing. This, in turn, requires the elements to be smaller in size in order to fit into a decreasing cell area for the grid. For wide bandwidth applications, to be discussed in the next section, we will see that element spacing, and thus element size, must be reduced as bandwidth is increased. Therefore, there is considerable emphasis on using a compact element, at least in the dimensions of the array grid (x- and y-directions for the planar array of Fig. 8-28). In the remaining dimension (z-direction for our planar array example), the element can be large if the application permits. The depth of an element may not be important for fixed antennas on land and sea platforms, where size and weight are less important than for air and space vehicles. The requirement for a low profile (i.e., shallow depth) will further limit the choices of element type. Before discussing specific element types, we review general goals for element performance; more details on phased array specifications and evaluation are found in [H.6: Lo and Lee, Eds., Chap. 18].

For scanning in any plane, an element pattern that is rotationally symmetric (i.e., balanced) is desired. This prompts the concept of an ideal element pattern. The directivity expression in (8-110) indicates that one cell of a planar array in the xy-plane has directivity proportional to its area, A_{Cell}. Directivity as a function of angle varies as the projection of the cell area $\cos\theta$ viewed from angle θ off broadside as reasoned by Hannan [8]. This is similar to the element pattern for a linear current segment along the z-axis, which is $\sin\theta$ from (2-116) and is the projection factor for the length of the segment viewed from angle θ. The corresponding field pattern for the cell area is $\cos^{1/2}\theta$, which is called the *ideal element pattern* as proposed by Wheeler [23]. The average active element-gain pattern including impedance mismatch created by mutual coupling is given by (8-120) as $G_i(\theta,\phi)[1-|\Gamma(\theta,\phi)|^2]$, which is the gain variation with angle of an element with all other elements terminated in matched loads. The angular variation of the isolated element-gain pattern (normalized pattern) is approximated as $\cos\theta$, which is the square of the ideal element pattern to make it a power pattern. The maximum directivity of a cell in the array in (8-110) extends to gain as a function of angle by including the angular variation and impedance mismatch just mentioned, giving the *ideal element-gain pattern*:

$$G_{\text{EG, ideal}}(\theta,\phi) = \frac{4\pi}{\lambda^2} A_{\text{Cell}} \left[1-|\Gamma(\theta,\phi)|^2\right] \cos\theta \tag{8-121}$$

If the array is infinitely large, the element patterns will be identical and often well approximated by (8-121). In finite arrays, of course, element patterns vary with location in the array. But for sufficiently large finite arrays, the full array gain is often approximated by multiplying by the number of elements, as discussed in Sec. 8.8. An approximation for the gain of the full array as a function of scan angle with all elements excited adding in-phase in direction (θ,ϕ) is to assume that the equal power supplied to all N elements adds, giving $G_{\text{Array}}(\theta,\phi) = N\ G_{\text{EG, ideal}}(\theta,\phi)$. This does not include array pattern effects, just gain variation with scan angle. It follows from the discussion in Sec. 8.8 for directivity approximations and is discussed further in [H.6: Hansen, Vol. II, p. 303].

A perfect element would be impedance matched for all angles $(1-|\Gamma(\theta,\phi)|^2 = 1)$. The peak gain at $\theta = 0$ in (8-121) of a planar array of half-spaced elements $(d = d_x = d_y = \lambda/2)$ would be $G_{\text{MaxEle}} = 4\pi(\lambda/2)^2/\lambda^2 = \pi = 5\,\text{dB}$. Thus, a perfect element has a

Table 8-2 Elements for Array Antennas

Element	Examples	Advantages; Disadvantages
Dipole-based elements, backed by a ground plane		
Dipole	Fig. 3-20 Fig. 8-35*a*	Wide beam, simple structure; narrow band
Bow-tie	Fig. 7-32	Wide beam, simple structure, broadband
Microstrip elements	Sec. 11.2	Wide beam, low-profile; narrow band in basic form
Slot elements	Fig. 8-35*b* Fig. 8-34*b*	High-power applications; many are narrow band
Aperture elements		
Open-ended waveguide	Fig. 9-9	Compact, moderate bandwidth; bulky structure
Horn antenna	Fig. 9-11	Moderate bandwidth, fewer array elements; limited scan due to wide spacing
Tapered slot antennas	Fig. 8-35*c* and *d*	Wide beam, broadband; not low-profile
Low-profile, broadband elements	Fig. 8-38 Sec. 8-11	Broadband, low-profile

unidirectional $\cos^{1/2}\theta$ pattern and 5 dB gain.[5] As explained in Sec. 8.9.1, a wide beam pattern such as $\cos^{1/2}\theta$ is appropriate for wide-scanning phased arrays. Scanning such a pattern 60° off broadside gives a gain loss of ($\cos^{1/2} 45^\circ = 0.841$) of only 1.5 dB. When designing large arrays that are capable of wide scan angles off broadside, it is recommended to select elements with wide beams and to perform tests with a small array before proceeding to full-scale hardware. [H.8.2: Milligan, 2nd ed., p. 128] In general, the desired element pattern depends on the array application. For fixed-beam arrays, a narrow-beam element pattern together with wider element spacing will lead to fewer elements in the array and lower cost.

Table 8-2 provides a list of commonly used array elements, along with references to places in the book where example realizations of the element are found. All of the major element categories have or will be discussed. The same is true for the subcategories, except for a few. Also noted in the table for each element are the features that are advantages or limitations. All the elements are suitable for fixed-phase arrays, but some have limited use in phased arrays, as noted in the table. In the remainder of this section, we comment on the listed elements. Elements for unidirectional beam arrays rather than bidirectional beams are assumed.

Dipoles and their variations to improve bandwidth are very popular array elements because of their wide beamwidth and easily matched input impedance, as well as their simple structure. They are used both for fixed-phase, broadside beam operation and for phased arrays capable of wide-angle scan off broadside. Dipoles, including drooping dipoles, are usually backed by a ground plane to produce a unidirectional pattern. Properties of dipoles in free space are given in Table 3-2 and in Sec. 6.1, where it was noted that about 16% bandwidth can be obtained with a wire dipole. A half-wave dipole backed by a ground plane a quarter-wavelength away produces a unidirectional as shown in Fig. 3-20. An integrated balun and mechanical support attached to the ground plane are shown in Fig. 6-40*b*. A printed form of the dipole with balun is shown in Fig. 8-35*a*.

[5] Note that the directivity of the $\cos^{1/2}\theta$ pattern from integration gives 6 dB because the classic formula of (8-121) is approximate.

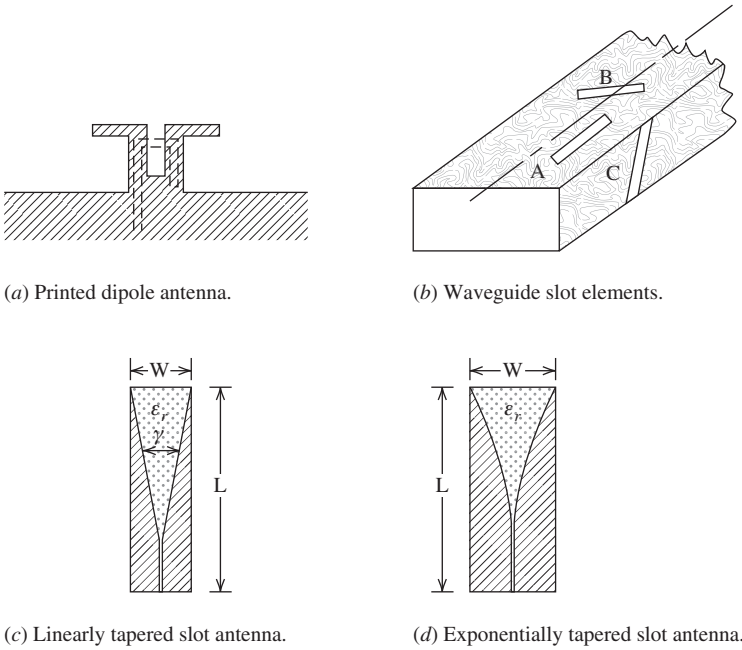

(*a*) Printed dipole antenna.

(*b*) Waveguide slot elements.

(*c*) Linearly tapered slot antenna.

(*d*) Exponentially tapered slot antenna.

Figure 8-35 Selected elements for array antennas.

The dipole is etched on to a printed circuit board together with a capacitively coupled loop, microstrip feed line, and is capable of 40% bandwidth. [H.8.2: Mailloux, 2nd ed., p. 236] Often the printed dipole is an integral part of a transceiver module. By lowering the ends of the dipole toward the ground plane, a *drooping dipole* is formed that can have 48% bandwidth. [H.8.2: Haupt, p. 271] Bandwidth can be increased to as high as 68% [24] by expanding the printed dipole into a bow-tie antenna; see Fig. 7-32. A bow-tie antenna array complete with feed network can be fabricated onto a single substrate as illustrated in Fig. 8-33. Monopole elements based on counterpart dipoles are used for fixed-phase endfire arrays and for phased arrays that scan off endfire.

Perhaps the best choice for a low-profile element is the microstrip antenna; see Sec. 11.2. It is ideally suited for printed circuit construction and has a fractional wavelength thickness. Its main disadvantage is that in its basic form, it has a bandwidth of only a few percent. Microstrip arrays are discussed in Sec. 11.3.

Another low-profile element is a slot antenna, which is a narrow slot in a ground plane as shown in Fig. 16-23. The slot is a complementary structure to the strip dipole of Fig. 6-8, where the air is replaced by metal and the metal is replaced by air to form the slot antenna. This complementary feature makes the strip dipole and slot antenna electromagnetic duals (see Sec. 3.4.1), so that the radiated electric and magnetic fields behave the same with their roles reversed. That is, any plane containing the long axis is an *E*-plane for the strip dipole but is the *H*-plane for the slot antenna. So, in Fig. 16-23, the *xz*-plane is the *E*-plane, whereas if the slot were replaced by metal forming a strip dipole, the *yz*-plane would be an *E*-plane. The patterns of a resonant half-wavelength slot in a finite ground plane are shown in Fig. 16-26. Practical single slot antennas are backed by a cavity to give a unidirectional pattern. Slot arrays are usually constructed with rectangular waveguides forming a *waveguide slot array antenna* as shown in Fig. 8-35*b*, often fabricated by milling slots in the waveguide. The array is series fed, giving a compact feed network. The slots are always designed to be resonant slots, but the array itself can be a traveling-wave (or non-resonant) or standing-wave (or resonant) array, which are terminated in a dummy load or a short, respectively. Traveling-wave arrays can be frequency scanned, whereas standing-wave arrays are used for broadside beams. Slots

are placed in the waveguide walls to interrupt the currents flowing in the walls, creating an electric potential across the narrow dimension of the slot causing it to radiate. Thus, the narrow wall of the slot determines the polarization; this was noted previously by it being the *E*-plane. The location, orientation, and length of the slots all enter into the design of a slot array, which can be complicated; see [H.6: *Ant. Eng. Hdbk*., 4th ed., Chap. 9] for design procedures. The slots can be longitudinal (i.e., parallel to the waveguide axis as shown in A of Fig. 8-35*b*) in the waveguide broadwall, inclined (rotated) in the broadwall (B of Fig. 8-35*b*), or inclined in the narrow wall (C of Fig. 8-35*b*)—also called an edge slot. The amplitude of excitation of each slot in the array is determined by the offset from the center axis for longitudinal slots and the amount of angular rotation for the inclined slots. Excitation phase is determined by which side of the center axis the longitudinal slots are placed and the direction of rotation for inclined slots, as well as the slot length. Waveguide slot arrays have good efficiency and are an excellent choice for high-power applications, but usually are narrow band (less that 5%). An example is the AWACS array of Fig. 8-35*b*, which is a traveling-wave array with 160 narrow wall slots in the longest row.

Aperture elements such as horn antennas (see Sec. 9.4) are used only for limited scan arrays with large element spacings that can accommodate the large aperture size of a horn. An exception is an array of open-ended waveguides (see Sec. 9.2.2), which have fractional wavelength dimensions. The open-ended waveguide radiator of Example 9-3 is $0.7\,\lambda$ by $0.3\,\lambda$. Being waveguide based, the element has moderate bandwidth (40% or more), but the physical structure can be large and heavy. Many types of directive elements can be used in limited scan arrays such as Yagi-Uda, helix, and others.

The *tapered slot antenna* (TSA),[6] also sometimes referred to as a *notch antenna* (or *flared notch antenna*), produces a useful endfire pattern over a bandwidth of 10 : 1 or more. It has moderate gain (7 to 10 dB) and balanced *E*- and *H*-plane beamwidths, making it a good array element candidate. [H.8.4: Lee and Chen, Chap. 9] There are several forms the TSA can have, but the *linearly tapered slot antenna* (LTSA) of Fig. 8-35*c* and the *exponentially tapered slot antenna* (ETSA) of Fig. 8-35*d* are two popular ones. They are constructed by etching a slot into a metal film, usually on a low-ε_r substrate. As a recent antenna innovation, the full understanding of its operation is incomplete, but basic principles are clear as we now discuss. The length L varies from about more than one wavelength up to many wavelengths over the operating band. The low frequency limit is determined by the slot width, W, which must be greater than $\lambda_L/2$. The feed region dictates the high-frequency limit. The TSA's traveling-wave behavior is responsible for its broad bandwidth. For operation near mid-band, the wave is bound in a transmission mode in the small-gap slot region near the feed, and when the wave reaches a region where the slot has widened to around a half-wavelength the power is converted to a radiation mode. TSAs are often fed using a microstrip-to-slotline transition at the slot line input. The LTSA is similar in geometry to the two-dimensional TEM (transverse electromagnetic) horn that is a planar version of a waveguide horn like the one in Fig. 9-11*b*. [H.8.2: Hansen, 2nd ed., p. 149] However, TSAs function more like a frequency independent antenna instead of an aperture antenna.

The LTSA has sides that expand linearly. With a flare angle γ in the range of 15 to 20°, it has nearly equal *E*- and *H*-plane beamwidths around 30°, even though the antenna is larger in the *E*-plane (the plane of the paper is the *E*-plane in Fig. 8-35*c* and *d*). [25] The ETSA has sides conforming to an exponentially flaring curve and is also called a *Vivaldi antenna*, a name coined in 1979 [26].

When TSAs are used as elements in an array there are unexpected benefits associated with the mutual coupling, which is explored further in the next section. The element performs best with a smaller size than when used as a single antenna. [27] The length can

[6] The term slot in this context does not imply there is radiation through a slot as in Fig. 16-23.

be reduced to under a wavelength and the width to under a half wavelength. This result allows closely spaced elements, which makes wide bandwidth possible. An experimental study of a dual-linearly polarized array (formed with orthogonal TSA element pairs) in a 9×8 grid demonstrated performance over a $5.9:1$ bandwidth. The element spacing (in both planes of the planar array) varied from about $0.1\,\lambda_L$ to $0.6\,\lambda_U$ over the band. [28] Simulations with the array showed that scanning out to 45° in all scan planes is achievable. [29] The high-frequency performance of TSA arrays is limited by narrow-band resonances introduced by the mutual coupling, but they can be reduced by adding plated-through vias. [28]

Additional elements are introduced in the next section that are low-profile as well as being suitable for broadband arrays.

8.11 WIDEBAND PHASED ARRAYS

In Sec. 7.1 we defined a broadband antenna as one with a bandwidth of about 2:1 or greater. Broadband behavior is more difficult to achieve with an array than with a single element. In this section, we address arrays that operate over a significant bandwidth, typically around $2:1$ or more, and refer to such an array as a **wideband array**. The distinction between the terms broadband and wideband are minimal, but it is common to use wideband with arrays with large bandwidth, so we adopt that convention. In this section, we first discuss fundamental principles for wideband array operation and then present types of wideband arrays that are of low-profile geometry. Multiband antennas that have multiple narrow operating bands spanning a wide frequency range are not included in this section, but instead we address arrays that operate over a continuous wide bandwidth. In some cases the array needs to support instantaneous bandwidth (see Sec. 7.1) over the band, such as with an UWB application discussed in Sec. 7.10.

A conventional wideband array with a periodic grid requires elements that span the same wide bandwidth. As discussed in Sec. 8.9.1, the element spacing d is limited by the appearance of grating lobes and other effects such as blind spots with (8-117) being the guideline. The spacing limit must be satisfied over the operating band and will give the largest physical distance value at the lowest operating frequency, f_L. Of course, the maximum physical extent of the element, D, in a row or column of the array must not exceed the spacing, so $D < d$. As an example, for a 50° scan angle off broadside ($\Delta\theta = 50^\circ$, $\theta_o = 40^\circ$), (8-117) gives $d < 0.57\,\lambda$ and then the maximum extent of the element is $D = 0.57\,\lambda$. It turns out that this physical size limitation is usually more difficult to satisfy than finding an element with sufficient bandwidth. The array bandwidth limitation can be quantified using the graph in Fig. 8-36 which compares popular broadband antennas used as elements in phased arrays. [30] The maximum lateral extent (diameter) of the Archimedean and equiangular spirals is about $D = 0.5\,\lambda_L$ and for the sinuous antenna is about $D = 0.4\,\lambda_L$, based on principles in Sec. 7.7. The Foursquare antenna of Fig. 8-38, to be discussed, has a maximum lateral extent of $D = 0.35\,\lambda_L$. The minimum element spacing is obtained by equating to the element extent, $d = D$, which corresponds to zero separation between elements edges. As frequency is increased from the low end of the operating band where $\lambda = \lambda_L$, the spacing normalized by wavelength increases as given by $d/\lambda = (d/\lambda_L)(f/f_L)$, which is used to plot the straight lines in Fig. 8-36. For example, at $f/f_L = 2$ the spiral antennas have a minimum spacing of $d/\lambda = (d/\lambda_L)(f/f_L) = 0.5 \cdot 2 = 1$. The maximum scan angle off broadside $\Delta\theta$ found from the grating lobe appearance limit of (8-117) is shown on the right ordinate of Fig. 8-36. For the preceding scan limit example, it is seen that $\Delta\theta = 50^\circ$ on the right ordinate corresponds to $d/\lambda = 0.57$ on the left ordinate. The plot is used to find candidate elements for an array of a given bandwidth. We illustrate for an array with a 50% bandwidth, which is a ratio bandwidth of $B_r = f_U/f_L = 1.67$. Drawing a vertical line from 1.67 on the ordinate intersects the three curves at 0.58, 0.67, and 0.84 for the element types. The corresponding maximum scan angles read from the right ordinate are 46°, 30°, and 11°. That is, the

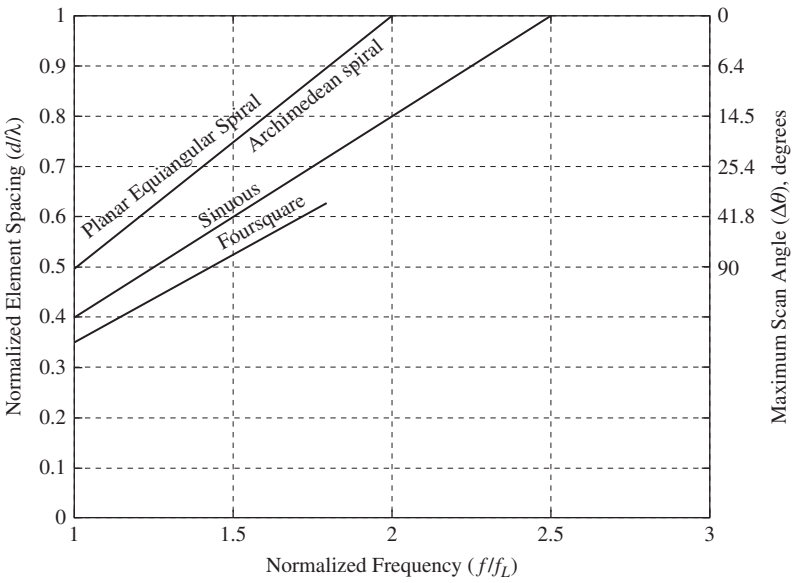

Figure 8-36 Minimum element spacing normalized to a wavelength versus normalized frequency for various broadband element types based on the physical extent of the elements. The right ordinate shows the maximum scan angle. (From [3] © 2000. Reprinted with permission from *Microwave Journal*.)

Foursquare array can scan to 46° at the upper frequency while the spiral arrays can only scan to 11° without a grating lobe appearing. Thus, we see that as the bandwidth requirement is increased for an array, the more compact the element must be in addition to covering the array bandwidth. For most applications, an extremely broadband element is unnecessary. Having a compact element is usually the most important factor.

For broadside operation there is no bandwidth limitation due to array size or feed network architecture. Of course, in all wideband arrays the element and feed network components (phase shifters, power dividers, etc.) must be wideband. However, when a phased array is scanned off broadside the main beam will steer to the intended scan angle of θ_o only at the center frequency f_c. This effect is illustrated for simplicity with a linear array along the z-axis. The phase shifters are selected to produce an array factor peak at angle θ_o at f_c, and then the phase terms in (8-5) are zero, or $0 = \beta_c d \cos\theta_o + \alpha$. When frequency is changed to f, the peak shifts to angle θ, or $0 = \beta d \cos\theta + \alpha$. Solving these two equations gives

$$\theta = \cos^{-1}\left(\frac{f_c}{f}\cos\theta_o\right) \tag{8-122}$$

This equation gives the angle for the peak of the beam of a linear array along the z-axis at frequency f with the phase shifters set to give a beam peak at angle θ_o at frequency f_c. For $f = f_c$, (8-122) gives $\theta = \theta_o$ as expected. As frequency deviates more from the center frequency, the beam peak direction correspondingly deviates ("squints") more from the desired pointing direction θ_o. The beam peak angle is closer to (farther from) broadside compared to the center frequency direction for frequencies above (below) the center frequency. Frequency dependent scan can be avoided by using time delay, as discussed in Sec. 8.9.2. See [H.8.2: Mallioux, 2nd ed., p. 31] for more details on bandwidth effects on phased arrays.

Recent innovations in arrays have led to array architectures that avoid the compact element size requirement of conventional uniform grid arrays, including reconfigurable arrays, aperiodic-grid arrays, variable element size arrays, and tightly coupled arrays. A *reconfigurable array* is altered dynamically to change its frequency band and, thus, does not fit the topic of this section. Reconfigurable arrays, discussed in Sec. 12.5, are usually implemented by activating switches internal to the elements to change their frequency range, often with MEMS switches. An *aperiodic-grid array* (i.e., an unequally spaced array) avoids the appearance of full grating lobes of a conventional periodic grid array because grating lobe formation requires a periodic geometry. Aperiodic arrays are more difficult to design because the mutual coupling environment is not repeatable across the array, leading to varying element impedances and patterns.

A special type of aperiodic-grid array employing different size elements is called an *interlaced-element array*, with one form being the *wideband array with variable element sizes* (*WAVES array*). [31] An example of a basic unit used to make large WAVES arrays shown in Fig. 8-37*a* consists of eight elements with two sizes of spiral antennas to cover two octaves (4 : 1) of bandwidth. The small spirals have diameter D_S and the large spirals have diameter D_L which are twice as large as the small spirals ($D_L = 2D_S$). The large elements operate over the full band of two octaves of f_1 to $f_2(= 2f_1)$ and f_2 to $f_4(= 2f_2)$. The small elements are operational only over the upper octave from f_2 to f_4. The patterns of the large spiral are shown in Fig. 7-29. At the lowest operating frequency f_1, the element spacings in the principal directions are a half-wavelength, so $S = S_x = S_y = \lambda_1/2$. At the top of the first octave $f_2 = 2f_1$ the electrical spacing is $S = \lambda_2$, which will lead to grating lobes. At f_2 the small elements become operational, lowering the spacing between the active elements to $\lambda_2/2$. Increasing frequency further to $f_4 = 2f_2$, the spacing once again becomes one wavelength, λ_4. The patterns for the array were computed using simple array theory and were measured for an experimental model operating from 2.5 to 8 GHz. [31] Representative patterns are shown in Fig. 8-37*b* and *c* for the low end of the band at 2.5 GHz with the four large elements active where the spacing is a half wavelength, and for the top end of the band at 10 GHz with all eight elements active where the spacing is one wavelength. Note that the pattern for one-wavelength spacing is acceptable because the element pattern of the spiral (see Fig. 7-29) diminishes the grating lobe effect, but smaller spacings would be needed in low-side lobe or wide-angle scanning arrays. The WAVES concept has been extended to at least three octaves of bandwidth (8 : 1) by distorting the large elements to make room for the smaller elements [32] or by using multiple layers of radiating elements, one layer for each octave. [33]

A recent innovation in wideband phased arrays is the *tightly coupled array*. While conventional array design seeks to reduce mutual coupling, it turns out that there are advantages to tightly packed elements that have high coupling. The unexpected benefit is that the bandwidth of an embedded element antenna is larger than when isolated. As with any array, the factor limiting bandwidth is the ground plane. But the second surprise benefit for tightly coupled arrays is that the elements can be placed close to the ground plane, often under $\lambda/10$ at the lowest operating frequency of the array. A related concept is that of a *connected array*, where the elements are conductively connected; examples are connected dipoles joined at the ends [34] and tapered slot elements joined on the sides [35]. The types of tightly coupled arrays are the Foursquare array, the current sheet array, the fragmented array, and the long slot array.

Perhaps the first successful tightly coupled array was developed at Virginia Tech in the 1990s. [36] Related geometries for isolated elements have evolved, such as the Fourpoint antenna shown in Fig. 12-7*a* which offers dual polarization and balanced patterns over 2.7 : 1 bandwidth (see Fig. 12-7*b*), covering common wireless bands in one compact antenna, and is an excellent choice for base stations. [37] The Foursquare element has four squares excited with a balanced feed for each opposing pair of squares, giving simultaneous dual linear polarizations. A 2×2 illustrative array is shown in Fig. 8-38. [38] The inactive squares can be thought of as sleeves for the active squares, thus

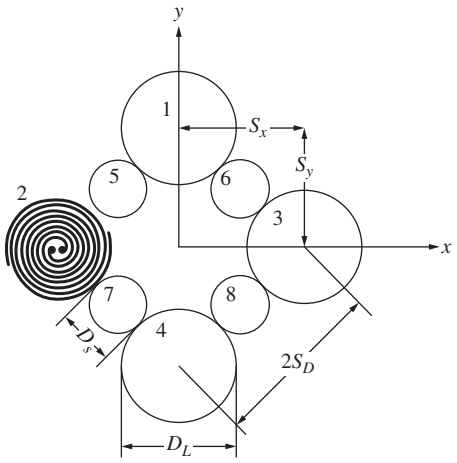

(*a*) Geometry for an eight-element, two-octave concept demonstration array.

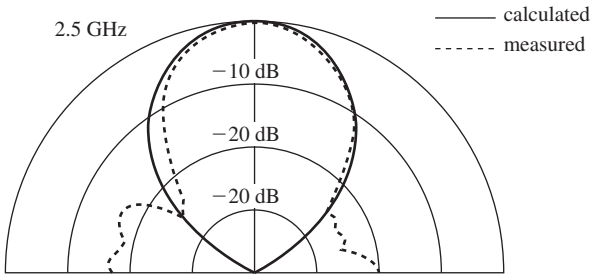

(*b*) Pattern at 2.5 GHz with four large elements active.

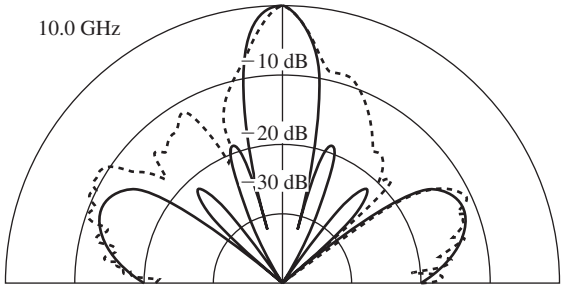

(*c*) Pattern at 10 GHz with eight large elements active.

Figure 8-37 An eight-element example wideband array with variable element sizes (WAVES array). (From [31] © 1990. Reprinted with permission from IET.)

widening bandwidth of an element as explained in Sec. 7.5. In an array, the neighboring elements support current associated with radiation from an element through coupling across the narrow gap between elements. [38] The original Foursquare arrays had a bandwidth of about 2 : 1. [38] The elements were about a quarter wavelength on each side and a tenth wavelength above the ground plane at the low end of the band. Subsequent research has shown 3.5 : 1 bandwidth is possible. [39]

The *current sheet array* (*CSA*), whose name comes from Wheeler's current sheet [23], is an array of electrically small collinear dipoles in each principal plane and backed by a ground plane less than a tenth of a wavelength away at the low end of the band. The

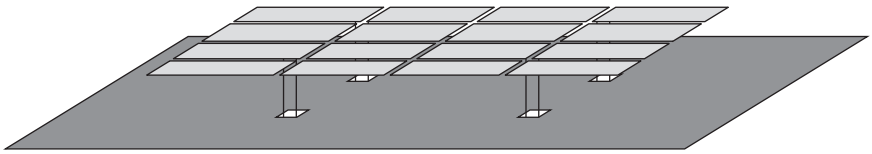

Figure 8-38 The Foursquare antenna used in a 2×2 tightly coupled array. [38]

largest element spacing is a half-wavelength at the high end of the band, just like the Foursquare array. The element ends are joined with capacitors to increase coupling. Experiments at Harris Corp. demonstrated a 9 : 1 bandwidth. [40] Additional details are available in [H.8.2: Munk, Chap. 6] and [H.6: Balanis, Ed., Sec. 12.2].

The *fragmented array* is designed using a genetic algorithm routine to form pixilated features. Bandwidths close to 10 : 1 are possible with simple ground planes. [H.6: Balanis, Ed., Sec. 12.4] The *long slot array* is a low-profile array of about $\lambda_L/8$ thickness and 4 : 1 bandwidth with a ground plane. [41] Array bandwidth is usually limited by the presence of a ground plane. Ground plane options include good conductors (i.e., metals), absorbing materials, or artificial materials, or a combination of these. For conducting ground planes, the conventional requirement of quarter-wavelength spacing away from the radiating elements limits the bandwidth to about 25% with conventional arrays. We have seen that tightly coupled arrays with conducting ground planes are capable of much wider bandwidths, a decade or so. Even greater bandwidths are possible by including absorbing materials such as resistive sheets or ferrite materials, but the associated loss reduces the gain. *Artificial materials* are artificial in the sense that they are not naturally occurring but are engineered using common materials in textured structures to create special electromagnetic properties. Such materials have origins in *frequency selective surfaces* that are constructed to pass certain frequency bands and reflect others for use in reflector antenna and radome applications. An example is an *artificial magnetic conductor* (*AMC*), which is the dual of a PEC. An electric antenna (such as a dipole) can be spaced arbitrarily close to a AMC ground plane. Similarly, a magnetic antenna (such as a loop) can be spaced arbitrarily close to a PEC ground plane. Close ground plane spacing enables antennas that are physically much thinner at VHF frequencies (and below) than conventional quarter-wave ground plane spaced antennas. See [H.6: *Ant. Eng. Hdbk*., 4th ed., Chap. 34] and [H.6: Balanis, Ed., Chap. 15] for more details.

In closing, we mention that there are wideband arrays that cover multiple frequency bands by using different types of elements for each band. In this *shared-aperture array* approach, the elements of one frequency band are interleaved with elements of different frequency bands. Such an array is often used to support multiple functions (communications, radar, sensing, position location, etc.) and thus is called *multifunctional wideband array.*

REFERENCES

1. C. T. Tai, "The Optimum Directivity of Uniformly Spaced Broadside Arrays of Dipoles,"*IEEE Trans. on Ant. & Prop*., Vol. AP-12, pp. 447–454, July 1964.
2. R. C. Hansen, "Hansen-Woodyard Arrays with Few Elements," *Microwave and Optical Technology Letters*, Vol. 5, pp. 44–46, Jan. 1992.
3. H. Bach, "Directivity Diagrams for Uniform Linear Arrays," *Microwave J.*, Vol. 15, pp. 41–44, Dec. 1972.
4. H. Bach, "Directivity of Basic Linear Arrays," *IEEE Trans. on Ant. & Prop.,* Vol. AP-18, pp. 107–110, Jan. 1970.
5. N. A. McDonald, "Approximate Relationship between Directivity and Beamwidth for Broadside Collinear Arrays," *IEEE Trans. on Ant. & Prop.,* Vol. AP-26, pp. 340–341, Mar. 1978.

6. W. L. Stutzman, "Estimating Directivity and Gain of Antennas," *IEEE Trans. on Ant. & Prop. Mag*., Vol. 40, pp. 7–11, Aug. 1998.
7. J. Rashed-Mohassel, "Optimum Directivity of a Uniformly Spaced Broadside Array of Collinear Half-Wave Dipoles," *Microwave and Optical Technology Let*., Vol. 7, pp. 193–196, Mar. 1994.
8. Peter Hannan, "The Element-Gain Paradox for a Phased-Array Antenna," *IEEE Trans. on Ant. & Prop.,* Vol. AP-12, pp. 423–433, July 1964.
9. A. Parfitt, D. Griffin, and P. Cole, "Mutual Coupling between Metal Strip Antennas on Finite Size, Electrically Thick Dielectric Substrates," *IEEE Trans. on Ant. & Prop*., Vol. 41, pp. 108–115, Jan. 1993.
10. D. Pozar, "A Relation between the Active Input Impedance and the Active Element Pattern of a Phased Array," *IEEE Trans. on Ant. & Prop*., Vol. 51, pp. 2486–2489, Sept. 2003.
11. D. Kelley and W. Stutzman, "Array Antenna Pattern Modeling Methods That Include Mutual Coupling Effects," *IEEE Trans. on Ant. & Prop*., Vol. 41, pp. 1625–1632, Dec. 1993.
12. K. Takamizawa and W. Stutzman, "Analysis and Synthesis of Microstrip Antennas Including Mutual Coupling," Virginia Tech Antenna Group Report 88-2, Aug. 1988.
13. D. Pozar, "Analysis of Finite Phased Arrays of Printed Dipoles," *IEEE Trans. on Ant. & Prop*., Vol. AP-33, pp. 1045–1053, Oct. 1985.
14. B. J. Forman, "Directivity Characteristics of Scannable Planar Arrays," *IEEE Trans. on Ant. & Prop.,* Vol. AP-20, pp. 245–252, May 1972.
15. H. King and J. L. Wong, "Directivity of a Uniformly Excited $N \times N$ Array of Directive Elements,"*IEEE Trans. on Ant. & Prop*., Vol. AP-23, pp. 401–404, May 1975.
16. D. Pozar, "The Active Element Pattern," *IEEE Trans. on Ant. & Prop*., Vol. 42, pp. 1176–1178, Aug. 1994.
17. J-P. Bayard, D. Schaubert, and M. Cooley, "E-Plane Scan Performance of Infinite Arrays of Dipoles Printed on Protruding Dielectric Substrates: Coplanar Feed Line and E-Plane Metallic Wall Effects," *IEEE Trans. on Ant. & Prop*., Vol. 41, pp. 837–841, June 1993.
18. D. Pozar, "Scanning Characteristics of Infinite Arrays of Printed Antenna Subarrays," *IEEE Trans. on Ant. & Prop*., Vol. 40, pp. 666–674, June 1992.
19. F. Zavosh and J. Aberle, "Infinite Phased Array of Cavity-Backed Patches," *IEEE Trans. on Ant. & Prop*., Vol. 42, pp. 390–398, Mar. 1994.
20. M. Deshpande and M. C. Bailey, "Analysis of Finite Phased Arrays of Circular Microstrip Patches," *IEEE Trans. on Ant. & Prop*., Vol. 37, pp. 1355–1360, Nov. 1989.
21. E. Brookner, "Phased-array Radars," *Scientific American*, pp. 94–102, Feb. 1985.
22. J. Butler and R. Lowe, "Beam-Forming Matrix Simplifies Design of Electronically Scanned Antennas," *Elec. Design*, Vol. 9, pp. 170-173, Apr. 12, 1961.
23. H. A. Wheeler, "Simple Relations Derived from a Phased-Array Antenna Made of an Infinite Current Sheet," *IEEE Trans. on Ant. & Prop*., Vol. 40, pp. 506-514, July 1965.
24. G. Zheng et al., "A Broadband Printed Bow-Tie Antenna with a Simplified Balanced Feed," *Microwave and Optical Tech. Let*., Vol. 47, pp. 534-536, Dec. 20, 2005.
25. P. Kool, T. Yeo, and M. Leong, "Parametric Studies of the Linearly Tapered Slot Antenna (LTSA)," *Microwave and Optical Tech. Let*., Vol. 4, pp. 200–207, Apr., 1991.
26. P. Gibson, "The Vivaldi Aerial," *Proc. 9th European Microwave Conf*., pp. 101–105, 1979.
27. J. Shin and D. Schaubert, "A Parameter Study of Stripline-Fed Vivaldi Notch-Antenna Arrays," *IEEE Trans. on Ant. & Prop*., Vol. 47, pp. 879–886, May 1999.
28. H. Holter, T-H Chio, and D. Schaubert, "Experimental Results of 144-Element Dual-Polarized Endfire Tapered-Slot Phased Array," *IEEE Trans. on Ant. & Prop*., Vol. 48, pp. 1707–1718, Nov. 2000.
29. T-H Chio and D. Schaubert, "Parameter Study and Design of Wide-Band Widescan Dual-Polarized Tapered-Slot Antenna Arrays," *IEEE Trans. on Ant. & Prop*., Vol. 48, pp. 879–886, June 2000.
30. W. Stutzman and C. Buxton, "Radiating Elements for Wideband Phased Arrays," *Microwave J.*, Vol. 43, pp. 130-141, Feb. 2000.
31. S. Shively and W. Stutzman, "Wideband Arrays With Variable Element Sizes," *IEE Proc., Pt. H*., Vol. 137, pp. 238–240, Aug. 1990.
32. E. Caswell, "Design and Analysis of Star Spiral with Applications to Wideband Arrays with Variable Element Sizes," Ph.D. Dissertation, Virginia Tech, 2001.
33. W. Stutzman, "Wide Bandwidth Antenna Array Design," *IEEE Southeastcon Proceedings* (Raleigh, NC), pp. 92–96, April 1985.
34. R. C. Hansen, "Linear Connected Arrays," *IEEE Ant. and Wireless Prop. Letters*, Vol. 3, pp. 154–156, 2004.

35. J. Lee, S. Livingston, and R. Koenig, "A Low-Profile Wide-Band (5:1) Dual-Pol Array," *IEEE Ant. and Wireless Prop. Let*., Vol. 2, pp. 46–49, 2003.
36. J. R. Nealy, "Foursquare Antenna Radiating Element," U. S. Patent 5,926,137, July 20, 1999.
37. S-Y. Suh, W. Stutzman, W. Davis, A. Waltho, K. Skeba, and J. Schiffer, "A Novel Low-profile, Dual-polarization, Multi-band Base-station Antenna Element—The Fourpoint Antenna," *IEEE Vehicular Technology Conference Proc.* (Los Angeles, CA), Vol. 1, pp. 225–229, Sept. 2004.
38. C. Buxton, W. Stutzman, and J. Nealy, "Implementation of the Foursquare Antenna in Broadband Arrays," URSI National Radio Science Meeting (Orlando), July 1999.
39. Terry Vogler, "Analysis of the Radiation Mechanisms in and Design of Tightly-Coupled Antenna Arrays," Ph.D. Dissertation, Virginia Tech, 2010.
40. M. Jones and J. Rawnick, "A New Approach to Broadband Array Design Using Tightly Coupled Elements," *IEEE Military Comm. Conf*., Oct. 2007.
41. J. J. Lee, S. Livingstone, R. Koenig, D. Nagata, and L. Lai, "Compact Light Weight UHF Arrays Using Long Slot Apertures," *IEEE Trans. on Ant. & Prop*., Vol. 54, pp. 2009–2015, July 2006.

PROBLEMS

8.2-1 Consider an array of two elements spaced one wavelength apart with currents that are equal in amplitude and 180° out-of-phase.
(a) Use the inspection method to rough sketch the polar plot of the array factor.
(b) Derive the exact array factor as a function of θ if the elements are on the z-axis.
(c) For what angles of θ is this array factor maximum?
(d) What is the expression for the normalized array factor $|f(\theta)|$?
(e) Show that (8-9) reduces to your answer in (d).

8.2-2 Use the techniques of Fig. 8-6 to obtain a polar plot of the array factor of the array given in Prob. 8.2-1.

8.2-3 Use the techniques of Fig. 8-6 to obtain a polar plot of the array factor of a two-element, one wavelength spaced array with equal amplitude and equal phase currents (Example 8-1).

8.2-4 Usually, the interelement spacing of an array is about one-half wavelength. Spacings much greater than this produce major lobes in undesired directions. To illustrate this point, use the techniques of Fig. 8-6 to sketch the array factor for a two-element array with equal amplitude, in-phase elements in polar form for the following spacings: (a) $d = 3\lambda/4$ and (b) $d = 2\lambda$. Examples 3-2 and 8-1 and this problem show the effects of spacing on an array of fixed excitation.

8.2-5 (a) Using the array factor for a two-element broadside array ($\alpha = 0$) with equal current amplitude point source elements, show that the directivity expression is

$$D = \frac{2}{1 + (\sin \beta d)/\beta d}$$

Hint: Change from variable θ to $\psi = \beta d \cos\theta$.
(b) Plot this expression as a function of d from zero to two wavelengths.

8.3-1 Prove that the array factor magnitude $|f(\psi)|$ for a uniformly excited, equally spaced linear array is symmetric about $\psi = \pi$.

8.3-2 Show that the array factor expressions (8-9) and (8-24) for a two-element uniformly excited array are identical.

8.3-3 Drive (8-33)

8.3-4 The expression for the half-power beamwidth of the array factor for a broadside, uniformly excited, equally spaced, linear array can be approximated as

$$\text{HP} \approx k\frac{\lambda}{Nd}$$

for $Nd \gg \lambda$. Determine k for $N = 10$ and 20, and compare to (8-34)

8.3-5 In this problem, the effect of phasings and spacings on a simple array are illustrated. Consider an equally spaced five-element array with uniform current amplitudes. Sketch the array factors for:

(a) $d = \lambda/2$, broadside case ($\theta_o = 90^\circ$)
(b) $d = \lambda$, broadside case
(c) $d = 2\lambda$, broadside case
(d) $d = \lambda/2,\ \theta_o = 45^\circ$
(e) $d = \lambda/2,\ \theta_o = 0^\circ$, endfire case

The five plots can be obtained from one universal pattern plot as discussed in Sec. 8.3. For the last two cases, determine the interelement phase shift α required to steer the main beam as specified.

8.3-6 Repeat Prob. 8.3-5 using a computer code.

8.3-7 Design a five-element uniformly excited, equally spaced linear array for:
(a) Main beam maximum at broadside
(b) Main beam maximum at 45° from broadside ($\theta_o = 45^\circ$)

In each case, select the element spacing and linear phasing such that the beamwidth is as small as possible and also so that no part of a grating lobe appears in the visible region. Sketch the polar plots of the patterns.

8.3-8 Design and plot the array factor for an ordinary endfire, five-element, uniformly excited linear array with spacings $d = 0.35\lambda$. Use $\theta_o = 180^\circ$ and find α.

8.3-9 Design a linear array of four isotropic elements for a single ordinary endfire beam using the maximum spacing. Plot the polar pattern.

8.3-10 Design a linear array of five isotropic elements for Hansen–Woodyard increased directivity with $d = 0.35\lambda$. Plot the polar pattern. (Note the differences in the results from Example 8-4.)

8.3-11 Design a linear array of 10 isotropic elements for Hansen–Woodyard increased directivity with $d = 0.4\lambda$. Plot the polar pattern.

8.3-12 Show that the array factor for a uniformly excited, equally spaced linear array approaches the pattern factor of a uniform line source (i.e., neglect the element factor) in the limit of small array element spacings.

8.3-13 Derive the pattern normalization factor used in (8-39). Consider both endfire directions (i.e., $\theta_o = 0$ and 180°).

8.4-1 Two collinear half-wave dipoles are spaced a half-wavelength apart (but not quite touching) and have the same amplitude and phase terminal currents. Calculate and plot the element pattern, array factor, and array pattern.

8.4-2 Repeat Prob. 8.4-1 for one-wavelength spacing.

8.4-3 Two parallel half-wave dipoles are spaced a one wavelength apart and have the same amplitude and phase terminal currents. Calculate and plot the full array pattern in the two principal planes.

8.4-4 A linear array of three quarter-wavelength-long, vertical monopoles is operated against an infinite, perfectly conducting ground plane. Let the element feeds be along the z-axis, the ground plane in the yz-plane, and the monopoles in the x-direction.
(a) Design the array as a Hansen–Woodyard increased directivity endfire array; that is, determine the element spacings and phasings (choose $d = 0.3\lambda$).
(b) Use the universal array factor plot for three uniformly excited elements to obtain a polar plot of the array factor for this problem.
(c) Write the expression for the complete pattern.
(d) Plot the complete far-field patterns in the xz-plane and yz-plane.

8.4-5 Three collinear half-wave dipoles are spaced $0.9\,\lambda$ apart and have the same amplitude and phase terminal currents. (a) Use the graphical techniques of Sec. 8.2 to sketch array factor. Then sketch the element and array patterns. (b) Use the computer to calculate and plot the array pattern.

8.4-6 An array of four small loop antennas oriented with the loops in the yz-plane are spaced 0.4λ apart along the z-axis, have uniform amplitudes, and are phased for ordinary endfire. Plot the full array pattern in the two principal planes.

8.4-7 Suppose a truck uses a Citizens Band radio to communicate at 27 MHz. The antenna system is two quarter-wave monopoles parallel to the x-axis (assumed to operate above a perfect ground plane) mounted on mirrors 2.78 m apart along the z-axis and fed with equal amplitude and phase. Use simple array theory to obtain sketches of the array patterns in the three principal planes.

8.4-8 *Design problem.* Design a broadside linear array of four parallel half-wave dipoles for as narrow a beamwidth as possible and with no level outside the main beam above -8 dB relative to the main beam peak. The excitations are uniform. (a) Determine the required element spacing. (b) Sketch the polar pattern in the H-plane.

8.4-9 Plot the principal plane full array patterns for the endfire array of Prob. 8.3-8 with parallel half-wave dipoles elements. Find the half-power beamwidths.

8.5-1 Calculate the directivities in decibels for the following broadside arrays of point sources:

(a) $N = 2,\ d = \lambda/2$.
(b) $N = 10,\ d = \lambda/2$.
(c) $N = 15,\ d = \lambda$.

8.5-2 Evaluate (8-67) for $d = 3\lambda/8$ and $N = 10$ for:

(a) Broadside, and compare the result to that of (8-69),
(b) Ordinary endfire, and compare the result to that of (8-70).

8.5-3 Evaluate (8-67) and plot D versus d/λ for $N = 10$ and ordinary endfire operation. Your results should look like the curve in Fig. 8-17.

8.5-4 The approximate directivity formula of (8-69) for long, broadside linear arrays of isotropic elements can be checked in the following two ways using HP $\approx 0.886\ \lambda/L$ from (8-34):

(a) Use $D = 4\pi/\Omega_A$ to derive an equation of the form $D = cL/\lambda$ by approximating Ω_A as 2πHP; find c.
(b) Begin with (8-74) to derive an equation of the form $D = cL/\lambda$; find c.

8.5-5 Develop a computer code to evaluate directivity using (8-67).

(a) Plot the D versus d/λ curve for a broadside array with eight isotropic elements; compare to the curve in Fig. 8-16.
(b) Plot the D versus d/λ curve for a broadside array of eight collinear short dipole elements.

8.5-6 Show that $D = N$ for an ordinary endfire linear array of uniformly excited isotropic elements when $d = \lambda/4$.

8.5-7 Evaluate the directivity of a broadside array of 12 collinear short dipole elements spaced 0.7λ apart in the following ways:

(a) Use (8-67).
(b) Use (8-69).

Determine the value of HP and use in the following to calculate directivity:

(c) Eq. (8-73).
(d) Eq. (8-74).

8.5-8 Calculate the directivity for the array of Example 8-5. How much more directivity is there compared to that of a single short dipole, in dB?

8.5-9 Calculate and plot the directivity of an array of 10 collinear short dipoles for spacings of 0.1 to $1.0\,\lambda$. Also, plot the curves for the approximate formulas (8-69) and (8-75).

8.5-10 A five-element array of five parallel short dipoles spaced $0.3\,\lambda$ apart is designed for Hansen–Woodyard endfire operation. Evaluate the directivity and compare to the directivities for the same array with isotropic elements and a similar ordinary endfire array of isotropic elements.

8.5-11 *Design problem.* Base station communication antennas are often constructed using a collinear array of half-wave dipoles oriented vertically to produce an omnidirectional pattern in the horizontal plane. The objective in this problem is to maximize gain by selecting the proper element spacing. Assuming uniform amplitude and phase excitation, design a maximum-directivity four-element array for the middle of the cellular telephone band (824 to 894 MHz). Show solution details. Give the values of spacing d in wavelengths and directivity D in decibels at midband and at the band edges. Plot the vertical-plane pattern in polar-linear form. Sketch the array, showing its physical length along, with a feed network.

8.5-12 The approximate array directivity formula $D \approx D_e D_i$ of (8-75) is attractive because of its simplicity, but can yield inaccurate results in many cases as this problem shows. Evaluate the directivity of the following arrays of short dipoles using the exact formula of (8-72).

(a) $N = 4$, broadside, collinear short dipoles, $d = \lambda/2$.
(b) $N = 4$, endfire, parallel short dipoles, $d = \lambda/2$.
(c) $N = 3$, broadside, collinear short dipoles, $d = \lambda/2$.
(d) $N = 3$, endfire, parallel short dipoles, $d = \lambda/2$.

Then compare results to (8-75) for cases to which (8-75) is applicable.

8.5-13 *Array directivity computation.*

(a) Write a computer program to evaluate the directivity of an array by direct integration. Validate the code by comparing to values obtained using (8-72) for an array of four collinear dipoles that are spaced a half-wavelength apart.
(b) Use the direct-integration directivity code to evaluate the directivity of arrays of collinear half-wave dipoles of 2, 3 and 4 elements spaced a half wavelength apart and uniformly excited. Compare to directivity of the same arrays with isotropic elements.

8.6-1 Calculate and plot the polar pattern for the five-element array with the triangular distribution in Fig. 8-21*b*. Find the half-power beamwidth in degrees and side lobe level in dB.

8.6-2 Calculate and plot the polar pattern for a five-element array with a triangular distribution similar to Fig. 8-21*b*, but with collinear half-wave dipole elements. Compare values of half-power beamwidth in degrees, side lobe level in dB, and directivity to the isotropic element case.

8.6-3 Prove that (8-83) follows from (8-82).

8.6-4 Prove that (8-85) follows from (8-83).

8.6-5 Verify the directivity values given in Figs. 8-20*c* through 8-20*e*, and in Fig. 8-22.

8.6-6 *Binomial array.* For a linear array of N isotropic elements spaced a half-wavelength apart and that have binomial current weightings:

(a) Derive the normalized array factor expression in terms of θ.
(b) Derive an expression for the directivity. The result will only be a function of N.
(c) Evaluate the directivity expression derived in (b) for five elements.

8.7-1 Two antennas have the following self- and mutual impedances:

$$Z_{11} = 70\angle 0^\circ, \qquad Z_{22} = 100\angle 45^\circ, \qquad Z_{12} = 60\angle -10^\circ$$

(a) Find the input impedance to antenna 1, if antenna 2 is short-circuited.
(b) Find the voltage induced at the open-circuited terminals of antenna 2 when the voltage applied to antenna 1 is $1\angle 0^\circ$ V.

8.7-2 Derive (8-94), making use of Fig. 8-24.

8.7-3 For the parallel dipoles of Fig. 8-25 and $d = 0.6\,\lambda$, calculate the coupling level between the dipoles in dB.

8.7-4 *Mutual impedance calculation.* (a) Mutual impedance is calculated using simulation data in (8-87) for the case of antenna 1 excited and antenna 2 open circuited to find $Z_{12} = V_2/I_1$. Evaluate Z_{12} for parallel half-wave dipoles of the type in Fig. 8-25 and spaced $0.2\,\lambda$ apart. (b) Mutual impedance can also be calculated using the following formula:

$$Z_{12} = \frac{Z_{1,\text{in}} - Z_{1,\text{out}}}{2}$$

where $Z_{1,\text{in}}$ and $Z_{1,\text{out}}$ are the input impedances for antenna 1 for the two cases of two sources on the two dipoles that are in phase and then out of phase. Derive this formula. (c) Repeat the mutual impedance calculation in (a) but using the formula in (b) and appropriate simulations.

8.8-1 A planar array of four isotropic elements is arranged in the *xy*-plane with the following positions and currents: $(\lambda/4, \lambda/4), +1; (-\lambda/4, \lambda/4), +1, (-\lambda/4, -\lambda/4), -1; (\lambda/4, -\lambda/4), -1$. Use simple array modeling techniques to obtain sketches of the *xz*- and *yz*-plane patterns.

8.8-2 A four-element linear array of parallel, in-phase, half-wave dipoles is located $\lambda/4$ in front of a large planar reflector in the *xy*-plane. Assume the reflector to be a perfect ground plane. If the dipoles are parallel to the *x*-axis and spaced $\lambda/2$ apart, plot the complete pattern in the *xy*- and *yz* planes.

8.8-3 A two-element array of vertical short dipoles is operated a quarter-wavelength above a perfect ground plane as shown. The elements are a half-wavelength apart and are excited with

equal amplitude and opposite phase. Obtain polar plots for the radiation pattern of this radiating system in the *xz*- and *yz*-planes.

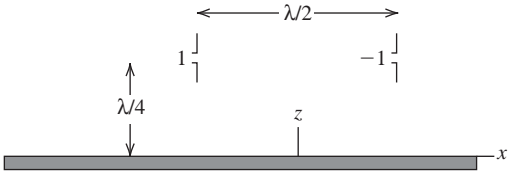

8.8-4 A two-dimensional, uniformly excited array of isotropic elements as shown below is to be analyzed. Use the principle of pattern multiplication with a pair of elements oriented vertically as an "array" and the four elements in a row as an "element." Plot the patterns in the *xz*-, *yz*- and *xy*-planes.

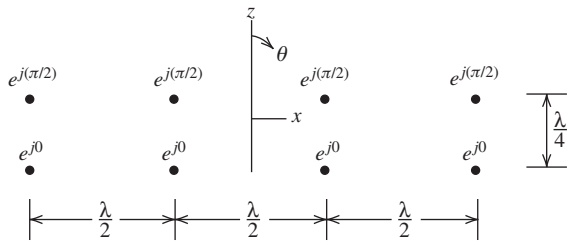

8.8-5 A planar array in the *xy*-plane has four isotropic elements in *x*- and *y*-directions with 0.5λ-spacings. Plot the radiation pattern (linear, polar plot) in the 45° plane. Then use the projection technique to find the equivalent linear array and then obtain the 45°-plane pattern. Compare the patterns.

8.8-6 *Square and triangular grid planar arrays*. This problem compares square-grid and triangular-grid planar arrays in the *xy*-plane of the same area. The square-grid array has 25 isotropic elements consisting of five rows of five elements each with 0.5λ-spacings. The triangular grid has 16 isotropic elements consisting of four rows of four elements each with 0.625 λ between all adjacent elements. Sketch the array geometries. Plot the radiation pattern (linear, polar plot) in the 45° plane for both arrays and comment on the results.

8.8-7 Verify the directivity values in Example 8-8 using numerical pattern integration for $d = 0.5\lambda$.

8.8-8 *Project*. Research the topic and prepare a report on the antenna aspects of one of the following technical programs. Include calculations of as many antenna parameter values as you can. (a) The Square Kilometer Array (www.skatelescope.org). (b) The Long Wavelength Array (lwa.nrl.navy.mil). (c) The High Frequency Active Auroral Research Program (www.haarp.alaska.edu). (d) The Low Band Antenna (www.lofar.org). (e) The Widefield Array (www.mwatelescope.org). (f) A Wullenweber array.

8.9-1 Plot the full array pattern for 0° and 30° scan angles off broadside for the array of Fig. 8-30. Also plot the array factor for 30 degrees scan to see the grating lobe reduction effect of the element pattern.

8.9-2 The four-port Butler matrix beamformer of Fig. 8-32 is used to drive four isotropic elements. (a) Write the interelement excitation phases for all four beams. (b) Plot all four beam patterns on one polar pattern plot. (c) Give the values of the beam peak locations and crossover levels. (d) Calculate the beam peak directions for Beam 1 and 2 using beam scanning principles.

8.9-3 For the AN/PPS-18 radar example of Fig. 8-33, find the aperture efficiency based on a specified gain of 27 dB.

8.9-4 Derive an expression for the line length of a delay-line phase shifter to steer the beam of a linear array to angle θ_o starting with the required phase for element n of $\alpha_n = -(2\pi/c)f\,nd\cos\theta_o$.

8.9-5 *Project*. Investigate quantization lobes due to digital phase shifting.

8.9-6 *Project*. Investigate and report on how the Butler and Blass beamforming networks operate.
8.9-7 Compute the pattern of Beams 1 and 2 in Fig. 8-32 for the Butler matrix BFN and determine the value and angle where beams crossover.
8.10-1 Find the element spacing in wavelengths, d/λ, that gives a maximum element gain value of 6 dB for a planar array with $d = d_x = d_y$.
8.11-1 This problem examines frequency effects on beam steering with a linear phased array. (a) Derive (8-122). Now consider an array with the phase shifters set to steer the beam 30° off broadside at 2 GHz. Find the angle off broadside of the beam peak at (b) 1.6 GHz, and (c) 2.4 GHz.
8.11-2 A phased array is required to have a bandwidth of 40% and 45° scan to off broadside. Find which antenna types in Fig. 8-36 are possible choices as elements.